

REPORT DOCUMENTATION PAGE			Form Approved OMB No. 0704-0188	
Public reporting burden for this collection of information is estimated to average 1 hour per response, including the time for reviewing instructions, searching existing data sources, gathering and maintaining the data needed, and completing and reviewing the collection of information. Send comments regarding this burden estimate or any other aspect of this collection of information, including suggestions for reducing this burden, to Washington Headquarters Services, Directorate for Information Operations and Reports, 1215 Jefferson Davis Highway, Suite 1204, Arlington, VA 22202-4302, and to the Office of Management and Budget, Paperwork Reduction Project (0704-0188), Washington, DC 20503.				
1. AGENCY USE ONLY (Leave blank)		2. REPORT DATE 4 May 1998	3. REPORT TYPE AND DATES COVERED	
4. TITLE AND SUBTITLE COMPARISON OF AMPLITUDE NOISE PROPERTIES OF SOLID STATE LASER OSCILLATORS AND AMPLIFIERS			5. FUNDING NUMBERS	
6. AUTHOR(S) Roberta Marie Ewart				
7. PERFORMING ORGANIZATION NAME(S) AND ADDRESS(ES) STANFORD UNIVERSITY			8. PERFORMING ORGANIZATION REPORT NUMBER  98-007	
9. SPONSORING/MONITORING AGENCY NAME(S) AND ADDRESS(ES) THE DEPARTMENT OF THE AIR FORCE AFIT/CIA, BLDG 125 2950 P STREET WPAFB OH 45433			10. SPONSORING/MONITORING AGENCY REPORT NUMBER	
11. SUPPLEMENTARY NOTES				
12a. DISTRIBUTION AVAILABILITY STATEMENT Unlimited distribution In Accordance With AFI 35-205/AFIT Sup 1			12b. DISTRIBUTION CODE	
13. ABSTRACT (Maximum 200 words)  <div style="text-align: center; border: 1px solid black; padding: 10px; font-size: 2em; font-weight: bold;">19980514 166</div>  <div style="text-align: right; font-weight: bold; transform: rotate(-10deg);">DWC QUALITY INSPECTED 3</div>				
14. SUBJECT TERMS			15. NUMBER OF PAGES 126	
			16. PRICE CODE	
17. SECURITY CLASSIFICATION OF REPORT	18. SECURITY CLASSIFICATION OF THIS PAGE	19. SECURITY CLASSIFICATION OF ABSTRACT	20. LIMITATION OF ABSTRACT	

COMPARISON OF AMPLITUDE NOISE PROPERTIES  
OF  
SOLID STATE LASER OSCILLATORS AND AMPLIFIERS

A THESIS

SUBMITTED TO THE DEPARTMENT OF ELECTRICAL ENGINEERING  
AND THE COMMITTEE ON GRADUATE STUDIES  
OF STANFORD UNIVERSITY

IN PARTIAL FULFILLMENT OF THE REQUIREMENTS

FOR THE DEGREE OF

ENGINEER

Roberta Marie Ewart  
March 1998

Approved for the department:

Robert L. Byer  
Adviser

Approved for the Committee on  
Graduate Studies:

Thomas Wasow

## ACKNOWLEDGMENTS

I wish to acknowledge the assistance and support I received from numerous people while completing my Stanford Graduate program.

First and foremost I am indebted to my adviser, Dr. Robert Byer. I was extremely fortunate to have been accepted into his research group in the last year of my graduate studies. Without his guidance and encouragement this thesis would not have been possible. Professor Byer provided the environment, both physically and mentally to allow me to make a contribution to laser noise studies. I felt "at home" almost immediately with his research group and this feeling is a product of his leadership and interaction with his staff and students.

Though there was not a great deal of time to build many in-depth relationships, I want to recognize the sacrifices made on my behalf by my fellow student, Bill Tulloch. Without hesitation he assisted me throughout the data gathering phase of this effort and substantially decreased the amount of time required to obtain data. His knowledge of the laser system and his continual maintenance efforts afforded me the luxury of focusing on the theory and analysis of data. I am certain he often put his work aside to help me. I hope somehow to return the favor.

A wider sphere of people contributed to my studies. I thoroughly enjoyed Professor Yamamoto's noise theory course, Professor Siegman's laser classes and Professor Byer's laser labs. They provided the foundation for my work. Professor Fejer and Eric Gustafson offered advice and invaluable insights and demonstrated how a well rounded and cohesive research organization should operate. I am also indebted to a fellow researcher, Xe-Shun Sun, who graciously loaned a photodetector to assist in the data gathering.

There are also people who work quietly and often without recognition to keep the entire research organization running. I salute the Stanford administrative support staff. In particular, I want to thank Kellie Koucky. Her positive and "can do" attitude kept me going on more than one occasion, and her assistance on flowing the paperwork and drafts was critical to completion of this thesis.

I wish to acknowledge the United States Air Force for supporting me financially throughout this period. Allowing me over three years to study with the finest scientists and engineers in the world will be an investment upon which I will guarantee a return. I especially want to thank Colonel Robert Duryea, USAF, who allowed me the time to finalize the thesis while on duty at the Air Force Research Lab.

Lastly and most importantly I want to recognize those who supported me personally through the challenging moments of graduate school. Above all my family should be recognized for their unswerving support and encouragement during my entire career. Over the years they have been the foundation from which I could extend my Air Force endeavors. To them I owe my system of values and work ethics and their training has served me well. Also, thanks go to John Lewellen, my first, and now forever, Stanford friend. He imposed sanity and reset my "frustration meter" on more than one occasion. Our motorcycling adventures are cherished memories.

This thesis was written over the last year and a half on my off duty time. This was time that was robbed from the most important person in my life. Robert, thank you for waiting so patiently, and sweetheart, I am coming home.

Roberta M. Ewart, Major, USAF  
Air Force Research Lab  
Albuquerque, NM  
March 1998

# CONTENTS

<b>Preface.....</b>	<b>iii</b>
<b>List of Figures.....</b>	<b>vii</b>
<b>Chapter 1. Background.....</b>	<b>1</b>
1.0 Introduction and Motivation.....	1
1.1 Thesis Content.....	2
1.2 Laser Noise Overview.....	3
1.3 Noise : Definitions and Types.....	4
1.4 Noise Measurement Units.....	10
1.5 Laser Amplifier and Oscillator Configurations.....	15
1.6 Detector Properties Affecting Amplitude Noise Measurements.....	17
Chapter 1 References.....	20
<b>Chapter 2 Theory I: Historical Approaches to Amplitude Noise Calculations.....</b>	<b>21</b>
2.1 Historical Overview of Linear Amplification Noise .....	21
2.2 Historical Overview of Saturated Amplification Noise.....	28
2.3 Historical Overview of Oscillator Noise .....	29
Chapter 2 References.....	33
<b>Chapter 3 Theory II: Derivations of Theoretical Expressions for this Study .....</b>	<b>36</b>
3.1 Linear Amplifier Amplitude Noise .....	36
3.2 Linear Amplifier Chain Amplitude Noise.....	49
3.3 Non-Linear Amplifier Amplitude Noise.....	50
3.4 Injection Locked Oscillator Amplitude Noise.....	56
Chapter 3 References.....	64
<b>Chapter 4 Experiment .....</b>	<b>68</b>
4.0 Introduction .....	68
4.1 The Laser Amplifier.....	69

4.2 Detection Systems.....	72
4.3 Experimental Process .....	75
4.3.1 Characterization and Calibration .....	75
4.3.2 Experimental Layout .....	82
4.3.3 Technique for Gain and Noise Measurements .....	84
5.4 Results and Analysis.....	87
Chapter 4 References.....	94
<b>Chapter 5 Conclusion.....</b>	<b>95</b>
5.1 Summary .....	95
5.2 Future Work.....	97
<b>Appendices</b>	
A1 Summary of Useful Equations.....	100
A2 Difference Between Optical and Electrical RIN.....	101
A3 Noise Floor Considerations.....	103
A4 Photodetector Frequency Analysis Procedure.....	108
A5 Quantum Efficiencies for Narrowband and Broadband Sources.....	109
A6 FP Cavity with Gain Medium.....	114
A7 Injection Locked Laser Calculations.....	119

## List of Tables and Figures

<b>Table 1. LIGO Laser Amplitude Noise Performance Parameters.....</b>	<b>2</b>
<b>Figure 1. Diagram of Noise Power and RIN.....</b>	<b>12</b>
<b>Figure 2. Conversion Chart for RIN and QNEL.....</b>	<b>13</b>
<b>Figure 3. Amplitude Noise of a Tungsten Source and the 300mW NPRO.....</b>	<b>18</b>
<b>Figure 4. Probability Representation of Photon States vs Photon States.....</b>	<b>37</b>
<b>Figure 5. Diagram of Noise Propagation through an Amplifier System .....</b>	<b>43</b>
<b>Figure 6. Linear Amplifier Amplitude Noise Versus Gain.....</b>	<b>45</b>
<b>Figure 7. Linear Amplifier Amplitude Noise Figure vs Gain.....</b>	<b>46</b>
<b>Figure 8. Noise Figure Referenced to the Detector.....</b>	<b>47</b>
<b>Figure 9. Double Pass Amplifier Block Diagram.....</b>	<b>48</b>
<b>Figure 10. Double Pass Linear Amplifier Amplitude Noise.....</b>	<b>49</b>
<b>Figure 11. Linear Amplifier Chain Amplitude Noise.....</b>	<b>50</b>
<b>Figure 12. NF for Linear and Non-Linear Amp Chains and Oscillator.....</b>	<b>56</b>
<b>Figure 13. Schematic of the RLC Model of an Injection Locked Oscillator....</b>	<b>60</b>
<b>Figure 14. Schematic of the Injection Locked Ring Laser.....</b>	<b>61</b>
<b>Figure 15. Injection Locked Oscillator Amplitude Noise Spectral Density.....</b>	<b>62</b>
<b>Figure 16. Single Pass Gain vs. Laser Diode Pump Level.....</b>	<b>70</b>
<b>Figure 17. Double Pass Gain vs. Laser Diode Pump Level.....</b>	<b>70</b>

<b>Figure 18. Amplified Spontaneous Emission vs. Gain for Single and Double Pass Systems.....</b>	<b>71</b>
<b>Figure 19. Schematic of InGaAs Detector/Receiver.....</b>	<b>74</b>
<b>Figure 20. InGaAs Detector Linearity at 15 MHz.....</b>	<b>76</b>
<b>Figure 21. Upward Drift in SA Noise Trace vs. Video Averaging Function....</b>	<b>77</b>
<b>Figure 22. Horizontal Intensity Profiles (Single Pass Amplifier).....</b>	<b>78</b>
<b>Figure 23. Vertical Intensity Profiles (Single Pass Amplifier).....</b>	<b>78</b>
<b>Figure 24. Horizontal Intensity Profile (Double Pass Amplifier).....</b>	<b>79</b>
<b>Figure 25. Vertical Intensity Profile (Double Pass Amplifier).....</b>	<b>79</b>
<b>Figure 26. Saturation Characteristics of the Nd:YAG Amplifier Slab.....</b>	<b>80</b>
<b>Figure 27. NPRO Serial # 118 Noise Power Spectral Density Plot.....</b>	<b>81</b>
<b>Figure 28. NPRO Serial # 282 Noise Power Spectral Density Plot.....</b>	<b>82</b>
<b>Figure 29. Layout of Linear Amplifier (Single Pass Set Up).....</b>	<b>83</b>
<b>Figure 30. Layout of Double Pass Set Up.....</b>	<b>83</b>
<b>Figure 31. Layout of Saturated Amplifier.....</b>	<b>84</b>
<b>Figure 32: Nd:YAG Linear Amplifier Noise.....</b>	<b>88</b>
<b>Figure 33. ASE Intensity Profiles for the Slab Amplifier.....</b>	<b>90</b>
<b>Figure 34. Efficiencies for Single Pass Case.....</b>	<b>91</b>
<b>Figure 35. Efficiencies for Double Pass Case.....</b>	<b>91</b>
<b>Figure 36. Homodyne Detection Parameter Degradation with Increasing Phase Front Misalignment.....</b>	<b>93</b>

# Chapter 1

## Background

### 1.0 Introduction and Motivation

There is an ongoing need for more capable laser sources that combine high average power with quantum noise limited performance for applied physics and photonic engineering applications, including free space optical communications systems, heterodyne spectroscopy and laser interferometry for gravity wave detection. At this time, one of the most plausible laser candidates to meet the application requirements is the diode laser pumped solid state laser (DPSSL)<sup>1</sup>. To push the state of the art of these lasers to the next level, technologists need to understand and characterize the noise properties. It is well known that amplitude and frequency-phase noises are coupled and hence it is important to characterize both frequency and amplitude noise to fully understand the noise properties of lasers. The question posed by this comparative study is, given the need for coherent optical power, on the order of tens of watts to kilowatts, what is the best amplitude noise performance attainable? Will the best amplitude noise performance for a given optical output power be obtained from a laser oscillator or from a master oscillator power amplifier (MOPA) approach?

The primary technological motivation for this thesis is to understand the relative intensity noise (RIN) of a laser system required for the Laser Interferometer Gravitational - Wave Observatory (LIGO). Table 1 displays the expected RIN performance parameters for the initial LIGO laser and the advanced LIGO laser system as defined in the 1995 Galileo Proposal to the National Science Foundation. The two key frequency ranges of interest are the phase modulation frequency at 15 MHz and the gravity wave system interaction frequency regime between 10 Hz and 10 kHz. The acronyms and units used in the table will be explained in subsequent sections.

**Table 1. LIGO Laser Amplitude Noise Performance Parameters**

	Initial LIGO Requirements	Advanced LIGO Requirements
<b>Laser Power</b>	<b>10 W</b>	<b>100 W</b>
<b>RIN @ 15 MHz</b>	<b>Shot Noise Limited (SNL)</b>	<b>SNL</b>
<b>RIN @ 100 Hz <math>1/\sqrt{\text{Hz}}</math></b>	<b><math>4 \times 10^{-7}</math></b>	<b><math>8 \times 10^{-9}</math></b>
<b>RIN @ 10 kHz <math>1/\sqrt{\text{Hz}}</math></b>	<b><math>4 \times 10^{-6}</math></b>	<b><math>8 \times 10^{-9}</math></b>

This study is bounded by the following comments. This study does not include theory or experimentation leading to the decrease of technical or environmental noises most often associated with or encountered from acoustic or thermal sources, such as: water coolant turbulent flow, vibration of mounts or thermalization of laser components. This study does not include parametric amplifiers or wave mixing amplifiers. In many cases the system discards the idler wave, rendering these devices, in many cases, too inefficient for the high power applications. It must be noted that these types of systems have very low quantum noise. Also, squeezed light, is not included experimentally in this study. Theoretically it may be possible to use this non-classical type of light to lower the amplitude noise of a laser system in particular applications and at particular frequencies below the expected quantum limit, but this simultaneously has deleterious effects on the conjugate quantum variable, the phase. Since, phase changes represent the key experimental parameter in an interferometer such as LIGO, care must be taken not to over optimize the amplitude noise and drive the phase noise to unacceptable levels.

## 1.1 Thesis Content

The content of this thesis is divided into chapters devoted to theory, experimentation and the comparison of the two. The first chapter discusses the background information and the definitions of terms. Here, emphasis is placed on clearly describing the different noise power measurement systems to prevent confusion when later comparing the theoretical and experimental outcomes of different authors. The theory portions are detailed in Chapters two and three. Chapter 2 contains the historical overview of theoretical approaches to laser

amplitude noise, while Chapter 3 encapsulates the noise power derivations for the particular solid state laser systems tested in the experimental portion of this study. Very simple theoretical expressions for the amplitude noise of traveling wave amplifiers are derived. These derivations are followed by a comparison of three approaches to calculating the amplitude noise of an injection locked oscillator. Chapter 4 details the experimental procedures. The noise power spectral density for the laser amplifiers is characterized at 15 MHz, (the LIGO interferometer signal frequency), and is shown to support the theory. Chapter 5 offers concluding remarks comparing the theory to the experimental results and providing comments on future work. Appendices are provided for the material which is too detailed or pedantic for the main body of the study.

This concludes a very brief introduction to the goal and content of this study. The next step is to relate this study effort to the studies of laser noise as a whole.

## 1.2 Laser Noise Overview

Laser noise studies actually began with studies of noise in the maser, the predecessor of the laser. As would be expected, electrical engineers viewed the laser noise as being similar to noise in standard RF amplification systems and used terms with which they characterized those systems. Terms such as noise factors and signal to noise ratios were keys for characterizing laser radiation for communications, especially as the field of guided wave or fiber optic communications developed. Applied physicists used different terminology including photon statistics and spatial modes to characterize the noise properties of predominantly free space communication systems. The two disciplines have since overlapped and created a large body of knowledge which lacks some coherence, common nomenclature and units.

With current technology it is not possible to remain entirely in an electronic or photonic regime to obtain the noise information about the laser systems themselves. There is no way to electronically “query” the atomic dipoles just prior to stimulated emission to determine the laser noise properties. There also is no current way to query the photonic stream, once it exists, without converting it to an electronic counterpart. Surely, if there were a purely photonic method for measuring the noise of a laser it would be much easier than converting the photons to electrons, determining their noise and then implying the noise characteristics of

the photon stream. The crux of the experimental study of laser noise is the crossover that occurs in the photodetection process. The photodetector can be viewed as converting the purely optical noise into noise which has components both from the optical noise, and from the detection processing of the photons themselves. Therefore, it is important to understand the noises created by the photodetection process as well as the photonic noise generated in the lasing process. These noises are categorized and explained in the next section. Following the definitions of noise are brief descriptions of the systems under comparison and a short background summary of detector related noise concerns.

### 1.3 Noise: Definitions and Types

It is not possible to have a deterministic or "noise free" measurement of coherent optical power. There are uncertainties in the location, momentum, energy or arrival time of the photons. So, in the case of photons, noise can be viewed as an inherent randomness in a physical process or it can be viewed as the inherent uncertainty involved in any measurement. Random fluctuations as studied in the statistics of random variables are often characterized mathematically by the concepts of the probability density function (PDF) and probability generating functions (PGF). These functions are used to describe the noise statistics of both the electrons and photons. Associated with these density functions are the mean, or average or entities called "expectation values", and the variance, or its root, the standard deviation. These qualities are also related to what statisticians call the first and second moments of the probability distribution. In most cases of CW laser operation only the first two moments are needed to characterize the noise. Higher moments are needed when dealing with noise properties of coherent photon streams in the study of digital communication systems. The equations for the first two moments of any distribution of random discrete variables are given by

$$\langle n^1 \rangle = \sum_{n=0}^{\infty} n^1 P(n) \quad (1.1)$$

and

$$\langle n^2 \rangle = \sum_{n=0}^{\infty} n^2 P(n), \quad (1.2)$$

where  $P(n)$  is the probability that the random variable takes the value  $n$ . Throughout this study  $n$  will be representing numbers of photons. The  $\langle \rangle$  indicates either an ensemble or a time average, as it is assumed the processes under study are ergodic. The first moment serves as the mean value or expectation value. In many cases it will represent the signal. The variance,  $\sigma^2$  and standard deviation,  $\sigma$ , are derived from a combination of the first and second moments as follows.

$$\begin{aligned}\sigma^2 &= \langle (\Delta n)^2 \rangle = \langle (n - \langle n \rangle)^2 \rangle \\ &= \langle n^2 - 2n\langle n \rangle + \langle n \rangle^2 \rangle \\ &= \langle n^2 \rangle - \langle 2n\langle n \rangle \rangle + \langle n \rangle^2 \\ &= \langle n^2 \rangle - 2\langle n \rangle \langle n \rangle + \langle n \rangle^2 \\ &= \langle n^2 \rangle - 2\langle n \rangle^2 + \langle n \rangle^2\end{aligned}$$

$$\sigma^2 = \langle n^2 \rangle - \langle n \rangle^2 \quad (1.3)$$

$$\sigma = \sqrt{\langle n^2 \rangle - \langle n \rangle^2} \quad (1.4)$$

The standard deviation (1.4) is also referred to as the RMS noise in the literature. The variance (1.3) is called the “noise power” is the observable data taken from a spectrum analyzer as a power spectral density per Hz, as it has traditionally been used to characterize noise in RF systems. However, a complete explanation of statistical concepts, including the PDF and PGF is better left to a text<sup>2</sup>. The only other statistical knowledge required for this study is the statistical distributions which photons can assume and which produce given PGF and PDF functions. The photon statistical distributions for a completely (perfectly) coherent source are Poissonian and for an incoherent or thermal source are Bose-Einstein. This will be explained in more depth shortly. Standard statistical calculations can be done on these photon distributions and assuming the photoelectrons are created via a Bernoulli random process, it can be assumed that the photoelectrons also follow the photon statistics. The difficulty then lies in converting the theoretical statistical values for the first two moments of the photon distributions into the

photoelectron noise power spectral density which is the observable obtained from a spectrum analyzer in an actual amplitude noise experiment.

Now that the mathematical background for characterizing noise has been briefly introduced, it is necessary to categorize noise in a useful way. The first category will focus on the radiation (photon) noise. This is the inherent noise on a photonic stream. It cannot be directly measured but a theoretical value can be determined. The second category is the noise associated with electrons after they have been photogenerated. It will include shot noise and the Nyquist or thermal noise in the measurement system. The third category will be called excess noise. This will be the noise which cannot be accounted for by either the photon statistics which evolve as the photon stream passes through a passive system or the electronic noise created in the receiver. It will be the noise created by the interactions of the original photonic streams with active media which supply both stimulated emission or gain and amplified spontaneous emission (ASE). In other words, any increase in the variance of the original photon statistics is deemed excess noise and is added by an amplification system. Technical noise, which covers macroscopic effects in the laser environment, such as acoustical coupling to coolant flow and microphonics will not be discussed. It is assumed in this study that the laser systems are free of these technical noises.

In this study, the interaction of a laser oscillator's (Nd:YAG non-planar ring oscillator (NPRO)) photonic stream with a laser amplifier will be investigated and characterized. Several interesting features will be exposed. Some excess noise can be viewed as either a classical beating of signal and noise fields at a "square law" detector or as the statistical outcome of quantum mechanical interactions which change the photonic stream's statistics (total number or phase) as it passes through the optical amplifier. It is a classic example of a wave, particle duality. It is also possible to show that spontaneous emission not only adds amplitude noise, it also broadens the spectral width by adding random phase noise. This is in accordance with the Schalow-Townes equation for the linewidth of a photonic stream from a laser. This phenomenon is an example of the Heisenberg uncertainty relation because photon number (amplitude) and phase are non-commuting observables. So, an increase of amplitude noise is reflected as an increase in the spectral width of the signal. As indicated earlier, amplitude and frequency noise are inextricably linked.

The first noise category of interest, radiation noise, arises from the original distributions of photons created by the radiating source, which is usually an atomic

dipole undergoing a transition. The subsequent photon statistics depend on these initial distributions. There are two types of photon statistics: Poisson statistics arising from a coherent light source and Bose-Einstein statistics arising from a thermal, i.e., blackbody source. All sources create radiation whose statistics fall between these two distributions. The Poisson distribution is used because it is in good agreement with experimental estimates of discrete processes, in this case, photon emission. The discrete processes assume the probability of detecting a photon goes to zero as the time goes to zero. Also, the emission of a photon is binary in nature, i.e., the particle is present or not. Multiple binary processes, or the train of randomly occurring emission events, then lead to a binomial distribution which becomes the Poissonian distribution as the number of particles per sample time approaches infinity. The photon emission events are time independent, or in other words the probability of detecting a photon is independent for non-overlapping time intervals. Only “perfectly” coherent light meets this criteria. The Nd:YAG laser oscillator used in this experiment operates in a single mode with a very narrow linewidth and a high degree of coherence and hence the Poisson assumption is a good one<sup>3</sup>. The Poisson probability distribution function is given by<sup>4</sup>

$$P(n) = \frac{\langle n \rangle^n}{n!} \exp(-\langle n \rangle)$$

from which the first two moments are found

$$\begin{aligned} \langle n^1 \rangle &= \langle n \rangle \\ \langle n^2 \rangle &= \langle n \rangle [\langle n \rangle + 1] \end{aligned}$$

using equations (1.1) and (1.2). The moments inserted into equation (1.3) yield the variance

$$\sigma^2 = \langle n \rangle. \quad (1.5)$$

So the noise power of a coherent photon stream is directly proportional to the mean number of photons in that stream.

At the other extreme of photon distributions, where the light is incoherent or chaotic, we have the Bose-Einstein statistics. These statistics were first applied to the study of noise from masers<sup>5</sup>. The probability distribution is given by

$$P(n) = \frac{1}{1 + \langle n \rangle} \frac{\langle n \rangle^n}{(1 + \langle n \rangle)^n}.$$

Using this probability function and equations (1.1), (1.2) and (1.3) we obtain

$$\sigma^2 = \langle n \rangle^2 + \langle n \rangle \quad (1.6)$$

for the noise power<sup>6</sup>. It is clear that an incoherent field is far “noisier” than a coherent one, as expected. Equations (1.5) and (1.6) will be used in the theoretical discussions of noise in the subsequent sections.

The second category of noise includes noise associated with electrons, regardless of whether they were generated through photoelectron pair production or exist due to the flow of charges in the measurement system. This category includes shot noise and the Nyquist noise or thermal noise. Shot noise is an inherent outcome of the randomness involved in the interaction of a charged particle with a radiation field. The granularity of charge is ultimately responsible for the existence of shot noise, but this is not the complete explanation. Shot noise occurs only under the conditions of DC flow and the presence of a potential barrier over which the electrons must leap. These conditions are met in a square law photodetector converting photons to electron-hole pairs and they are not met when electrons flow through a linear resistor. As electrons hop the barrier there is a discontinuity in the current which translates to a random arrival time. The shot noise power equation has been derived by numerous authors, but a succinct explanation is found in Yariv<sup>7</sup>. The shot noise equation is

$$\sigma_i^2 = 2qI_{DC}\Delta f, \quad (1.7)$$

where  $q$  represents the electron charge,  $I_{DC}$  is the direct current flow and  $\Delta f$  refers to the bandwidth of the measurement. From this equation two qualitative statements can be made. Shot noise power drops linearly with the DC photocurrent. So, for example, to calibrate a photodetector just decrease the

intensity linearly and verify the noise power goes down linearly. This linear relationship implies that more intense laser beams are inherently noisier. Also notice that as the bandwidth increases, the precision of the time measurement is increased. When this occurs, the precision in the count of the electrons in the stream decreases as one would expect from the uncertainty principle. Hence the shot noise increases. For consistency, all noise measurements need to be referenced to a particular bandwidth, which in this study will be 1 Hz. For this reason, often the bandwidth will not appear in the shot noise power equation in this study. However, for correct units the bandwidth needs to be indicated.

Shot noise has an underlying assumption which is worthwhile summarizing here for completeness. Shot noise is postulated to have a white noise or constant power spectrum. However, since this would imply infinite energy--through the integration of the power spectral density over an infinite set of frequencies--there must be some characteristic fall-off at high frequencies. It is assumed that the rolloff occurs at frequencies outside of the bandwidth across which the experimental measurements were taken. However, rather than just postulating a rolloff, the difficulty can be resolved by considering that in the case of photodetectors, there are non-zero carrier transit times across a potential barrier, such as a depletion region in a PIN photodiode. The transit times impose a type of bandwidth limitation or roll-off. The shot noise should decrease once the noise frequency becomes comparable to the inverse transit time of the charge carrier. So, the linear shot noise equation only holds for noise spectral components whose frequencies are small compared with the inverse transit time. Above that critical value, the shot noise equation over estimates the noise.

If a charge carrier passing through a depletion layer of a diode creates a rectangular current pulse, whose duration is equivalent to the transit time, the noise equation (1.7) is slightly modified via a Fourier transform and produces the following expression for the shot noise

$$\sigma_i^2 = 2qI_{DC}\Delta f \left( \frac{\sin \pi f \Delta t}{\pi f \Delta t} \right)^2 .$$

For frequencies up to  $0.25 / \Delta t$ , where  $\Delta t$  is the transit time, the correction is smaller than 10%. The InGaAs PIN photodiodes used in this study have transit times up to 1 nS. This gives bandwidths of 1 GHz. If the noise measurements are

conducted at 15 MHz, the value of the sinc function at 0.015 will give the correct value within 0.03 % of the simpler theory. Experimental error will be much greater than this, so the simpler equation is adequate for this study. It should be noted that if the noise power measured in a detection system is dominated by the shot noise contributions, the detection system is said to be operating in the “quantum-limited” detection regime. This is the most desirable detection regime in which to operate. Sometimes, however, another noise power comes into play, Nyquist or thermal noise.

Nyquist or thermal noise is the result of the random walk of electrons through any lossy device. It is an inherent noise in any electronic circuit with a lossy component. Since measurement involves adding a load to the system under test and this load represents a lossy component, thermal noise will be present. The derivation of the thermal noise can be found in numerous texts, and similar to the shot noise discussion above there is a correction which takes into account rolloff of the noise at high frequencies. This correction, called the Plank correction, is not used when operating below a terahertz at room temperature. The simplified formula for the mean square current density is<sup>8</sup>

$$\sigma^2_{thermal} = \frac{4kT\Delta f}{R},$$

where as before  $\Delta f$  refers to the bandwidth of the measurement,  $k$  is Boltzman’s constant,  $T$  is the temperature in Kelvins, and  $R$  is the resistance. Assuming the loads are matched throughout the experimental set up, the value of thermal noise for a 50 ohm system at room temperature, in a 1 Hz bandwidth is -174 dBmW. This value is well below the shot noise measurements made with the Hewlett Packard spectrum analyzer used in this experiment. The HP 71000 system spectrum analyzer has a noise floor of approximately -143 dBmW through out the megahertz region with a standard 50 ohm terminator on its input. Therefore, thermal noise will not be discussed for the remainder of this study.

## 1.4 Noise Measurement Units

Having briefly discussed the types of noise which are under study it is now appropriate to clarify the units which are used to quantify noise and to provide nomenclatures for the observables in the experiment. The most important mental

picture is that of the noise power represented by the power spectrum. This is a continuum of noise power spread from DC to frequencies well beyond what the experimental apparatus can measure. This particular experiment focuses on the noise power gathered in one second at a particular frequency, 15 MHz, and is called the power spectral density at that point. The unit for measuring this particular observable is the dBmW in 1 Hz, abbreviated dBm/Hz.

Any power which is gathered by the experimental apparatus which is not derived from the desired signal is considered to be noise. (Note that it is critical to determine what the power of the signal actually is in order to understand what the noise may be.) To put noise into the proper perspective with the signal, the term relative intensity noise (RIN) is used. RIN should be viewed as a ratio of the intensity of the noise versus the signal intensity. Since both electric field and optical intensity terms occur in these experiments, the term RIN can be used with both photonic and electronic noises. (However, the electrical and optical RIN are not equal -- see Appendix 2) RIN is not expressed in power density units, but as a relative unit in dB, depending on the DC level of the signal, which is linked to the DC photocurrent or the electrical current. If, for example the majority of the noise is shot noise (the ideal case), then the RIN due to shot noise can be found by plotting the shot noise power and the detected signal power and subtracting the two in units of decibels. Converting the detected photonic intensity into photocurrent in a 1 Hz bandwidth or a 1 second integration results in the diagram in Figure 1.

As noted above, in the ideal case, the shot noise is the predominant noise in the system under test (SUT) and it basically implies that the limits to the measurement are the experimental apparatus themselves. It is assumed here that if the intensity and original statistics of the signal are known then the shot noise can be calculated and subtracted from the total noise measured to determine the excess noise added by the amplification process. It is the excess noise created by the interaction of the photonic stream with the amplifier or oscillator under test which is of ultimate interest. The RIN increases with an increase in the signal power, as indicated in Figure 1. So, just amplifying a signal, for example adding coherent photons to increase the total number of photons in the stream, will automatically result in greater RIN.

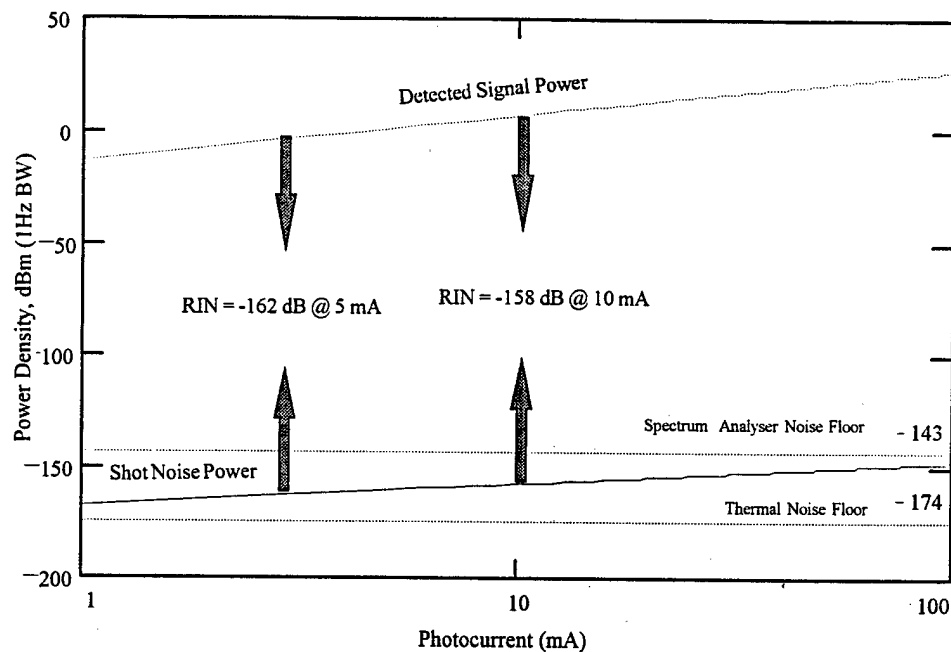


**Figure 1. Diagram of Noise Power and RIN. The relative intensity noise increases with increasing optical power.**

If the device under test (DUT) gives a RIN value which is due only to the contribution of the shot noise then the SUT is considered shot noise limited (SNL) and this is classically the very best noise performance one can expect from that system. As an aside, it can be very tempting to make noise measurements at high photocurrents such as 10 mA, to take advantage of the increased shot noise power over and above the spectrum analyser noise floor and thereby forego adding an additional amplifier stage. However, it is important to take into account the effects this higher current can have on the photodetector and amplifier response and design accordingly. For example, higher photon fluence can lead to saturation effects which are different at different frequencies. Detection saturation was encountered early on in this study and is described in greater depth in the following section. Appendix 4 describes an apparatus to determine the photodetector frequency response which is very convenient when undertaking broadband noise analysis.

In addition to the RIN (in either electrical or optical units) another term is often used, called the quantum noise equivalent level (QNEL). This is also a frequency normalized form for comparing the noise power and the signal power and it is often seen in the literature as a ratio of optical intensities or powers. The RIN (in electrical units) is twice the QNEL when both are given in dB. The QNEL

is in units of  $1/\sqrt{\text{Hz}}$  and the mathematical relationship between the QNEL and the RIN is:  $QNEL = \sqrt{RIN_{linear}}$ . (Note: In Table 1, strictly speaking, the units of amplitude noise for LIGO should have read QNEL not RIN.) A handy conversion chart is provided in Figure 2.

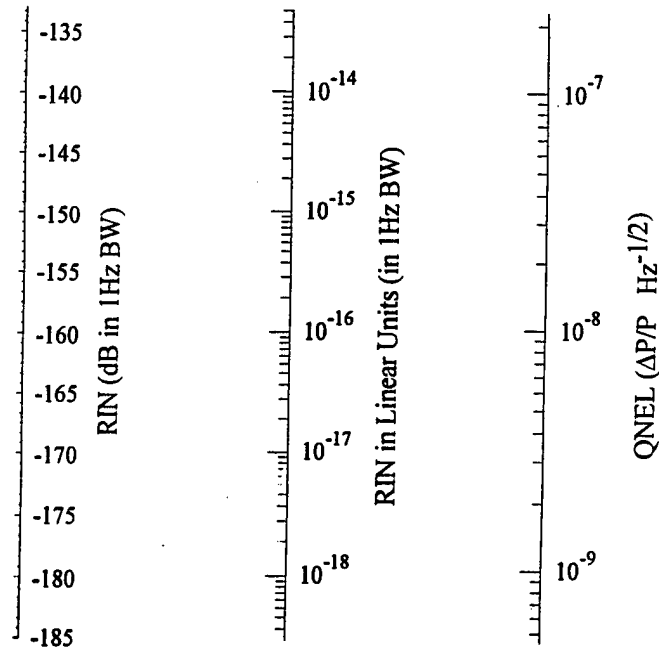


**Figure 2. Conversion Chart for RIN and QNEL**

Another commonly used term for discussing noise properties is the signal to noise ratio (SNR). It is particularly useful when discussing the properties of amplifiers, which are judged by how much they degrade the SNR of an incoming signal. SNR can be defined if the measurements of the noise and signal are time averaged over a time which is long compared to the inverse bandwidth of both of them. The measurements made in this study were for time averages over milliseconds while the inverse bandwidths were on the order of microseconds. The signal to noise ratio in the electrical and optical sense can be viewed as either ratios of power quantities or signal quantities. This study will use the convention of the power ratio given by

$$SNR \equiv \frac{\langle n \rangle^2}{\sigma^2}.$$

In electrical terms,

$$SNR \equiv \frac{\langle I_{DC} \rangle^2}{\sigma_i^2},$$

while the optical terms,

$$SNR \equiv \frac{\langle n \rangle^2}{\sigma_n^2}.$$

The SNR values for the Poisson and Bose-Einstein photon distributions are derived using substitution and algebraic rearrangement.

For Poisson Statistics

$$SNR = \langle n \rangle,$$

and it is apparent that Poisson statistics are highly desirable due to the fact their optical signal to noise ratio scales with average photon number.

For Bose Einstein Statistics

$$SNR = \frac{\langle n \rangle}{\langle n \rangle + 1},$$

and it is clear that the optical SNR cannot be greater than 1 regardless of the number of photons. Hence, it is not feasible to use Bose-Einstein distributions for systems where signal to noise is an important parameter, as it is in communication systems for example.

The optical signal to noise ratios just derived have assumed well defined photon statistics. This study is aimed at finding the noise and hence the SNR for an as yet unknown statistical distribution which will not be mathematically as simple as these two pure cases. It will become clear in the theory section that there is another approach to find the noise using a semi-classical calculation which evokes the concepts of "beats" or the visualization of heterodyning of photon fields on a square law detector. The use of this heterodyning approach in this particular case requires the current associated with the local oscillator (NPRO probe beam) be much greater than the current due to the amplified spontaneous

emission (ASE). This implies that the noise used in the SNR calculation is predominantly the shot noise from the local oscillator photoelectrons.

Comparisons of SNRs can be tricky because in some cases the SNR is in optical terms and in the other it is in electrical terms. For now, the electrical SNR for a heterodyned system as found in the fiber optic communications or IR astronomy field of study will be quoted for reference and then later compared to the derived theory. The equation for SNR for a heterodyned system where  $n_{ASE}$  is the number of ASE photons is

$$SNR = 2\langle n_{ASE} \rangle.$$

The last units discussed in this section are the noise factor, the noise figure and the Fano Factor. Noise Factor, commonly given the term “F”, is the ratio of the SNR input to the SNR output of a system, usually measured at 290 K and Noise Figure, commonly given the term “NF”, is the noise factor converted to decibels. An ideal amplifier would have a noise factor of 1 and a noise figure of 0dB. Amplifiers whose noise figures are 3 dB or less are considered very good amplifiers. The Fano Factor, “f”, is slightly different. It is defined as

$$f = \frac{\sigma^2}{\langle n \rangle}. \quad (1.8)$$

For Poisson statistics  $f=1$  and for Bose-Einstein  $f=\langle n \rangle + 1$ . A system whose Fano Factor approaches one is also a very good system.

## 1.5 Laser Amplifier and Oscillator Configurations

A clear definition of units is mandatory. It is also important to clearly define the configuration of the systems whose noise properties will be compared. In this case, a traveling wave amplifier operating in two regimes, the linear and the non-linear or saturated, will be compared to the oscillating or recursive wave amplifier. In addition, the concepts of noise properties of amplifier chains which use relay imaging will be touched upon because these types of amplifier chains are the next logical step when power scaling a solid state laser system. It is also important to briefly add a comment about coherent and incoherent amplifiers. Those that preserve both the phase and amplitude information of the original signal are

coherent and those that destroy one or both are considered incoherent. Linear amplifications will be viewed as coherent and non-linear amplification or saturated amplification will be incoherent.

The linear traveling wave amplifier, also called less precisely an “unsaturated” amplifier, operates under conditions where so few photons enter the amplifier that their presence does not substantially change the stimulated emission and absorption cross sections and hence the probabilities of emission. It is also called the small signal case. The linear amplifier can also be considered “coherent” since it preserves the phase information of the original signal. The saturated traveling wave amplifier is one whose medium is pumped to a full inversion and then a large number of photons are flooded into the material to cause the absorption or emission characteristics to roll off. It is important to clearly understand which cross sections or which set of atomic transitions are affected--be it saturation of the pump transition or the radiation transition. Fundamentally, the amplifier is saturated when the photon populations and the excited state populations are coupled such that the input pump or signal (NPRO probe) significantly affects these two populations. In this study the saturation refers to the stimulated radiation transitions.

The third configuration used in this study is the oscillator or recursive wave amplifier which can be as basic as a traveling wave amplifier with a Fabry Perot cavity imposed around it or as complex as an injection locked oscillator. This type of amplification has generated great interest because it can be built into a feedback system which should provide greater control over several types of noise properties. The only type of oscillator configuration examined in this study, in depth, is the injection-locked oscillator. The reason is that generally high power oscillators, which are seeded from their own noise, require intracavity elements to ensure the single mode operation desired for laser gravity wave interferometry and using these elements robs the system of power. Injection locked oscillators may be a candidate for the applications of interest to this study, but are more complex to operate and do not offer convenient power scaling with high operational reliability. Briefly, the injection locked oscillator studied here is a small, low noise oscillator, like an NPRO, which is used to seed and thus control the oscillating modes of a higher power slave laser oscillator. The system is set up so that the frequency difference between the lasers is small so that the locking range is fairly robust. In the case used here, a small, 200 mW Nd:YAG NPRO is used to lock a Nd:YAG slab laser at 20 Watts. Other general rules of operation for this system include

good mode matching of the master and slave laser optical fields and a careful tradeoff of the ratios of the master and slave laser powers and the locking range. The theory section gives more details on the characteristics of this system.

Lastly, lumped amplifier chains, especially relay imaged versions, are gaining in popularity. The idea is to relay the beam from amplifier to amplifier such that the last amplifier is the only one in saturation. The major difficulties which need to be overcome are that of keeping the beam quality throughout the free space optical chain and preventing optical damage. By ensuring that optical foci occur in either vacuum or air there is less chance that the high intensities will damage system optical coatings. Up till now, the only amplifier chains were found in the fiber optic communications field, where chains of erbium doped amplifiers were used for transatlantic cables and in very high power glass lasers for fusion research. The fiber optic systems operate with very low photon flux and a guided wave channel. This is in direct contrast to the free space high power systems. However, fiber amplifier chains provide a departure point for the free space amplifier chain calculations.

## **1.6 Detector Properties Affecting Amplitude Noise Measurements**

As indicated earlier, the detector is the crux of the noise problem in converting from the photonic to electronic regimes. Several detector properties influence the interpretation of data as the detector converts noise power between the two worlds. Two properties are particularly important in the study of noise in photodiodes, the quantum efficiency and the response time. The reason these two are chosen is because it has now become common in the industry to form a responsivity and bandwidth product for comparison of detectors in high speed work. As is well known, the quantum efficiency is directly linked to the responsivity and the response time is inversely related to the bandwidth. The quantum efficiency term is used when converting noise measurements between the photonic and electronic regimes and the bandwidth is important when setting up measurements of noise power spectral densities. Both of these properties are affected by the materials chosen for the detector and the detector's physical layout in a receiver circuit. These two properties are considered in addition to the property of detector saturation which must be considered in all detectors. Though saturation might be considered the most straight forward of the three properties to be measured, in this

particular experimental set up saturation became the most difficult property to characterize.

Quantum efficiency is the probability that a photon will be converted to an electron-hole pair that contributes to the detector current. Because of the nature of the coupling between the photonic fields and the semi-conductor bands which represent collections of various electronic states, photodiode detectors have slightly different responses to broadband or thermal light characterized by Bose-Einstein statistics and the very narrowband nearly coherent light typified by the Poisson statistics. For a broadband source, instead of one quantum efficiency for the entire stream, one has to introduce a spectrum of quantum efficiencies normalized for the entire photon stream intensity. As the light becomes more narrowband, the approximation of a single quantum efficiency is acceptable. One of the advantages of the homodyne technique used in this experiment was that the single longitudinal and transverse mode of the local oscillator laser selected only one ASE mode so effectively, by default, the noise measurements were made with only one quantum efficiency value. Figure 3 shows the comparison of the broadband tungsten source (MAG Flashlight) versus the coherent narrowband 1064  $\mu\text{m}$  output of the NPRO at 1mA.

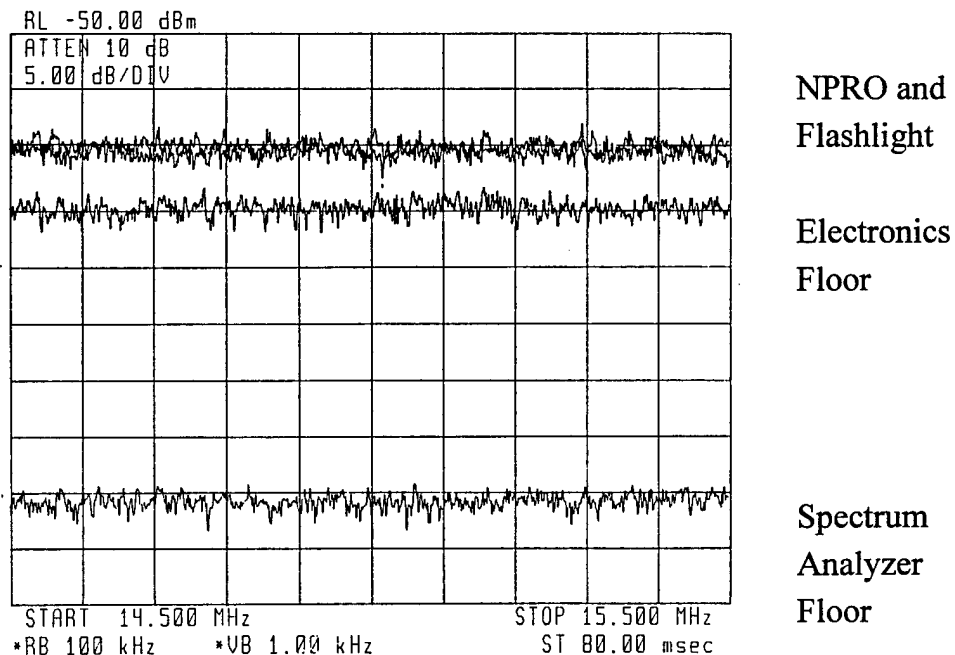


**Figure 3. Amplitude Noise of a Tungsten Source and the 300 mW NPRO @ 3.8 mA photocurrent using a Si detector. The amplitude noise is found to be indistinguishable between the flashlight and the coherent laser source.**

It should be pointed out that although in the lab environment the standard flashlight is viewed as a shot noise limited source, it is incorrect to make direct comparisons with the narrowband sources arbitrarily. Calculations of the differences in detector efficiencies between broadband and narrowband sources are provided in Appendix 5.

Also, because this experiment was conducted at the fairly low frequency of 15 MHz, the responsivity and hence the quantum efficiency was more important than the detector bandwidth. Since responsivity and bandwidth are inversely related, this led to a decision to move to a detector with higher quantum efficiency, but not substantially better response times, for these measurements.

The second major trait of photodiode detectors which is of concern in noise work is the response time which is composed of the transit time and the RC time constant. Transit time is the time allotted for the photoelectrically generated carrier to physically drift to the electrical contact and enter the detector circuit. Some photodiodes also have a restriction for diffusion time, whereby carriers generated outside of the depletion region take time to arrive in the depletion zone and then can be collected. In the design of the detectors the lifetime of charge carriers is also taken into account such that the dimensions are chosen to allow most of the carriers to be gathered before they experience recombination. The RC time constant is formed by the resistance and the capacitance of the photodetector and the receiver circuitry. It lengthens the impulse response which represents the creation of a photoelectron. When the RC time constant is convolved with the transit time response the result provides the total response time restriction. Response times convert directly and inversely to the bandwidth of the detector. For the InGaAs detectors used in this study the response times were on the order of 100 psec which converts to GHz of bandwidth.

For the sake of completeness, there is an additional detector trait, the dark current noise, which should be examined in low photon fluence noise work but was not examined here because the mW photon fluences essentially swamped the effect. Essentially, photoelectrons are created by thermal processes or tunneling in the absence of light. Often when biasing the detector to a higher voltage to attain a higher responsivity, and shorter transit times, dark current increases. Engineering trade-offs must then be done to optimize the detector.

Now that the definition of terms is complete and the basic outline of the devices under test and the detector characteristics have been briefly discussed, it is time to turn to the theory of noise in both the linear and saturated amplifier cases.

## Chapter 1 References

1. Robert L. Byer, "Diode Laser-Pumped Solid-State Lasers", *Science*, Vol. 239, p. 742 (1988).
2. Alberto Leon-Garcia, *Probability and Random Processes for Electrical Engineering*, 2nd Ed., (Addison-Wesley Publishing, Menlo Park, CA, 1994).
3. E. Dereniak, and D. Crowe, *Optical Radiation Detectors*, (Wiley, New York 1984), p. 18.
4. Herbert Kroemer, *Quantum Mechanics for Engineers and Applied Scientists*, (Prentice Hall, Englewood Cliffs, NJ, 1994), p. 609.
5. K. Shimoda, H. Takahasi, and C.H. Townes, "Fluctuations in Amplification of Quanta with Application to Maser Amplifiers", *Journal of the Physical Society of Japan*, Vol. 12, No. 6, p. 688 (1957).
6. B. Saleh and M. Teich, *Fundamentals of Photonics*, (Wiley, New York, 1991), p. 407.
7. Amnon Yariv, *Optical Electronics*, 4th Edition, (Holt, Reinhart and Winston, Inc., San Francisco, 1991), p. 364.
8. Amnon Yariv, *Optical Electronics*, 4th Edition, (Holt, Reinhart and Winston, Inc., San Francisco, 1991), p. 369.

## **Chapter 2**

### **Theory I: Historical Approaches to Amplitude Noise Calculations**

#### **2.1 Historical Overview of Linear Amplification Noise**

The theory associated with laser amplification amplitude noise began with the studies of maser noise in 1957 with the work of Shimoda, Takahasi and Townes<sup>1</sup> (STT). They derived the photon statistics master equation for the simple case of linear amplification. It was based on the stochastic process of birth, death and immigration (BDI), a process which was well characterized for such studies as animal population evolution and cosmic ray showers. In the case of a laser/maser, birth is viewed as emission, death as absorption and immigration as that of a photon passing through the amplifier. Various authors since then have derived variants of the STT model where time dependence of the emission and absorption coefficients as well as some saturation phenomenon have been included. Authors have also looked at traveling wave configurations versus oscillator configurations and tried adjusting for spontaneous and stimulated emission processes to derive similar equations for oscillators. In all cases the basic idea of a population statistics approach for the interaction of the excited states and the photon population were retained. The original STT approach assumed a uniformly pumped laser medium, where all atomic coefficients were constant with length and unperturbed by the influx of photons from outside. Though not explicit, it was also assumed that light of a single optical longitudinal and transverse mode in a single polarization state was employed.

The STT approach used particle distributions which followed Bose-Einstein statistics (geometric distribution) i.e., a thermal but narrowband source. However, a coherent laser source with Poisson statistics<sup>2</sup> would result in a slightly different answer, though the procedure would be the same. Deviations from Poisson statistics at the exit point of the amplifier can be viewed as “excess noise” or the noise added to the photon stream by the amplifier. The STT calculations gave the

evolution of the probability of a particular number of photons existing at a particular time, or if visualizing a traveling wave amplifier this number equates to number of photons evolving with distance, so that a set of photon statistics at the exit of the amplifier could be derived. It was not clear that this technique could be used with oscillators because the recirculation of the photons would invariably result in a saturation effect down to a steady state value which their model could not calculate. Though their approach was to solve a partial differential rate equation in a classical sense, other methods have been developed which included quantum mechanical states. Their rate equation for the evolution of the photon number with time, or conversely with elapsed distance in a traveling wave amplifier, is as follows

$$dm/dt = (a - b)m + c$$

where:  $m$  is the total number of particles (photons)

$a$  is the probability of producing another particle--birth

$b$  is the probability of destroying the particle--death

$c$  is the rate of adding new particles--immigration.

Let  $m=n$  at  $t=0$  and the **classical** solution is

$$m = \left( n + \frac{c}{a-b} \right) \exp[(a-b)t] - \left( \frac{c}{a-b} \right).$$

However, since  $m$  must represent an integral number of particles, this equation needs to be revised to reflect the probability of a particular number of photons at a particular time. Probability is denoted by the term  $P_{n,m}$ , which is shorthand for "the probability of  $m$  particles at time  $t$  assuming  $n$  particles at  $t=0$ ". The functional dependence on time is dropped in the notation. The subsequent probabilistic representation of the change in the number of photons with time then becomes<sup>3</sup>

$$\frac{dP_{n,m}}{dt} = -[(a+b)m+c]P_{n,m} + [a(m-1)+c]P_{n,m-1} + b(m+1)P_{n,m+1}. \quad (2.1)$$

Hence the rate of change of the probability of a particular photon number is composed of the probabilities of the three system states, three “photon number states”, one in which there are  $m$ ,  $m+1$  or  $m-1$  photons. In these three states, different probabilistic processes can give  $m$  photon states. If one is in the  $m-1$  state, to get to the  $m$  state one has the possibility of adding a photon via birth (“a”) or by immigration (“c”). If one is in the  $m+1$  state, to get down to the  $m$  state, one needs to have one of the  $m+1$  photons die (“b”). Finally, to stay at the  $m$  state all the processes affecting the  $m$  state, birth, death and immigration must be accounted for. If there is no change in the probability of  $m$  photons existing at time  $t$ ,  $dP_{n,m}/dt = 0$ , then the first term will equal the sum of the second and third term, as it is assumed sub-probabilities can evolve with time but the total photon number probability is fixed. This equation is called the **photon statistics master equation** and is the foundation for most of the noise work that followed. From this equation the first and second moments for the photon number can be derived. As detailed earlier, these two moments contain the information needed to obtain the variance or noise expected on the photon stream. The solutions for the first two moments are<sup>4</sup>

$$\langle m \rangle = \left( \langle n \rangle + \frac{c}{a-b} \right) \exp[(a-b)t] - \frac{c}{a-b},$$

$$\langle m^2 \rangle = \left[ \langle n^2 \rangle - \frac{c(a-b)}{(a-b)^2} + \left( \langle n \rangle + \frac{c}{a-b} \right) \left( \frac{a+b+2c}{a-b} \right) \right] \exp(2(a-b)t) - \left( \langle n \rangle + \frac{c}{a-b} \right) \left( \frac{a+b+2c}{a-b} \right) \exp((a-b)t) + \frac{c(b+c)}{(a-b)^2}$$

Assume that  $a$ , the birth probability, is equivalent to the emission probability in the laser, which can be written as the emission cross section times the number of excited states,  $a = \sigma_e N_2$ , and  $b$  written as the absorption cross section times the unexcited states,  $b = \sigma_a N_1$ . In a fully inverted Nd:YAG amplifier,  $a \gg b$  because  $N_2 \gg N_1$ , due to the four level architecture of the lasing scheme, while the cross sections are comparable, due to the small degeneracy of the sublevels. Also, assume that the only immigration is from the spontaneous emission photon into the single spatial mode, this implies  $c=a$ . Letting

$G = \exp(a - b)t$ , and applying the foregoing assumptions, the moment equations can be simplified. The results are

$$\begin{aligned}\langle m \rangle &= (\langle n \rangle + 1)G - 1, \\ &\text{and} \\ \langle m^2 \rangle &= [\langle n^2 \rangle + 3\langle n \rangle + 2]G^2 - 3(\langle n \rangle + 1)G + 1.\end{aligned}$$

Now calculating the variance from these two moments using equation (1.3),  $\sigma^2 = \langle m^2 \rangle - \langle m \rangle^2$ , the noise power on the photon stream leaving the traveling wave amplifier will be

$$\sigma^2 = \sigma_0^2 G^2 + G(G - 1)(\langle n \rangle + 1), \quad (2.2)$$

where  $\sigma_0^2 = \langle n^2 \rangle - \langle n \rangle^2$  is the noise power on the photon stream entering the detector. These results are quite general because particular input photon statistics were not assumed. The output noise power will therefore be the input noise power increased by the amplifier gain and an additional term which is added by the amplifying medium. When the  $G=1$  or the material is passive, then the photon stream passes through the material unaffected. This is the case when traversing optical elements such as lenses in the beam train. When the amplifier is above the transparency gain threshold and  $G>1$  then the noise power increases. If the medium is below the transparency gain threshold, and  $G<1$ , then noise power still increases. This output noise power has not included any effects due to the photodetection process, it is only the noise power inherent in the optical amplification process. Other than introducing the requirement for discrete particles, this is a classical derivation using algebra and statistics alone. As a semi-classical derivation it will subsequently be shown to reduce to the quantum mechanically derived solution. Also note, if no photons enter the amplifier there is still a noise power output,  $\sigma^2 = G(G - 1)$ , which classically is not intuitive, but will be shown to be related to the amplified spontaneous emission, (ASE), and the ASE-ASE beat terms once a photodetection process takes place. Lastly, if the input photon stream obeys Poisson statistics, and  $\langle n \rangle$  is much larger than 1, and  $\langle n \rangle$  is also much larger than  $G(G-1)$ , then the semi-classical noise power equation takes on a simpler form given by

$$\sigma^2 = G(G-1) + G\langle n \rangle [2G-1],$$

which can be rewritten as

$$\sigma^2 = G\langle n \rangle [1 + 2(G-1)]. \quad (2.3)$$

Once a photodetection process takes place, this noise power equation will be shown to actually contain 4 terms: the shot noise term, the ASE-signal term, the ASE and the ASE-ASE term. Prior to photodetection the semi-classical noise power equation cannot really be interpreted in terms of observables. There is only a quantum mechanical interpretation.

In 1992, Diament and Teich<sup>5</sup>, in addition to providing a good summary of linear amplifier noise work up to that time, used the BDI approach to discuss the evolution of the statistical properties of photons as they passed through a linear traveling wave amplifier. In their model a single photon initiates its own BDI process rather than being represented by part of the immigration parameter. Their technique was aimed at the steady state laser amplifier used in a digital communications system's doped fiber amplifier where the input of photons is modeled as numbering in the tens to hundreds. Because the system was at steady state, the parameters for the BDI process were independent of time. They went on to prove that if the input is a Poisson distribution a noncentral-negative -binomial (Laguerre) distribution<sup>5</sup> will occur at the output. Their technique of using the PDF and PGF to solve the output distribution moments proved to be more useful for higher order moments needed for studying the digital SNR than the STT approach for solving the differential moment equations, as long as the number of photons did not exceed approximately 1000 and if particular input distributions were given which could simplify the calculations. However, for this study the number of photons is on the order of  $10^{15}$  to  $10^{18}$  which makes that technique difficult, unless perfect Poisson input distributions are assumed. Since the analog system noise in this study is easily modeled by the first two moments of the photon distributions, it proved easier to solve the differential equations using the STT approach.

In early 1962, Hugh Heffner<sup>6</sup>, of Stanford University's Ginzton Laboratory, added another chapter to the book of linear amplifier noise with his derivation of the fundamental amplifier noise limit from the Heisenberg uncertainty principle.

His approach was to assume an ideal noiseless linear amplifier (either a maser type or a parametric amplifier) and subsequently showed that it violated the uncertainty relation which exists between the photon number and their phase. He went on further to derive the minimum noise power associated with optical amplification<sup>6</sup>,

$$P_N = h\nu B(G - 1),$$

where B is the amplifier single sided optical bandwidth and G is the gain as defined above. This relation can also be rewritten to highlight the association of this minimum power with the ever present zero point energy of half a photon per Hz which comes about when the electromagnetic field is quantized

$$P_N = \frac{h\nu}{2T}(G - 1),$$

where T is the sample period. This result is applicable to this study as it sets the lower bound of noise power for the amplifiers.

Just a few months earlier, Louisell, Yariv and Siegman published their studies of quantum fluctuations and noise in parametric processes<sup>7</sup>. This was the first of many papers which took the quantum mechanical approach to the noise theory for the laser amplification process. Their results showed the same fractional noise power for a single frequency input as the STT theory. Though their work focused on very high gain parametric processes which are not discussed in this study, they set the stage for subsequent quantum mechanical noise work. A more general paper which encapsulated the results of STT and LYS and simultaneously produced Heffner's result appeared in late 1962. This paper, by Haus and Mullen<sup>8</sup>, also derived expressions for the noise figures, and the SNR. They showed that the minimum noise figure is 2 (i.e., 3 dB) under the condition that the quantum noise (uncertainty noise) is dominant and a linear amplifier of high gain is used<sup>8</sup>. In 1963, Glauber<sup>9</sup> laid down the mathematical formulation for coherent and in-coherent photon streams which when used with the density operator representing the amplification process, allowed a statistical distribution to represent the photon stream output. (The only caveat is that the number of photons in the system under consideration be much larger than 1.) This output distribution could be compared to the input distribution to determine the qualities of the variance or noise. This is the approach which will be used in the subsequent

derivation of the prediction for noise power from the linear and saturated amplifiers based on the quantum mechanical technique. It will be shown in Chapter 3 that the semi-classical and quantum mechanical results for the noise theory are compatible.

The first step in the quantum mechanical approach is to define the type of input photon stream. There are two approaches. The first approach is to define a pure photon number stream as the input. The advantage to this approach is a simplified mathematical picture. A pure photon number state is not realizable with conventional laser sources but may be created via squeezing. Basically, electromagnetic waves emanating from these sources do not contain a specific number of photons. The other approach is to define a statistical mixture of pure photon number states. In this case, a linear superposition of states has an associated probability distribution which indicates how much of each pure photon number state is present. Strictly speaking because the coherent states do not form an orthogonal set, the probability density cannot truly be associated with a particular coherent state. However, when the number of photons is large, the overlap between coherent states is minimal and the coherent states are essentially orthogonal, allowing the probability density formalism to be used.

For the coherent photonic streams emanating from a laser like the NPRO, the probability distribution is Poisson<sup>10</sup>. To keep track of all the elements of the statistical mixture a subscript and summation notation is needed which complicates the mathematics. It is therefore common to use the pure photon number state to calculate the output distributions and then generalize the results to the linear superposition which represents the coherent states. Once the input statistical distribution is determined the next step is to describe the density matrix operator detailing the evolution of the photon statistics as they pass through the amplifiers. It is important in this step to ensure that the diagonal elements represent the probability densities and the off diagonal elements are zero. This simplifies the math without sacrificing validity. With these modifications the derivation of the linear optical noise expression is completed using statistical methods to find the first and second moments. The optical noise expression is subsequently converted to linear electrical noise. Once in terms of electrical noise, the theoretical results are directly comparable to the experimental results of this study. This is done in section 3.1

## 2.2 Historical Overview of Saturated Amplification Noise Processes

The next logical step after determining the linear amplification noise power is to determine the saturated traveling wave (TW) amplifier noise power. This came about naturally with the desire to run high power laser amplifiers as oscillators in which saturation effects begin to appear. Work on saturation began with work by Sargent, Skully, and Lamb<sup>11</sup> (SSL) in 1967 and continued through Abraham<sup>12</sup> and Bendjaballah and Oliver<sup>13</sup> in 1980. More recently there was a great deal of interest in determining whether it was a good idea to optically pre-amplify signals in fiber optic transmission systems. These studies were driven by the fiber optic communications field which began to blossom in the 1980's and included two approaches. One approach was to look at the noise from semiconductor lasers<sup>14</sup> and the other was the fiber laser amplifiers<sup>15</sup>. Each of these approaches sheds some light on the problem of calculating noise in the solid state amplifier. However, in the case of the semiconductor systems some of the assumptions and physical processes do not apply because the electron interactions in the active material are not applicable to Nd:YAG and in the case of the Er fiber laser, the lasing scheme is for a three level system versus the four level Nd:YAG. Nevertheless, the techniques, when modified, prove very germane to this study. Another simplification provided by the 4-level Nd:YAG system is there is no need to model saturation effects in the lower state because the population of this state is practically zero, due to the fast decay to the ground level. This allows the earlier and simplified saturation models to be used.

In all saturation studies, beginning with (SSL), the approach is to multiply the photon numbers by an additional term whose denominator is of the form  $(1 + sn_{\text{sat}})$ . "s" is called the saturation parameter and is also often annotated as  $s = 1/n_{\text{sat}}$ , where  $n_{\text{sat}}$  is defined as the number of photons for which the  $sn_{\text{sat}}$  term becomes 1. This technique is used in models of saturation of gain in laser amplifiers.

Saturation effects are responsible for the decrease in spontaneous emission which lowers the noise one expects from the non-linear amplifier and was succinctly derived by Abraham<sup>16</sup>. Abraham also derived a simple semi-classical approach for determining the decrease in the noise using normalized second and third order moments but it is valid only up to 10% saturation, due to the use of a truncated power series approximation. He additionally derived a modified

probability density matrix term following SSL which could be used to show at what rate the noise **decreases** with length in an amplifier at a particular saturation, but only under limiting cases. One limiting case was the linear case, for which we already have the theoretical noise expression, (see the section immediately preceding this one), one was for saturation onset, i.e., <10% and the third was for traveling photon distributions which are in completely saturated mediums and hence see no gain. By qualitatively piecing together the results, the evolution of a coherent signal, according to Abraham should follow this pattern. Initially the Poisson distribution is mixed with ASE which broadens the distribution, i.e., makes it noisier, then as saturation sets in, the distribution narrows, returning to the Poisson distribution with a different mean corresponding to the mean of the amplified signal.

The saturated noise problem is a difficult one and numerical solutions have been attempted. Oliver and Bendjaballah<sup>17</sup> completed an exact numerical integration of the probability density equations in August 1980 which used a limited parameter set (number of particles (1000) modeled, number of moments calculated (2) and a coherent input field), yet it also showed that the laser noise initially increased with saturation, becoming greatest with modest saturation, then decreased to a constant at complete saturation, reinforcing the Abraham finding.

For approximately seven years these findings were neither challenged nor improved upon. In 1987 additional higher order moments were calculated by Ruiz-Moreno et. al.<sup>18</sup> (RJS) based on improvements in computer platforms. These higher order moments were needed to calculate bit error rate (BER) in digital communications and the theory was modified to fit semiconductor lasers. In section 3.2, the basic solution methodology of RJS is used but is modified to fit the Nd:YAG system.

### **2.3 Historical Overview of Oscillator Amplitude Noise**

The third and final system of interest to this study is the laser oscillator. As indicated in the introduction and initial background of noise studies, the noise of a laser depends very much on its configuration. Gas, solid state and semiconductor lasers have all been found to have unique noise properties. It is necessary to understand the amplitude noise of these systems because they will probably seed the amplifiers already discussed or as has been discovered recently, they may have some particularly useful amplitude noise characteristics of their own.

There are numerous difficulties in attempting to generate vast quantities of perfectly coherent photons to attain the lowest noise solution, or in other words generating the highest powered, narrowest line width optical outputs. The ultimate noise trade off will be found in choosing the balance of amplitude and phase noise which is bounded by the spectral Heisenberg relation. Since the phase noise ultimately sets the natural linewidth, the lowest theoretical amplitude noise can also be determined. In what follows, a brief overview of noise studies on oscillators is given with the intent of then focusing solely on the amplitude noise properties of injection locked oscillators for high power applications in section 3.4.

The oscillator amplitude noise studies historically began with the maser and the van der Pol negative conductance oscillators in the RF frequency spectrum and evolved to the higher frequencies associated with the laser. The initial efforts to determine noise used a simple and intuitive method based on modeling an oscillating (RLC) electrical circuit with internal and external noise inputs. An example of this approach was provided by Nilsson, Yamamoto and Machinda in 1986.<sup>19</sup> Their model did not relate to any particular laser structure so care had to be taken when comparing the outputs of the model to actual laser systems. Subsequent work derived a model for an injection locked system. However, to obtain a theoretical expression to compare to actual observables, the noise spectrum of the pump source, in the case of this experiment, the diode laser arrays, must be known. A simplified calculation for the injection locked DPSSL system using this technique is included in section 3.4. This method of determining oscillator noise will be denoted the RLC approach throughout this study.

The second approach to evaluating noise in laser oscillators followed from the photon statistic rate equations technique used so successfully in evaluating the noise in the traveling wave amplifiers, denoted here as the STT approach. Basically, the STT method is used and the birth, death and immigration parameters are modified to obtain the appropriate coefficients for the recursive systems. This approach was attempted by Yamamoto<sup>20</sup> and Goldstein and Teich<sup>21</sup>. The Yamamoto recursive solution was derived by considering the effects a simple Fabry Perot (FP) cavity would have on the standard STT traveling wave solution. This work relied heavily on taking the original forms of the STT solution for the linear case and rewriting the gain portions to reflect the effects of phase lag imposed by the boundary conditions of an oscillator system.

Taking the formalism of the STT approach and following Yamamoto's modifications, the basic form of the noise equation for the oscillator do not change

compared to the traveling wave amplifier amplitude noise equations found in sections 3.1 (linear) and 3.3 (saturated or non-linear). This assumes once again a large number of Poisson distributed photons in a single mode arriving at the entrance to the FP cavity. The change in the noise equation occurs in the representation of the gain term. Interestingly enough, in representing the Yamamoto equations in the same format as the linear and non-linear cases derived above and in Chapter 3, it is found that the FP cavity amplifier will produce lower or equivalent noise. This can be seen from the following calculations. Taking the total cavity gain from Yamamoto's paper given by

$$G_c = \frac{(1-R_1)(1-R_2)G}{(1-\sqrt{R_1 R_2} G)^2},$$

where  $G$  is equal to the single pass gain, and the equations for the average output number of photons and the variance (noise )

$$\begin{aligned} \langle n_1 \rangle &= G_c \langle n_0 \rangle \\ \sigma^2 &= G_c \langle n_0 \rangle + 2 \frac{(1+R_1 G)(1-R_1)(1-R_2)^2 (G-1)G}{(1-\sqrt{R_1 R_2} G)^4}, \end{aligned} \quad (2.4)$$

it is possible to rewrite the variance equation in the form

$$\sigma^2 = G_c \langle n_0 \rangle (1 + 2(G_c - 1 - X)),$$

$$\text{where } X = R_1 \frac{\left(G - \sqrt{\frac{R_2}{R_1}}\right)^2}{(1-\sqrt{R_1 R_2} G)^2}.$$

It is apparent that "X" is always positive. This implies that for a given single pass gain it is possible that the FP resonator with amplifying medium could have a lower noise than its traveling wave counterpart. In Appendix 6 there is a Mathcad document displaying these results graphically. It appears there is a possibility of improved noise performance when the single pass gain is between 1

and 2 and the mirror reflectivities of the FP are dissimilar and low. However, this low a gain may not be useful in LIGO power amplifier configurations.

A third approach for calculating the noise behavior of an oscillator is a hybrid of the STT rate equation approach and the RLC approach. It was derived by Farinas et al.<sup>22</sup> and uses the concept of the system transfer function to model the injection locked oscillator amplitude and frequency noise spectrum. Since this approach does not deal with pure oscillators it will not be explained here but rather in section 3.4. Results from the transfer function approach (TFA) can be directly compared to the RLC approach as they are both semi-classical approaches solved with nearly steady state conditions. They will also be compared to the next and final approach for discussing oscillator noise, the Quantum Langevin Approach (QLA).

The last and most complex oscillator noise modeling approach is the full quantum mechanical treatment using the Langevin equations and modeling the effects the evolution of internal and external noise reservoirs have on the laser. A seminal paper in this area was published by Yamamoto and Imoto in 1986<sup>23</sup>. However, there was a difficulty in modeling the evolution of the noise reservoirs themselves. More recently, the QLA approach has been simplified and applied directly to injection locked lasers by Ralph et. al.<sup>24</sup> By using a linearized analysis they were able to derive amplitude noise properties of the injection locked system in a broader frequency range than the previous approaches. A more complete discussion of their efforts and the comparisons of the RLC, TFA and QLA amplitude noise modeling for the injection locked lasers is found in section 3.4.

## Chapter 2 References

1. K. Shimoda, H. Takahasi, and C.H. Townes, "Fluctuations in Amplification of Quanta with Application to Maser Amplifiers", *Journal of the Physical Society of Japan*, Vol. 12, No. 6, p. 686 (1957).
2. E. Dereniak and D.Crowe, *Optical Radiation Detectors*, (Wiley, New York 1984) p.18.
3. K. Shimoda, H. Takahasi, and C.H. Townes, "Fluctuations in Amplification of Quanta with Application to Maser Amplifiers", *Journal of the Physical Society of Japan*, Vol. 12, No. 6, p. 687 (1957).
4. K. Shimoda, H. Takahasi, and C.H. Townes, "Fluctuations in Amplification of Quanta with Application to Maser Amplifiers", *Journal of the Physical Society of Japan*, Vol. 12, No. 6, p. 689 (1957).
5. P. Diament, and M. Teich, "Evolution of the Statistical Properties of Photons Passed Through a Traveling-Wave Laser Amplifier", *JQE*, Vol. 28, No. 5, p. 1331 (1992).
6. H. Heffner, "The Fundamental Noise Limit of Linear Amplifiers", *Proceedings of the IRE*, p. 1607 (1962).
7. W.H. Louisell, A.Yariv, A.E. Siegman, "Quantum Fluctuations and Noise in Parametric Processes, I", *Phys. Rev.*, Vol. 124, No. 6, p. 1646 (1961).
8. H. Haus, and J.A. Mullen, "Quantum noise in linear amplifiers," *Phys. Rev.*, Vol. 128, No. 5, p. 2412 (1962).
9. R.J. Glauber, "Coherent and Incoherent States of the Radiation Field", *Physical Review*, Vol. 131, No. 6, p. 2766 (1963).
10. R.J. Glauber, "Coherent and Incoherent States of the Radiation Field", *Physical Review*, Vol. 131, No. 6, p. 2769 (1963).
11. M. Sargent, M.O. Skully, and W.E. Lamb, "Buildup of Laser Oscillations from Quantum Noise", *Applied Optics*, Vol. 9, No. 11, p. 2423 (1970).

12. N.B. Abraham, "Quantum theory of a saturable amplifier", *Physical Review A*, Vol. 21, No. 5, p. 1595 (1980).
13. C. Bendjaballah, and G. Oliver, "Detection of Coherent Light after Nonlinear Amplification", *IEEE Transactions on Aerospace and Electronic Systems*, Vol. AES-17, No. 5, p. 620 (1981).
14. Y. Yamamoto, "Noise and Error Rate Performance of Semiconductor Laser Amplifiers in PCM-IM Optical Transmission Systems", *IEEE Journal of Quantum Electronics*, Vol. 16, No. 10, p. 1073 (1980).
15. E. Desurvire, *Erbium Doped Fiber Amplifiers*, (Wiley and Sons, New York, 1994).
16. N.B. Abraham, "Quantum theory of a saturable amplifier", *Physical Review A*, Vol. 21, No. 5, p. 1595 (1980).
17. G. Oliver, and C. Bendjaballah, "Statistical Properties of Coherent Radiation in a Nonlinear Optical Amplifier", *Physical Review A*, Vol. 22, No. 2, p. 630 (1980).
18. S. Ruiz-Moreno, G. Junyent, M.J. Soneira, and J.R. Usandizaga, "Statistical Analysis of Nonlinear Optical Amplifier in High Saturation", *IEE Proceedings*, Vol. 135, Pt. J, No. 1, p. 34 (1988).
19. O. Nilsson, Y. Yamamoto, and S. Machinda, "Internal and External Field Fluctuations of a Laser Oscillator: Part II - Electrical Circuit Theory", *JQE*, Vol. 22, No.10, p. 2043 (1986).
20. Y. Yamamoto, "Noise and Error Rate Performance of Semiconductor Laser Amplifiers in PCM-IM Optical Transmission Systems", *IEEE Journal of Quantum Electronics*, Vol. 16, No. 10, p. 1073 (1980).
21. E. Goldstein and M. Teich, "Noise in Resonant Optical Amplifiers of General Resonator Configuration", *IEEE Journal of Quantum Electronics*, Vol. 25, No. 11, p. 2289 (1989).
22. A. Farinas, E. Gustafson, and R. Byer, "Frequency and Intensity noise in an Injection-Locked, Solid-State Laser", *Journal of the Optical Society of America B*, Vol. 12, No. 2, p. 328 (1995).

23. Y. Yamamoto, and N. Imoto, "Internal and External Field Fluctuations of a Laser Oscillator: Part I - Quantum Mechanical Langevin Treatment", JQE, Vol. 22, No.10, p. 2032 (1995).

24. T. Ralph, C. Harb and H. Bachor, "Intensity Noise of Injection Locked Lasers: Quantum Theory Using a Linearized Input-Output Method", Physical Review A, Vol. 54, No. 5, p. 4359 (1996).

## Chapter 3

### Theory II: Derivation of Theoretical Expressions for Laser Amplitude Noise

#### 3.1 Linear Amplifier Amplitude Noise

Following upon the comments made in the historical overview to the linear amplifier noise processes, the following assumptions will be used in the calculation:

- pure photon number states will be used to simplify the mathematics (though the experiment did not use these pure states);
- single optical mode is assumed throughout (single transverse, longitudinal and polarization singled out by the NPRO probe beam);
- the interaction Hamiltonian is dominated by the electric dipole interaction (which is true for most visible strong transitions in materials);
- the atomic dipoles are aligned with the interacting field (again simplifying the calculation);
- only two atomic states are considered:  $|1\rangle$ , the ground state and  $|2\rangle$ , the excited state;
- transitions only involve the emission or absorption of one photon in a single optical mode.

Any or all of these assumptions can be foregone for a more in-depth analysis. However, doing so will not change the qualitative aspects of the outcome. It will only raise the precision of absolute measurements which experimentally are difficult to make.

The calculation proceeds with the emphasis on the number of photons in the photonic stream and how the probability density for these photon number states changes versus the more standard approach of viewing the atomic transition probability as the item of interest. Hence all probabilities will apply to the photon number states. Using the Loudon<sup>1</sup> notation, the first step is to specify the

interaction Hamiltonian, which is the second quantized electric dipole Hamiltonian given by

$$\hat{H}_{ED} = \hat{a} \exp(-i\omega t) |2\rangle\langle 1| - \hat{a}^\dagger \exp(i\omega t) |1\rangle\langle 2|$$

where  $\hat{a}|n\rangle = \sqrt{n}|n-1\rangle$ , and  $\hat{a}^\dagger|n\rangle = \sqrt{n+1}|n+1\rangle$  are the lowering and raising operators. The matrix element for photon absorption is:  $\langle n-1, 2 | \hat{H}_{ED} | n, 1 \rangle = \sqrt{n} \exp(-i\omega t)$ , and the matrix element for photon emission is:  $\langle n+1, 1 | \hat{H}_{ED} | n, 2 \rangle = \sqrt{n+1} \exp(i\omega t)$ . The rate at which the photons are emitted or absorbed goes as the absolute square of the matrix element<sup>2</sup>, which leaves for the absorption a rate proportional to  $n$  and for emission a rate which is proportional to  $n+1$ . This rate is directly converted to a probability by assuming that the interaction time has occurred and the atom has either jumped to the upper state and absorbed a photon or gone to the lower state and emitted a photon. Basically, "transition rate to final state"  $\times t =$  "probability of final state at time  $t$ ".

Now that the probabilities of the absorption and emission of the photons are known, it is possible to compose the complete probability that a system will have  $n$  photons after any interaction. Since the system can only go up or down by one photon at a time, there are only three levels or pure photon states which are needed to specify the probability  $P_n$  of a specific photon number  $n$ , after an interaction:  $|n\rangle$ ,  $|n+1\rangle$  and  $|n-1\rangle$ . The probability of a final state will be equal to the probability of each of the initial states times the probability of the appropriate transition. Figure 4 shows a diagram to help clarify the derivation of the total probability from the component probabilities.

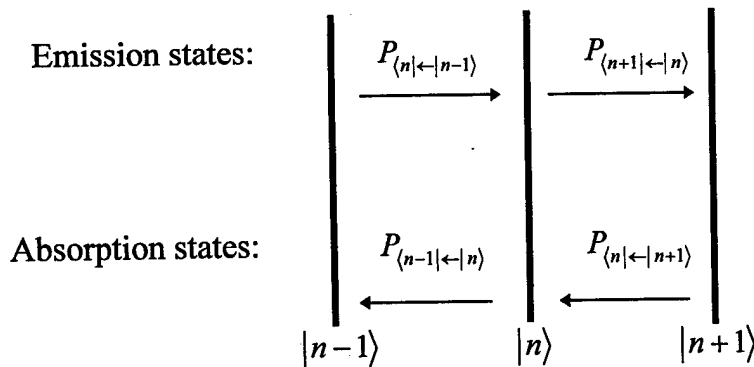


Figure 4. Probability Representation of Photon States versus Photon States

The photon number states are listed across the bottom of Figure 4 and the probability of being in one of these states prior to an interaction is:  $P_x$  where  $x$  can be  $n-1$ ,  $n$ ,  $n+1$ . By taking these initial state probabilities and multiplying by the appropriate term for the emission or absorption interaction the following four terms result

Absorption :

$$P_{(n-1|\leftarrow|n)} = n P_n \quad (3.1)$$

$$P_{(n|\leftarrow|n+1)} = (n+1) P_{n+1} \quad (3.2)$$

Emission :

$$P_{(n|\leftarrow|n-1)} = n P_{n-1} \quad (3.3)$$

$$P_{(n+1|\leftarrow|n)} = (n+1) P_n \quad (3.4)$$

To compose the equation which represents the change in the probability of a particular photon number state,  $dP_n$ , as the photon stream propagates through the amplifier, requires additional steps. The change in the probability will depend on the four terms (3.1 - 3.4) but it will also depend on the absorption and emission cross sections and how many atoms are in each of the two states,  $N_1$  and  $N_2$ . Using the notation from the semi-classical STT derivation where  $a = \sigma_e N_2$  and  $b = \sigma_a N_1$ , the photon number probability will evolve with distance,  $dz$ , as

$$dP_n = \{-bnP_n + anP_{n-1} + b(n+1)P_{n+1} - a(n+1)P_n\}dz.$$

The processes which move the photon number away from  $|n\rangle$  are given (-) and the processes which move the photon number towards  $|n\rangle$  are given (+). This equation can in turn be written in the more recognizable form

$$\frac{dP_n}{dz} = a\{nP_{n-1} - (n+1)P_n\} + b\{(n+1)P_{n+1} - nP_n\}. \quad (3.5)$$

This will be called the QM photon statistics master equation.

There are two approaches to solving for the first two moments of the photon number based on the probability density function. One approach follows the algebraic and differential equation solution method used by STT and by Sargent, Scully and Lamb<sup>3</sup>, (SSL) and the other approach uses the more general probability generating function used by Diamant and Teich<sup>4</sup>. The SSL approach is to start with the moment distribution

$$\langle n^k \rangle = \sum_{n=0}^{\infty} n^k P_n ,$$

then apply the derivative and shift it inside the summation

$$\frac{d}{dz} \langle n^k \rangle = \sum_{n=0}^{\infty} n^k \frac{d}{dz} P_n .$$

For the first moment or average photon number

$$\frac{d}{dz} \langle n \rangle = \sum_{n=0}^{\infty} n [ a \{ n P_{n-1} - (n+1) P_n \} + b \{ (n+1) P_{n+1} - n P_n \} ] .$$

Multiplying through by  $n$  and adjusting the summations and indices so that only  $P_n$  terms are left, gives

$$\frac{d}{dz} \langle n \rangle = \sum_{n=0}^{\infty} [ a \{ n+1 \} - b \{ n \} ] P_n ,$$

or substituting for the expectation of  $n$

$$\frac{d}{dz} \langle n \rangle = (a - b) \langle n \rangle + a .$$

At  $z = 0$ ,  $\langle n \rangle = \langle n(0) \rangle$  and assuming  $a$  and  $b$  are not functions of position in the amplifier, gives a solution for the average photon number at the output of the amplifier

$$\langle n \rangle = G \langle n_0 \rangle + A , \tag{3.6}$$

where  $G = \exp(a-b)z$  and  $A = a(G-1)/(a-b)$ . From this it is easy to see that the  $A$  represents an additional number of photons--the amplification spontaneous noise and it is present whether photons enter the amplifier or not. It is also apparent that the amplified spontaneous noise is lowest when  $b$  is zero, or when  $N_1$ , the ground state population, is zero. This occurs when the amplification medium is fully inverted--something which was easy to attain with the 4 level Nd:YAG solid state slab amplifiers used in this experiment.

The second moment is obtained using a similar procedure

$$\langle n^2 \rangle = G^2 \langle n^2(0) \rangle + 3G(G-1) \langle n(0) \rangle + 2N^2 + N, \quad (3.7)$$

where in addition at  $z = 0$ ,  $\langle n^2 \rangle = \langle n^2(0) \rangle$ . To obtain the optical noise power leaving the amplifier,  $\sigma_n^2 = \langle n^2 \rangle - \langle n \rangle^2$ , substitute the moments from equation (3.6) and (3.7) and algebraically manipulate the results. This leaves

$$\sigma_n^2 = G^2(\sigma_0^2 - \langle n(0) \rangle) + G \langle n(0) \rangle + 2GN \langle n(0) \rangle + N^2 + N, \quad (3.8)$$

where  $\sigma_0^2 = \langle n(0)^2 \rangle - \langle n(0) \rangle^2$ . It is common to highlight the 'classical' interpretation of these quantum mechanically derived optical noise power terms, a trend which began with Yamamoto<sup>5</sup>. Often the term "beat" is used to describe some of the terms in equation (3.8) as the photodetection process downstream from the amplifier squares the field amplitudes and results in mixed "beat" terms. This is strictly speaking not what this equation indicates, but one can assume a perfect detector is being used at this point and proceed with the beat analogy.

The first term in equation (3.8) represents the noise power added by the amplifier, over and above the noise of the input optical stream. It corresponds to the "excess" noise spoken of earlier. The second and last terms represent the photons which would fall on the detector and give the DC current shot noise. Hence, they are called the shot noise component. Term three is the beat noise between the signal and the spontaneous emission and the fourth term is the beat noise between the spontaneous emission and itself. To reiterate, at this point no photodetection process has occurred and no assumption was made regarding the

input photon statistics. This equation represents the photon stream statistics after the photons have interacted with a linear amplifier.

The next steps are to point out the qualitative aspects of the noise power equation (3.8) which might be observed in the experimental setting. If the device is passive,  $G=1$  then the input noise, regardless of the input statistics, equals the output noise. Hence, Poisson statistics or Bose-Einstein statistics are preserved when light is passing through a passive device. If the input stream obeys Poisson statistics and there are a large number of photons, the noise power equation (3.8) at the output of the amplifier can be rewritten as

$$\sigma_n^2 = G\langle n(0) \rangle [1 + 2(G - 1)], \quad (3.9)$$

and  $A = G-1$  has been used, assuming full inversion. There is no excess noise to deal with. However, if the input stream is Bose-Einstein, as ASE is expected to be, the excess noise does not cancel, using equation (1.6), but makes a substantial contribution to the overall noise. Note also, this full quantum theory derivation, equation (3.8), gives the same results as the semi-classical theory, equation (2.2), for absorption and stimulated emission and adds the information corresponding to the spontaneous emission. Probability generating functions can also be used to arrive at these results as mentioned earlier<sup>6</sup>. The mathematical foundations of PGFs give a far more general result and can extend to even higher moments, but they are limited by the computation time required for higher photon fluence.

A slight modification to the single mode noise power expression yields multiple mode noise power estimates. For example, if multiple transverse modes are needed to compose a square top or super Gaussian profile, which would be of interest in amplifier chaining for a higher powered LIGO laser system, Desurvire has calculated the effects of multiple modes as they effect fiber systems and found the noise equation<sup>7</sup>

$$\sigma_n^2 = G^2 (\sigma_0^2 - \langle n(0) \rangle) + G\langle n(0) \rangle + 2GA\langle n(0) \rangle + MA^2 + MA,$$

where  $M =$  the number of modes. As long as the number of modes is not a substantial fraction of the number of photons entering the amplifier the effects of the additional modes are negligible. This is the case for LIGO applications. From this point on only the single mode calculation will appear.

It is now appropriate to bring the theoretical results in line with the experimental processes by introducing the effects of the propagation and detection process on the noise power of a photon stream after the amplifier. The photon stream will experience loss as it propagates to the detector. The detection process of converting the photons to photoelectrons will be imperfect and the receiver will add additional noise power.

In this experiment the receiver was designed to add insignificant noise power to the photoelectron stream, leaving the loss processes as the major modification to the photon and hence photoelectron stream statistics. The key concept is the Bernoulli random deletion process occurring in the passive elements and the detector. This deletion process can represent the effects of channel loss through scatter or absorption and the imperfect conversion of photons to photoelectrons. However, the Bernoulli process maintains the form of the photon stream statistics<sup>8</sup>. By maintaining the form of the photon statistics through these elements, linear multipliers called efficiency factors appear in the first and second moments of the output statistical distributions and hence in the noise power representation (the variance).

Since the form of the photon statistics remains the same and only multiplicative efficiency factors are needed to account for the absolute changes in the photon statistics, this allows a matrix to represent the transfer of the photon statistics across a given element. The transfer matrix can be derived from the first two derivatives of the PGF evaluated at the lowest order z transform component<sup>9</sup>. The efficiency factors,  $\eta$ 's, factor out of the differentials of the PGF. It takes only a few steps to rearrange the results into a linear superposition of the average photon number and the variance.

The average photon number and the variance then compose a two element vector which when operated on by the transfer matrix, describes the change of those two quantities as they traverse the optical component represented by the matrix. The results are

$$\langle n_{out} \rangle = \langle n_{in} \rangle \eta$$

$$\sigma_{out}^2 = \langle n_{in} \rangle \eta (1 - \eta) + \sigma_{in}^2 \eta^2$$

where the subscripts refer to the input and output statistics for the single optical element with transmission efficiency,  $\eta$ . These vector representations can be

summarized compactly, just as ABCD matrix representations are compact representations for photon beam or ray calculations through a beam line. The transfer matrix is given by

$$\hat{D} = \begin{pmatrix} \eta & 0 \\ \eta - \eta^2 & \eta \end{pmatrix}.$$

The output statistics, in general, are given by

$$\begin{pmatrix} \langle n_{out} \rangle \\ \sigma_{out}^2 \end{pmatrix} = \hat{D} \begin{pmatrix} \langle n_{in} \rangle \\ \sigma_{in}^2 \end{pmatrix}.$$

With this handy tool it is now possible to write the form the photoelectron noise power expression will take, given an actual experimental apparatus. In the experiments conducted in this study both single and double pass amplifier set ups were used, but for simplicity the single pass photoelectron noise power will be derived first. For a single pass situation a block diagram details the efficiencies as follows

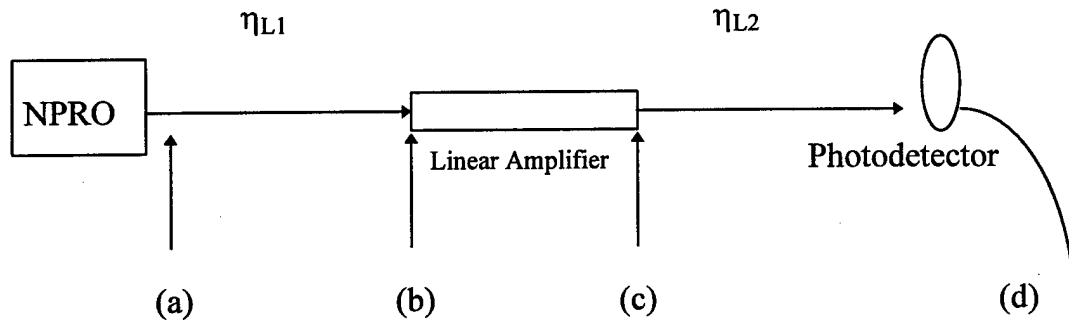


**Figure 5. Diagram of Noise Propagation through an Amplifier System under Test. The letters indicate measurement reference planes for amplitude noise.**

At point (a), the output of the NPRO is a stream of Poisson distributed photons, with statistical vector,  $[\langle n_a \rangle, \sigma_a^2] = [\langle n \rangle, \langle n \rangle]$ , where subscripts denote the locational letter and  $\langle n \rangle$  is the average value of photons leaving the NPRO. This photon stream will experience a reflective loss or clipping upon entry to the amplifier material and possibly passive loss in the channel which will result in another statistical vector at (b),  $[\langle n_b \rangle, \sigma_b^2] = \eta_{L1} [\langle n \rangle, \langle n \rangle]$  where L1 represents optical

path leg 1. In the amplifier the photons experience gain and upon exit, (c), they will have a statistical vector  $[\langle n_c \rangle, \sigma_c^2] = [\eta_{L1} G \langle n \rangle, \langle n_c \rangle [1 + 2(G - 1)]]$ . There is loss in the optical channel and at the cover glass of the detector, which leads to a transmission efficiency,  $\eta_{L2}$ . Finally there is an attenuation caused by a less than perfect quantum conversion efficiency,  $\eta_d$ , (assuming no detector effects due to bandwidth limitations), which leaves a statistical vector at (d) that can be represented by the linear vector equation

$$\begin{bmatrix} \langle n_d \rangle \\ \sigma_d^2 \end{bmatrix} = \eta_d \begin{bmatrix} 1 & 0 \\ 1 - \eta_d & 1 \end{bmatrix} \eta_{L2} \begin{bmatrix} 1 & 0 \\ 1 - \eta_{L2} & 1 \end{bmatrix} \begin{bmatrix} \langle n_c \rangle \\ \sigma_c^2 \end{bmatrix}.$$

This gives a photoelectron noise power of

$$\sigma_d^2 = \eta_{tot} G \langle n \rangle (1 + 2(G - 1) \eta_{L2} \eta_d),$$

with  $\eta_{tot} = \eta_{L1} \eta_{L2} \eta_d$  or

$$\sigma_d^2 = \sigma_{shot}^2 (1 + 2(G - 1) \eta), \quad (3.10)$$

where  $\eta_{tot} G \langle n \rangle$  represents the shot noise contribution and  $\eta = \eta_{L2} \eta_d$ . This expression shows that the excess noise due to the amplification process is seen as a multiplier of the shot noise. Once a photocurrent is established in an experiment, the shot noise level is also established and the excess noise measurements can then be made relative to that level. Data can then be represented in terms of 'shot noise units' above the theoretically perfect shot noise floor and with a linear dependency. No absolute measurements are required.

A theoretical plot of the linear amplifier amplitude noise, Equation 3.10, in shot noise units, expected for different  $\eta_{L2}$  efficiency values, is found in Figure 6. In Figure 6 the detector quantum efficiency,  $\eta_q$  was set to 0.4 and the optical efficiency after the amplifier,  $\eta_{L2}$ , was varied between 0.1 and 0.9. The slopes of the lines are directly related to the efficiency values. As expected, the higher efficiencies show the steepest slopes and the largest noise values.

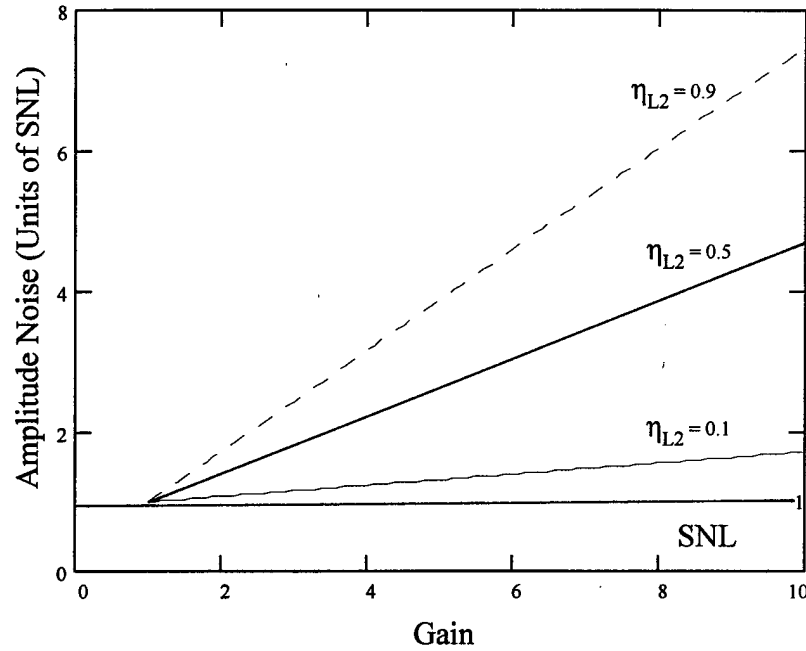


**Figure 6. Linear Amplifier Amplitude Noise versus Gain, Equation 3.10, for three different  $\eta_{L2}$  values (0.1, 0.5, 0.9). As the efficiency increases the amplitude noise increases. The shot noise level at the input to the detector is labeled for reference.**

The linear amplifier amplitude noise characteristics can also be depicted using the earlier defined optical  $SNR_o$ , the optical noise figure or the Fano Factor. Comparing the photon stream SNR just before the amplifier,

$$SNR_{in} = \frac{\langle n_b \rangle^2}{\sigma_b^2} = \eta_{L1} \langle n \rangle,$$

to the photon stream SNR just after the amplifier,

$$SNR_{out} = \frac{\langle n_c \rangle^2}{\sigma_c^2} = \frac{(\eta_{L1} G \langle n \rangle)^2}{\eta_{L1} G \langle n \rangle (1 + 2(G - 1))}$$

will give a noise figure

$$NF = 10 \times \log\left(\frac{SNR_m}{SNR_{out}}\right) = 10 \times \log\left(\frac{1+2(G-1)}{G}\right). \quad (3.11)$$

Notice that the efficiency is eliminated from the expression. The plot of the NF is found in Figure 7.

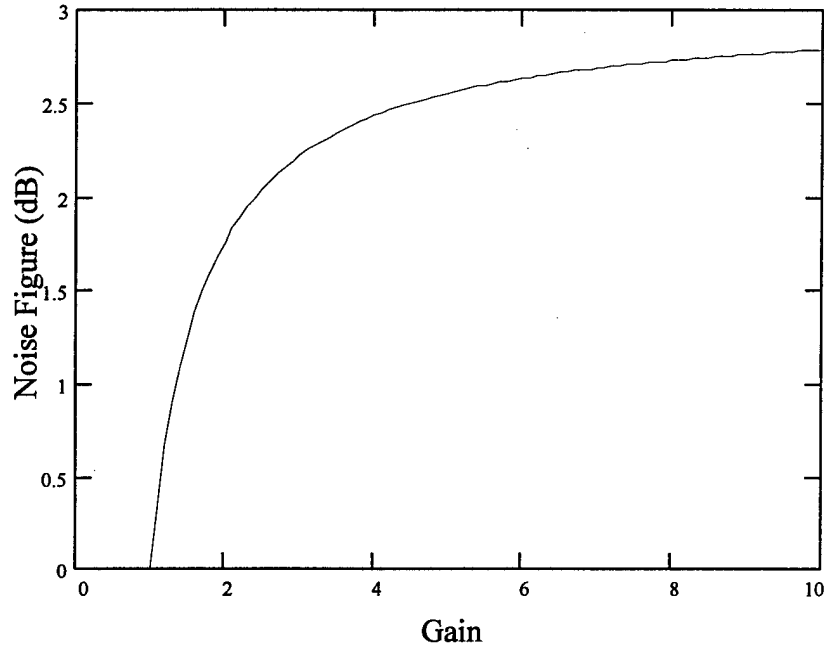


**Figure 7. Linear Amplifier Amplitude Noise Figure versus Gain, Equation 3.11.**

The Fano Factor, in linear units, is:

$$f = \frac{\sigma_d^2}{\langle n_d \rangle} = 1 + 2(G-1)\eta$$

and is the same form as Equation 3.10 plotted in Figure 6.

Lastly, what type of noise figure could be expected at the detector? The noise figure will now be composed of the SNR prior to the amplifier

$$SNR_m = \frac{\langle n_b \rangle^2}{\sigma_b^2} = \eta_{L1} \langle n \rangle$$

and the SNR at the detector

$$SNR_d = \left( \frac{\langle n_d \rangle^2}{\sigma_d^2} \right) = \left( \frac{G \eta_{tot} \langle n \rangle}{1 + 2(G-1)\eta_{L2}\eta_q} \right),$$

giving

$$NF_d = 10 \times \log \left( \frac{SNR_m}{SNR_d} \right) = 10 \times \log \left( \frac{1 + 2(G-1)\eta_{L2}\eta_q}{\eta_{L2}\eta_q G} \right). \quad (3.12)$$

This noise figure is plotted for different values of  $\eta_{L2}$  in Figure 8.

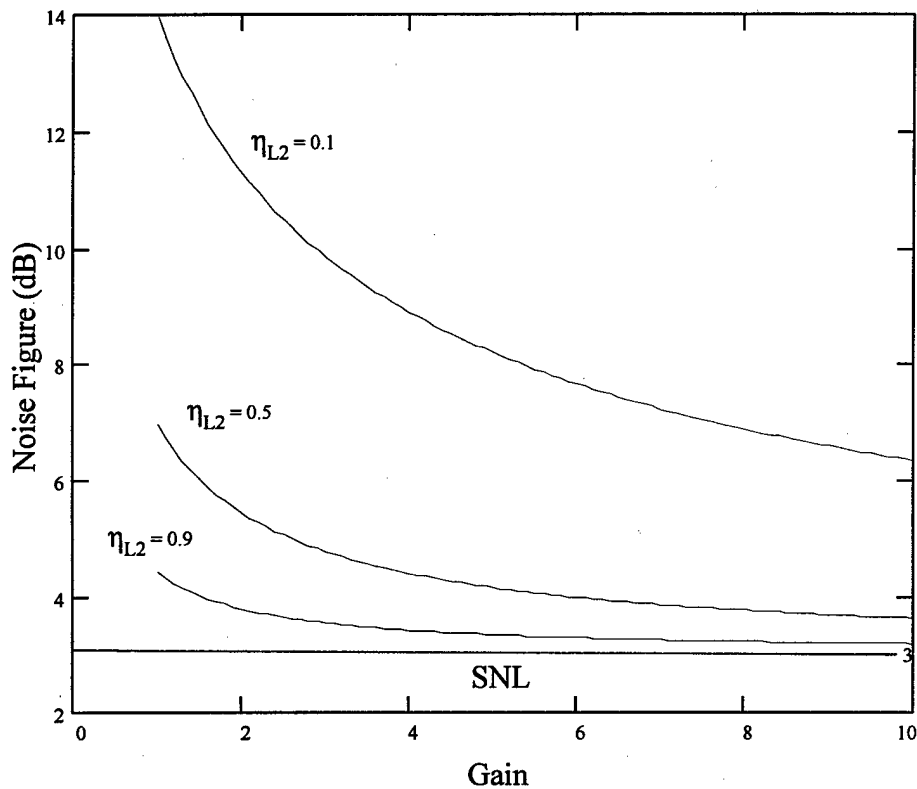


**Figure 8.** Noise Figure referenced to the detector for different values of optical efficiency between the amplifier and the detector, Equation 3.12. The NF for a perfect amplifier is drawn at 3 dB for reference.

Notice that the greater the attenuation in the path between the amplifier and the detector, for the same photocurrent, the higher the noise figure. Higher noise figures indicate that more noise is being added to the photon stream by amplification. So the most desired situation is to have as little attenuation as

possible after the amplifier. Figure 8 also graphically illustrates that optical amplifiers can never improve SNR. It also shows that even though attenuation does not change the Poisson statistics of the photon stream, it does degrade the SNR.

For a double pass amplifier the results will be derived in a similar manner but with a gain factor for each amplifier and more loss factors for the additional legs. The block diagram is

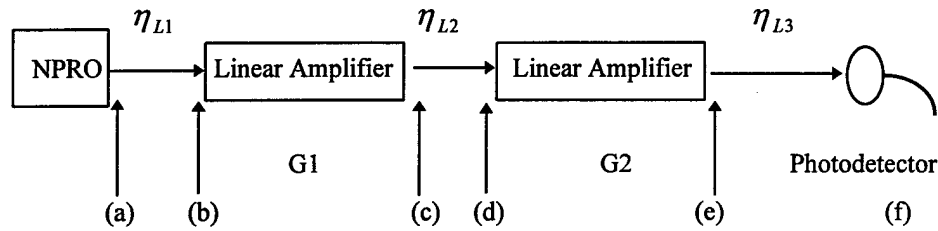


**Figure 9. Double Pass Amplifier Block Diagram**

and its noise equation is

$$\sigma_f^2 = \sigma_{shot}^2 \{1 + 2(G_2 - 1)\eta_{L3}\eta_d + 2(G_1 - 1)G_2\eta_{L2}\eta_{L3}\eta_d\}. \quad (3.13)$$

Again, the theoretical results can be plotted relative to the shot noise component in shot noise level units. Figure 10 shows the noise expected for several different gain values,  $G_2$ , in the second amplifier and where the loss in both legs is the same, 6% and the detector efficiency is now 80%. Note that the noise contributions are still roughly linear with gain and they increase with increasing gain in the second amplifier. This is the same behavior as the single pass amplifier case depicted in Figure 6. A single pass noise curve is given for reference. Notice the shot noise floor across the bottom of the plot.

The matrix methodology for determining amplitude noise power can be extended to a chain of 'k' amplifiers and the results are found in section 3.2 below. It is also interesting to note that each amplifier could have also been treated as a distributed amplifier versus a lumped amplifier where the gain and loss sections of the amplifier slabs form a continuum. That technique is used to describe the noise for very long fiber amplifiers with lengths of tens of kilometers.

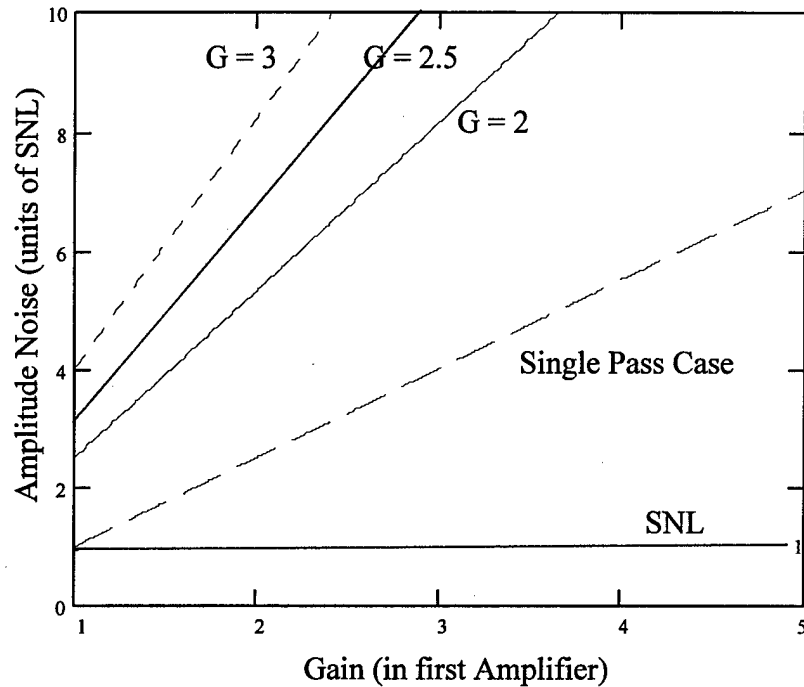


**Figure 10. Double Pass Linear Amplifier Amplitude Noise, Equation 3.13.** The top three curves are for increasing values of gain in the second amplifier, and the bottom curve is the amplitude noise for a single pass device. The shot noise level is labeled for reference. The units are the same as in Figure 6.

### 3.2 Linear Amplifier Chain Amplitude Noise

A natural extension of the linear double pass amplifier noise theories presented in section 3.1 above is to increase the number of amplifiers and generate a recursion relationship. This type of amplifier chaining has been well known in the fiber optic field as it is the basis for long haul optical communication along transoceanic cables. For a number of amplifier and loss elements chained together, assuming the input photon stream is Poisson, each amplifier is fully inverted, only one or a few modes propagate, the amplifiers have approximately the same gain,  $G$ , and the transmission efficiency between the amplifiers,  $\eta$ , is the same, a noise power relationship has been established<sup>10</sup>

$$\sigma_k^2 = (\eta G)^k \langle n_0 \rangle (1 + 2\eta(G-1)x_k) + \frac{\eta(G-1)x_k}{1+\eta G} \left\{ \frac{1-\eta G+2\eta(G-1)}{1-\eta G} \eta G [1-(\eta G)^{k-1}] + (1+\eta(G-1)) [1+(\eta G)^k] \right\}$$

where  $x_k = \frac{1-(\eta G)^k}{1-\eta G}$ , and k represents the number of amplifier stages. Since the number of photons  $\langle n_0 \rangle$  is so large, the second term can be eliminated, leaving the familiar formula already derived for the amplitude noise properties

$$\sigma_k^2 = \sigma_{SNL}^2 (1 + 2\eta(G-1)x_k). \quad (3.14)$$

This relationship produces amplitude noise plots indicating that as long as the gain is moderate, less than approximately 4 per stage, the additional noise is less than 10 times the shot noise level. The plot in Figure 11 shows the amplitude noise above shot noise, in shot noise level units, for 3, 5 and 10 stage amplifier chains with gain per stage as indicated along the x axis and an interstage transmission efficiency of 0.9. Figure 11 is directly comparable to Figures 6 and 10.

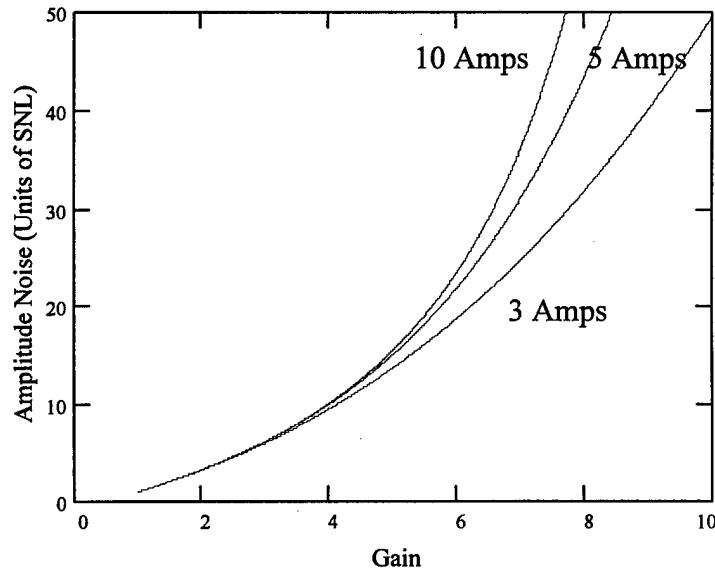


**Figure 11. Linear Amplifier Chain Amplitude Noise, Equation 3.14. The top curve is for 10 amplifiers the middle for 5 and the lower for 3. The chains have very similar behavior at low gain.**

### 3.3 Non-linear amplifier amplitude noise expression

From the historical background section in section 2.2 it is apparent that further study of the amplitude noise arising from non-linear amplification ceased in the late 1980's. It is also apparent that the evolution of the amplitude photon noise as the amplifier transitions from the linear regime to the saturated regime is not trivially derived for moderate to low numbers of photons, say under 1000, and for a large number of modes. However, it has been shown numerically by Bendjaballah and Oliver<sup>11</sup> and Abraham<sup>12</sup> that amplifier amplitude noise increases to a certain point and then decreases to a constant level at saturation. With the large number of photons found in the applications of interest to this study i.e., LIGO, a simpler result is available. In general, the outcome is that the output distribution of the amplitude noise variance is broader when compared to a coherent or Poisson distribution of the same mean, until complete saturation occurs. In the case studied here, as the amplifier becomes completely saturated and the gain approaches 1, the output photon stream approaches a Poisson distribution. Saturation has effectively turned the active lasing medium into a passive medium as far as the first two moments of the photon distribution are concerned. To study the effects of gain saturation on other photonic systems, such as communication systems, requires higher order moments be compared between the non-linear and linear amplifier output photon distributions.

As in the linear case, discussed in sections 2.1 and 3.1, the calculations presented here will begin with the probability density functions for the photon fields with similar assumptions to the linear case. As a reminder, these assumptions include a fully inverted four level lasing medium operating as a CW traveling wave amplifier and that the initial photon input distribution is Poisson and single mode.

The first step is to modify the unsaturated probability density evolution function or the QM photon statistics master equation, equation (3.5), by incorporating the saturation factor function

$$f_n = \frac{1}{1 + n/n_{sat}},$$

into

$$\frac{dP_n}{dz} = a\{nP_{n-1} - (n+1)P_n\} + b\{(n+1)P_{n+1} - nP_n\},$$

which becomes

$$\frac{dP_n}{dz} = a\{nf_n P_{n-1} - (n+1)f_{n+1} P_n\} + b\{(n+1)f_{n+1} P_{n+1} - nf_n P_n\}.$$

For a fully inverted medium  $b = 0$ , and the equation simplifies to

$$\frac{dP_n}{dz} = a\{nf_n P_{n-1} - (n+1)f_{n+1} P_n\}.$$

Using the moment distribution function

$$\langle n^k \rangle = \sum_{n=0}^{\infty} n^k P_n,$$

and taking the first derivative as before

$$\frac{d}{dz} \langle n^k \rangle = \sum_{n=0}^{\infty} n^k \frac{d}{dz} P_n$$

becomes

$$\frac{d}{dz} \langle n^k \rangle = \sum_{n=0}^{\infty} n^k a\{nf_n P_{n-1} - (n+1)f_{n+1} P_n\}.$$

Applying the translation property

$$\sum g(n) P_{n\pm 1} = \sum g(n \mp 1) P_n$$

gives

$$\frac{d}{dz} \langle n^k \rangle = \sum_{n=0}^{\infty} a\{(n+1)^{k+1} - n^k (n+1)\} f_{n+1} P_n.$$

Again applying the moment distribution gives

$$\frac{d}{dz}\langle n^k \rangle = a \left\langle \left\{ (n+1)^{k+1} - n^k (n+1) \right\} f_{n+1} \right\rangle.$$

For the evolution of the first moment, i.e.,  $k = 1$ , or the evolution of the average number of photons at a particular position in the amplifier the equation becomes

$$\frac{d}{dz}\langle n \rangle = a \left\langle \left\{ (n+1)^2 - n(n+1) \right\} f_{n+1} \right\rangle$$

or

$$\frac{d}{dz}\langle n \rangle = a \left\langle \left\{ (n+1) \right\} f_{n+1} \right\rangle.$$

This equation normally cannot be analytically solved due to the statistical correlation between the saturation factor function  $f_{n+1}$  and the term  $(n+1)$ . A solution can be obtained if the photon probability density function is known as a function of distance  $P_n(z)$ . Numerous authors have used decorrelation methods involving expansions and numerical routines to provide approximate solutions<sup>13-15</sup>. However, in this study, the saturation factor function is **not** correlated to the photon number states because the saturation of the gain medium in the laser amplifier is provided by another laser source, not by the probe signal stream  $\langle n \rangle$  from the NPRO. (This assumes the optical power of the saturating source is much greater than the NPRO.) This implies that the equation may be written as

$$\frac{d}{dz}\langle n \rangle = a \langle n+1 \rangle \left( \frac{1}{1+sn_e} \right)$$

where the saturation factor function,  $f_{n+1}$  has been rewritten with  $n_e$  representing the influx of photons from an external source. The saturation effect is encapsulated in the saturation parameter, "s". In addition, in this study,  $n \gg 1$  allows an even greater simplification and a straightforward solution given by

$$\langle n \rangle = \langle n_0 \rangle \exp\left( \frac{aL}{1+sn_e} \right), \quad (3.15)$$

where  $L$  is the optical length traversed by the probe beam through the amplifier and  $\langle n_0 \rangle$  is the average photon number at the input, or  $L=0$  point of the amplifier. For simplicity Equation 3.15 can be written as

$$\langle n \rangle = \langle n_0 \rangle G_s,$$

which is the same form as the linear solution for high photon numbers as derived in section 3.1. At the point of total saturation,  $G_s = 1$ , effectively the “a” or emission coefficient, has been driven to zero by driving the excited state population  $N_2$  to zero.  $G_s$  is the power gain experienced by a signal traversing the amplifier. In real systems there will be losses distributed throughout the length of the amplifying medium. The gain provided by the medium as well as the losses are encapsulated in the  $G_s$  term. By definition it cannot be less than 1.

The same approach can be used to obtain a second order moment and the variance. The saturated gain term  $G_s$  can encapsulate the effects of the non-linear amplification situation as long as  $n \gg 1$  and  $n \gg G$ , which is the case in this study. This leaves an equation identical in form to the linear amplifier Equation (3.9)

$$\sigma^2 = G_s \langle n_0 \rangle \left[ 1 + \left( 2 + \frac{1}{2} \right) (G_s - 1) \right] \quad (3.16)$$

Hence, all earlier material derived for the linear case including the equations for chains of amplifiers can be used in the non-linear case. The form of Equation 3.16 implies that the experimental approach used for verifying the linear amplifier noise, Equation 3.9, can also be used to verify the non-linear version. (Since the probe photon stream is continuous and the amplifier attains steady state saturation with an external photon stream uncorrelated to the probe, pulse saturation effects described by the Franz-Nodvik<sup>16</sup> equations do not apply).

If a saturated amplifier is designed as a multi-pass amplifier for the probe beam, with discrete losses at the output couplers and turning optics, the system can be modeled as an amplifier chain using Equation 3.14 and 3.16. (If the probe is multi-passed through the amplifier in an attempt to cause saturation using only the probe beam, Equation 3.16 does not apply). If the amplifying medium is hosted inside a simple oscillator configuration the equations in section 2.3 apply. It is possible to directly compare the amplitude noise performance of a linear, and non-

linear multi-passed amplifier to a simple oscillator by using the noise figures as defined in section 1.4. The noise figure for the multi-passed non-linear amplifier is given by

$$NF_{nlamp} = 10 * \log \left( \frac{1 + \left(2 + \frac{1}{2}\right) \eta (G_s - 1) x_{sk}}{(\eta G_s)^k} \right)$$

where k is the number of amplifier stages and

$$x_{sk} = \frac{1 - (\eta G_s)^k}{1 - \eta G_s}.$$

The noise figure for the oscillator is given by Equation 2.4

$$NF_{osc} = 10 * \log \left( \frac{1 + 2(G_c - 1 - X)}{G_c} \right)$$

where

$$X = \frac{R_1 \left( G - \sqrt{\frac{R_2}{R_1}} \right)^2}{(1 - \sqrt{R_1 R_2} G)^2} \quad \text{and} \quad G_c = \frac{(1 - R_1)(1 - R_2)G}{(1 - \sqrt{R_1 R_2} G)^2}.$$

Lastly, the linear amplifier chain noise figure is derived directly from Equation 3.14

$$NF_{amp} = 10 * \log \left( \frac{1 + (2) \eta (G - 1) x_k}{(\eta G)^k} \right)$$

where

$$x_k = \frac{1 - (\eta G)^k}{1 - \eta G}.$$

If  $G = G_s$ , then the oscillator and the amplifier chains can be directly compared as in Figure 12. Different combinations of mirror reflectivities in the oscillator can

lead to very different noise figure results. Appendix 6 describes the effects of using various mirror reflectivities on the SNR of the oscillator.

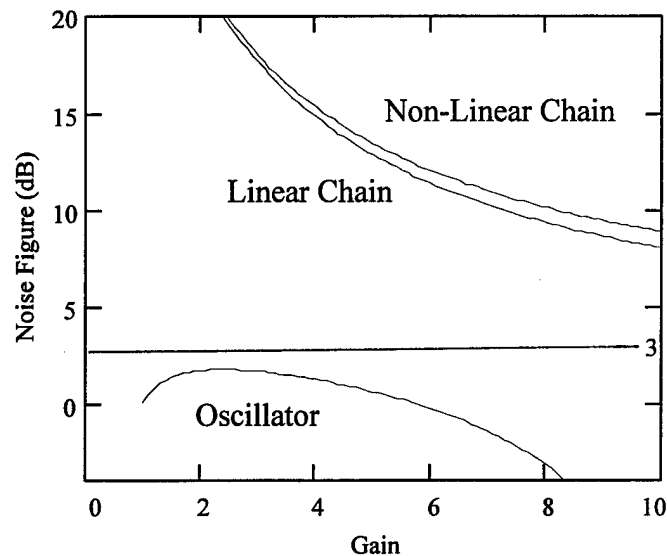


**Figure 12. Noise Figure for Linear and Non-Linear Amplifier Chains and the Simple Oscillator. ( $R_1 = R_2 = 0.1$ ,  $k = 3$  and transmission efficiency  $\eta$  of 0.9). The 3 dB Noise Figure for a perfect amplifier is drawn for reference.**

### 3.4 Injection locked oscillator amplitude noise

Extensive work has been done defining the operational characteristics and noise properties of injection locked DPSSLs.<sup>17,18</sup> This study did not attempt to reproduce the experimental data, rather use the published data and theoretical approaches to compare to the data taken on the amplifier systems. In particular, the Transfer Function Approach (TFA), Yamamoto's Circuit Approach (RLC) and the Quantum Langevin Approach (QLA) mentioned in section 2.3 will be compared.

The study of the amplitude noise of the injection locked systems often begins with a study of the decoupled, low power, low noise master oscillator and the high power, noisier slave laser. Then the noise equations are derived for the coupled system. In the case of this study and numerous others, the choice of master laser is straightforward and the discussion of how master lasers are designed for low noise operation will be limited to one type of master laser. It may be possible to use the low noise techniques traditionally reserved for just the master laser on combinations of master and slave oscillator. This would require simulation of the total system in which the laser is to be embedded and a

discussion of the engineering trade offs of the more complex system. This trade-off analysis will not be attempted here.

To date, one of the quietest master laser designs is the monolithic non-planar ring oscillator NPRO<sup>19</sup>. It is a diode pumped solid state laser, operates single mode, and has been built with electronic feedback systems to reduce two sources of noise. The first feedback control system is composed of the temperature stability loop to ensure the diode pump laser maintains the most efficient pump frequency for a given solid state material, avoids mode hops, and hence produces stable long term amplitude output for a given pump input. A second feedback loop senses the optical output of the laser and adjusts the current driving the diode laser to decrease the amount of amplitude noise over shorter periods of time. This loop is particularly useful in suppressing the resonant relaxation oscillation present in Nd:YAG systems<sup>20</sup>. This technique, employed in commercial systems from Lightwave Corporation, is known as a “noise eater” circuit. Though originally demonstrated by C.D. Nabors, at Stanford University<sup>21</sup>, Kane has demonstrated a 37 dB suppression in the amplitude noise attributed to the resonant relaxation oscillation.

NPRO lasers demonstrate shot noise limited performance in the Megahertz range making them very desirable for the LIGO systems employing phase modulation at 15 MHz. This is an impressive use of electronic feedback in a particular frequency range of laser operation. Another notable but lesser known stabilization effort was done by Tsubono and Moriwaki<sup>22</sup> in 1992. They were able to attain RIN values of  $< 10^{-7}$  within the range of 100 Hz to 10 kHz on an NPRO. This is the desired LIGO gravity wave interaction range and indicates that it may be possible to attain shot noise limited performance with DPSSLs in this region.

One of the most complete efforts to date to achieve the benefits of electronic feedback in the low frequency regime can be attributed to the collaboration between the Australian National University and the Laser Center in Hanover, Germany. In 1994, they demonstrated a feed back control system capable of reducing noise to  $1 \times 10^{-7} / \sqrt{\text{Hz}}$  for frequencies between 300 Hz and 10 kHz for an injection locked laser configuration<sup>23</sup>. This number is within the RIN requirements for the initial LIGO design. It is interesting to note that feedback control systems will always introduce excess noise such that a laser using this method for stabilization will always have amplitude noise at least 3 dB above the quantum noise limit. It may be possible to use external resonant “mode cleaners”

to reduce the amplitude and frequency noise of an injection locked or amplifier system without resorting to electronic feedback<sup>24</sup>. This would be a very important step in the design of the laser systems for LIGO.

Given all the attention devoted to finding an ultra-quiet injection locked laser, it is important to settle on one rendition of the master laser's power spectral density of amplitude noise. With this noise profile of the master laser in hand it will be possible to insert the master laser power spectral density of noise into the equations for the injection locked systems power spectral density of amplitude noise. The master laser noise equation used here will be the polynomial fit to the power spectral density of intensity noise of a feedback controlled NPRO<sup>25</sup>

$$\sigma_i^2(f) = 10 \log[2qI_{DC} \times 50\Omega] + (-0.024f^3 + 0.58f^2 - 5.71f + 21.42). \quad (3.17)$$

This is given in dBmW and where  $I_{DC}$  is in terms of mA of detected optical signal and  $f$  is in units of MHz. This choice will allow direct comparisons of the three injection locked amplitude noise power theories by agreeing to the same master laser (NPRO) input amplitude noise.

Having looked at the master oscillator amplitude noise it is now appropriate to consider the coupling of the master and the slave laser and compare the TFA, RLC and QLA approaches to the amplitude noise problem. The Transfer Function Approach<sup>26</sup>, is derived from a semi-classical approach to the laser rate equations based on Siegman<sup>27</sup>. It gives the internal photon number noise (unlike the external noise solution by Yamamoto which follows immediately thereafter). TFA assumes:

- the pump noise and externally incoupled master laser noise are uncorrelated, allowing a superposition of the two noise solutions as the square root of the sum of the squares;
- amplitude and frequency noise are decoupled;
- the slave laser remains in the locking range without electronic feedback;
- pump rate amplitude noise equates to the external amplitude noise of the slave;
- perfect master to slave mode matching.

This last assumption is not strictly correct but mode matching of 95% can be achieved. Though pump rate amplitude variations are directly related to pump

amplitude noise they are not necessarily directly related to the external photon number noise from the slave. However, it is very difficult to obtain relations and experimental data to verify this. If it were possible to obtain the laser diode pump amplitude noise spectral density and then compare that to the slave laser external amplitude noise, the predictions of this theory would be more precise. This is experimentally very difficult to do, especially with diode pump arrays, but the Australian and German groups have begun the process by studying the noise characteristics of single diode lasers and diode arrays<sup>28</sup>. They find a difference between the semiclassical TFA approach and their own QLA approach in the frequency regime well below the resonant relaxation oscillation. However, after comparing the results of these two theories, the difference appears minimal.

While working with the TFA approach it became apparent that the transfer function from the pump rate fluctuations to the internal photon number noise in the slave,  $G_p$  when multiplied by the spectral density of amplitude noise taken from external measurements of the slave,  $S_{N,p}$  rendered a problem with units<sup>29</sup>. In most cases, transfer functions need to be unitless or the corresponding spectral density functions need to have complimentary units. This was not the case. So, using the Yamamoto equations as a guide, the TFA approach was modified slightly to correct this problem. The results of the comparison of the amplitude noise from the TFA, RLC and QLA approaches with the same input master and pump noise are given in Figure 15 below. The calculations can be found in the “MathCad” document in Appendix 7. [Note that TFA uses QNEL units and RLC and QLA uses dB and dBmW units. The TFA numbers were changed to dB for comparison in the same figure.]

Yamamoto’s “RLC” approach to the injection locked oscillator begins with an RLC definition of the standard oscillator and assumes the injection locked system’s outcoupling resembles a connection to a standard transmission line, as depicted in Figure 13. The master oscillator amplitude noise  $v_{ex}$  is modeled as entering a circulator just as the load noise does

$$\left[ R_L + j\left(\omega L - \frac{1}{\omega C}\right) - R_a + jX_a \right] i = v_a + v_L + v_{ex}$$

where the subscript “a” refers to the gain material, and the subscript “L” refers to the load.

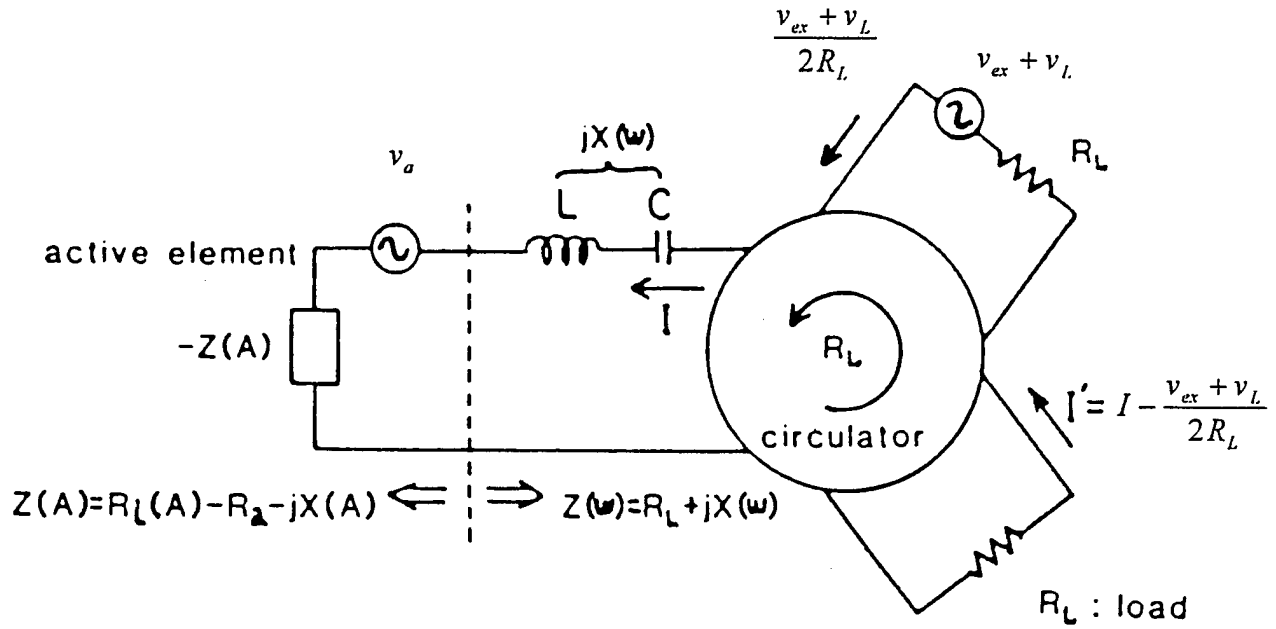


**Figure 13. Schematic of the RLC Model of an Injection Locked Oscillator**

A few assumptions are used in the derivation, such as:

- single mode operation,
- photon lifetime much longer than the excited state lifetime of the atoms in the gain medium,
- slave laser operating far above threshold,
- the noise sources of the load,  $v_L$ , and the gain medium,  $v_a$ , are uncorrelated,
- the master and slave lasers are locked
- and the injected signal is much smaller than the total output power.

With these assumptions it is possible to derive the power spectrum of the amplitude noise of the injection locked system regardless of the choice of master laser power spectral density of amplitude noise,  $\overline{S_{LC}(\Omega)}$ , and the slave laser power spectral density of amplitude noise,  $\overline{S_{ac}(\Omega)}$ , where both are spectrums of voltage values,  $[V^2 \cdot s]$  and arise from  $v_L$  and  $v_a$  respectively. This power spectrum is

$$\overline{S_{\Delta A_{ex}}(\Omega)} = \frac{1}{4R_L^2} \left[ \frac{(\Omega/\Omega_c)^2 + 4(A_{ex}/A)^2}{1 + (\Omega/\Omega_c)^2} \overline{S_{LC}(\Omega)} + \frac{1}{1 + (\Omega/\Omega_c)^2} \overline{S_{ac}(\Omega)} \right] \quad (3.18)$$

in units of  $[A^2 \cdot s]$  and where  $\Omega_c$  refers to the cavity resonant frequency.

At very high frequencies ( $\Omega$ ) the amplitude noise spectrum is dominated by the noise of the load, including the master laser input, which qualitatively can be understood as the external noise reflecting off the input coupler of the slave.

(Using the RLC analogy there is a mismatch between the load, which is modeled as a transmission line, and the source, which is the slave cavity.) Conversely at very low frequencies, the external noise is attenuated by the power ratio of the external and internal field amplitudes  $(A_{ex} / A)^2$ , in this case 0.01, so that the internal gain medium noise, composed mostly of the diode pump laser noise, dominates. In the middle region of frequencies a weighting of both external load noises and internal noises occurs. It is clear that if the external noise is quantum limited  $\overline{S_{LC}}(\Omega) = 4\hbar\omega R_L$ , then at high frequencies the injected system is also quantum limited,  $\overline{S_{\Delta A_{ex}}}(\Omega) = \frac{\hbar\omega}{R_L}$ . If the diode pump lasers are quantum limited then at very low frequencies the system should be nearly quantum limited.

To compare the three injection locked amplitude noise theories, Equation (3.17) was used to derive values for noise power spectral densities of the master laser while the pump noise spectral density is assumed to be shot noise limited. The calculations used a power ratio between the master and slave laser of 100:1, indicative of using a 200 mW NPRO and a 20 W slave. The parameters of the Shine<sup>30</sup>, injection locked ring laser were used to calculate the cavity resonances to insert into the three separate injection locked oscillator amplitude noise theories. The RLC calculations are done in MathCad and found in Appendix 7. The results of the comparison of the three theories are found in Figure 15. Note that the linear frequency is in units of MHz. The system is quantum limited at approximately 10 MHz in the RLC calculation.

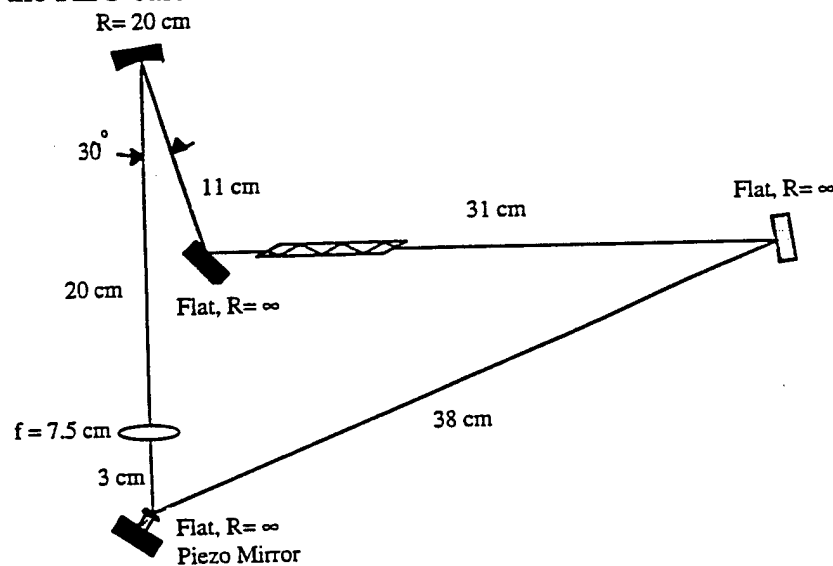
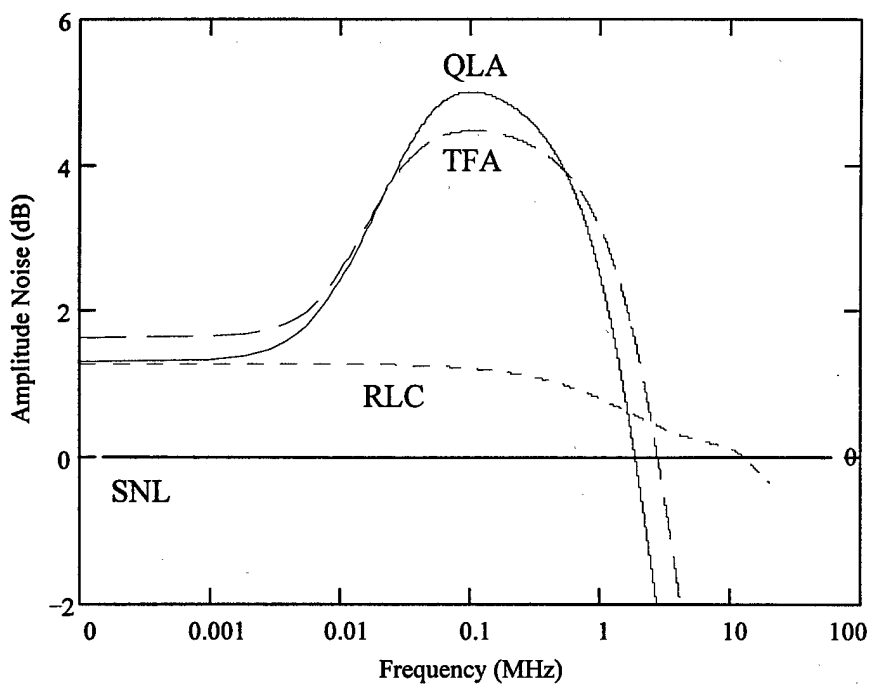


Figure 14. Schematic of the Injection Locked Ring Laser [After Shine<sup>30</sup>]

The third and final theoretical approach to the injection locked laser's amplitude noise calculation is the QLA approach. This theoretical contribution from Ralph, Harb and Bachor<sup>31</sup>, was to take previous Langevin representations of a laser system and apply a linearized analysis to the injection locked solid state laser operating near steady state. This approach provides more information about the behavior of the solid state laser in two regimes: that well below the frequency of the relaxation oscillation and well above the oscillation in comparison to the semi-classical rate equation approach. The results differ from the semi-classical TFA approach used by Farinas et. al.<sup>32</sup>, in the location of the crossover point for the laser into the shot noise limited regime beyond the relaxation oscillation and the amount of low frequency noise expected under the low pump noise approximation. The good news is that in either theory (and supported by experiment) the laser system for LIGO can be SNL at the 15 MHz phase modulation frequency due to the filtering effect of the injection locked cavity<sup>33</sup>.



**Figure 15. Injection Locked Amplitude Noise Power Spectral Density for three different theoretical approaches. The Quantum Langevin Approach (QLA) shows the highest relaxation oscillation noise but crosses into the SNL at the lowest frequency. The RLC approach does not reproduce the amplitude noise represented by the relaxation oscillation. The Transfer**

**Function Approach (TFA) and the QLA approach have very similar behavior.**

It should be possible to suppress the pump noise and obtain better noise properties (possibly sub shot noise performance) in the 100 Hz to 10 kHz regime<sup>34</sup>. Experimental results obtained by Harb and Ralph et. al.<sup>35</sup> demonstrated excellent agreement with their theory and imply that injection locked systems are capable of producing high power and shot noise limited outputs in the non-amplification regimes on either side of the relaxation oscillation. Calculations of the QLA amplitude noise power approach can also be found in Appendix 7. In Figure 15, the noise power for the same injection locked system is plotted using the three different injection locked theories. There is a strong similarity between the results for the TFA and QLA approaches.

### Chapter 3 References

1. R. Loudon, *The Quantum Theory of Light*, 2nd Ed., (Oxford University Press, NY, 1983).
2. R. Loudon, *The Quantum Theory of Light*, 2nd Ed., (Oxford University Press, NY, 1983) p. 171.
3. M. Sargent, M. O. Skully, and W.E. Lamb, "Buildup of Laser Oscillations from Quantum Noise", *Applied Optics*, Vol. 9, No. 11, p. 2423 (1970).
4. P. Diament and M. Teich, "Evolution of the Statistical Properties of Photons Passed Through a Traveling-Wave Laser Amplifier", *JQE*, Vol. 28, No. 5, p. 1325 (1992).
5. A. Yariv, *Optical Electronics*, 4th Edition, (Holt , Reinhart and Winston, Inc., San Francisco, 1991).
6. P. Diament and M. Teich, "Evolution of the Statistical Properties of Photons Passed Through a Traveling-Wave Laser Amplifier", *JQE*, Vol. 28, No. 5, p. 1325 (1992) p. 1332.
7. E. Desurvire, *Erbium Doped Fiber Amplifiers*, (Wiley and Sons, New York, 1994) p. 85.
8. E. Desurvire, *Erbium Doped Fiber Amplifiers*, (Wiley and Sons, New York, 1994) p. 159.
9. A. Leon-Garcia, *Probability and Random Processes for Electrical Engineering*, 2nd Ed., (Addison-Wesley Publishing, Menlo Park, CA, 1994) p. 147.
10. E. Desurvire, *Erbium Doped Fiber Amplifiers*, (Wiley and Sons, New York, 1994) p. 117.
11. C. Bendjaballah and G. Oliver, "Detection of Coherent Light after Nonlinear Amplification", *IEEE Transactions on Aerospace and Electronic Systems*, Vol. AES-17, No. 5, p. 620 (1981).

12. N.B. Abraham, "Quantum theory of a saturable amplifier", *Physical Review A*, Vol. 21, No. 5, p. 1595 (1980).
13. S. Ruiz-Moreno, G. Junyent, M.J. Soneira, and J.R. Usandizaga, "Statistical Analysis of Nonlinear Optical Amplifier in High Saturation", *IEE Proceedings*, Vol. 135, Pt. J, No. 1, p. 34 (1988).
14. C. Bendjaballah and G. Oliver, "Detection of Coherent Light after Nonlinear Amplification", *IEEE Transactions on Aerospace and Electronic Systems*, Vol. AES-17, No. 5, p. 620 (1981).
15. G. Oliver and C. Bendjaballah, "Statistical Properties of Coherent Radiation in a Nonlinear Optical Amplifier", *Physical Review A*, Vol. 22, No. 2, p. 630 (1980).
16. L. Frantz and J. Nodvik, "Theory of Pulse Propagation in a Laser Amplifier", *Journal of Applied Physics*, Vol. 34, No. 8, p. 2346 (1963).
17. T. Ralph, C. Harb, and H. Bachor, "Intensity Noise of Injection Locked Lasers: Quantum Theory Using a Linearized Input-Output Method", *Physical Review A*, Vol. 54, No. 5, p. 4359 (1996).
18. C. Harb, T. Ralph, E. Huntington, I. Freitag, D. McClelland, and H. Bachor, "Intensity Noise Properties of Injection Locked Lasers", *Physical Review A*, Vol. 54, No. 5, p. 4370 (1996).
19. T. Kane, and R. Byer, "Monolithic, unidirectional single-mode Nd:YAG ring laser", *Optics Letters*, Vol. 10, No. 2, p. 65 (1985).
20. T. Kane, "Intensity Noise in Diode-Pumped Single-Frequency Nd:YAG Lasers and its Control by Electronic Feedback", *IEEE Photonics Technology Letters*, Vol. 2, No. 4, p. 244 (1990).
21. C.D. Nabors, A.D. Farinas, T. Day, S.T. Yang, E.K. Gustafson, and R.L. Byer, "Injection Locking of a 13-W CW Nd:YAG Ring Laser", *Optics Letters*, Vol. 14, No. 21, p. 1189 (1989).
22. K. Tsubono, and S. Moriwaki, "Shot-Noise Limited Low Frequency Intensity Noise of a Nd:YAG Laser", *Japanese Journal of Applied Physics*, pt 1, Vol. 31, No. 4, p. 1241 (1992).

23. C. Harb, M. Gray, H. Bachor, R. Schilling, P. Rottengatter, I. Freitag, and H. Welling, "Suppression of the Intensity Noise in a Diode Pumped Nd:YAG Nonplanar Ring Laser", *JQE*, Vol. 30, No. 12, p. 2907 (1994).
24. B. Willke, E. Gustafson, R. Byer, P. King and S. Seel, "Spatial and temporal filtering of a 9.1 Watt Nd:YAG laser with a ring-cavity, Fabry-Perot, pre-mode cleaner", Submitted to *Optics Letters* (March 1998).
25. C. Harb, T. Ralph, E. Huntington, I. Freitag, D. McClelland, and H. Bachor, "Intensity Noise Properties of Injection Locked Lasers", *Physical Review A*, Vol. 54, No. 5, p. 4377 (1996).
26. A.D. Farinas, E.K. Gustafson, and R.L. Byer, "Frequency and Intensity noise in an Injection-Locked, Solid-State Laser", *Journal of the Optical Society of America B*, Vol. 12, No. 2, p. 328 (1995).
27. A.E. Siegman, *Lasers*, (University Science Books, 1986).
28. C. Harb, T. Ralph, E. Huntington, D. McClelland, H. Bachor, and I. Freitag, "Intensity Noise Dependence of Nd:YAG Lasers on Their Diode-Laser Pump Source", Submitted to *JOSA B*, (1997).
29. A.D. Farinas, E.K. Gustafson, and R.L. Byer, "Frequency and Intensity noise in an Injection-Locked, Solid-State Laser", *Journal of the Optical Society of America B*, Vol. 12, No. 2, p. 331 (1995).
30. R.J. Shine, A.J. Alfrey and R.L. Byer, "A 40 W cw, TEM<sub>00</sub> mode, diode-laser-pumped, Nd:YAG zig-zag miniature-slab laser", *SPIE*, Vol. 2379 p. 112 (1995).
31. T. Ralph, C. Harb, and H. Bachor, "Intensity Noise of Injection Locked Lasers: Quantum Theory Using a Linearized Input-Output Method", *Physical Review A*, Vol. 54, No. 5, p. 4359 (1996).
32. A.D. Farinas, E.K. Gustafson, and R.L. Byer, "Frequency and Intensity noise in an Injection-Locked, Solid-State Laser", *Journal of the Optical Society of America B*, Vol. 12, No. 2, p. 328 (1995).

33. C. Harb, T. Ralph, E. Huntington, I. Freitag, D. McClelland, and H. Bachor, "Intensity Noise Properties of Injection Locked Lasers", *Physical Review A*, Vol. 54, No. 5, p. 4376 (1996).
34. T. Ralph, C. Harb, and H. Bachor, "Intensity Noise of Injection Locked Lasers: Quantum Theory Using a Linearized Input-Output Method", *Physical Review A*, Vol. 54, No. 5, p. 4363 (1996).
35. C. Harb, T. Ralph, E. Huntington, I. Freitag, D. McClelland, and H. Bachor, "Intensity Noise Properties of Injection Locked Lasers", *Physical Review A*, Vol. 54, No. 5, p. 4370 (1996).

## **Chapter 4**

### **Experiment**

#### **4.0 Introduction**

The intent of the experimental portion of this study was to verify the linear and non-linear amplifier amplitude noise calculations. Up to this time the only experimental work in the area was conducted on argon gas lasers by Harris et. al. in 1992<sup>1</sup> Using an argon gas laser in a traveling wave amplifier configuration in both a single and double pass set-up, their results showed that the amplified beam acquired amplitude noise which was greater than would be expected from a perfect Poissonian distribution. Their technique was aimed at verifying the relationship between the degree of population inversion and the amount of ASE at a particular gain level. Though the results are not directly applicable in this study, due to the nearly perfect inversion quality of the Nd:YAG diode pumped system, the form of their equations and the emphasis placed on ensuring single mode operation of their systems is very similar to the approach taken in this study.

To obtain data which could be compared to the theory derived in Chapter 3, several important assumptions had to be converted into experimental reality. The first was the requirement for single optical mode operation. Recall the theory section wherein the noise equations were simplified by assuming that only one mode propagated. The second assumption was a completely inverted gain medium would be needed to simplify the expression for ASE. The third assumption was a Poisson stream of input photons would enter the amplifier under test.

All assumptions were satisfied by the choice of components and the experimental methodology. First, the probe laser must operate in a single mode, produce a Poisson light distribution and be shot noise limited at the frequency of interest. The Lightwave Model 122-300 non-planar ring oscillator (NPRO), met all the requirements. Second, the laser amplifier was fully inverted with gain and loss coefficients independent of position within the amplifier slab. This was achieved with a diode-pumped fiber coupled Nd:YAG zig-zag slab amplifier. In

addition, by using the single mode NPRO as a probe beam it was possible to use a homodyning technique to select a single ASE mode from the amplifier.

In addition, if a super Gaussian or flat top mode is used as a probe beam, since it is inherently a multi-mode structure, it must be carefully determined if these noise calculations apply to this situation, or if a multiplier must be used. In general, if the number of modes is far less than the average number of photons, which will almost always be the case for LIGO applications, these noise calculations will remain valid. As for a chain of amplifiers, if relay imaging is used properly, a single mode will propagate and the calculations for noise, as found in this study, will be valid.

#### 4.1 The Laser Amplifier

The laser amplifier for both the linear and non-linear experiments as well as the single and double pass work was the same. It was a zig-zag slab Nd:YAG diode pumped device. The active material was Brewster end cut with dimensions 1.7 mm x 1.8 mm by 58.9 mm long. The head was pumped through fiber coupled diode lasers which had computer controlled current sources and electronically controlled TECs for temperature stability.

The slab was face cooled with pure water and designed to have turbulent flow. To improve operational characteristics, the 25 separate pump sources were fiber coupled perpendicularly to a manifold parallel to the slab, so if one pump diode failed, the change in the smoothness of the inversion would be minimal. This was critical to ensure the  $a$  and  $b$  coefficients did not change along the length of the amplifier. Even with this design feature, there probably is some slight difference throughout the inverted region because the center frequency of each diode drifts slightly differently with temperature and each has a slightly different set point to attain the desired 808 nm pump frequency. However, the advantage of the zig-zag path design is that the wavefront traverses a path which averages out these different regions of gain. The pump diodes were operated with TEC coolers which would indicate when the temperature went more than 10% too high or too low. Tighter control could not be maintained with this design. The slab itself was pumped and cooled through the same surfaces. A more complete description of the head and the information about this particular device can be found in Shine<sup>2</sup>.

The head was removed from its laser configuration and used in the traveling wave amplifier configuration. As an amplifier it was important to characterize the

small signal gains for various diode laser pump levels. This would give a feel for the gain envelope the NPRO probe beam would experience and set the upper boundary of the noise that could be measured. The following figures display the single and double pass gains versus the laser diode pump level, stated as a percentage of maximum pump power of approximately 220 Watts.

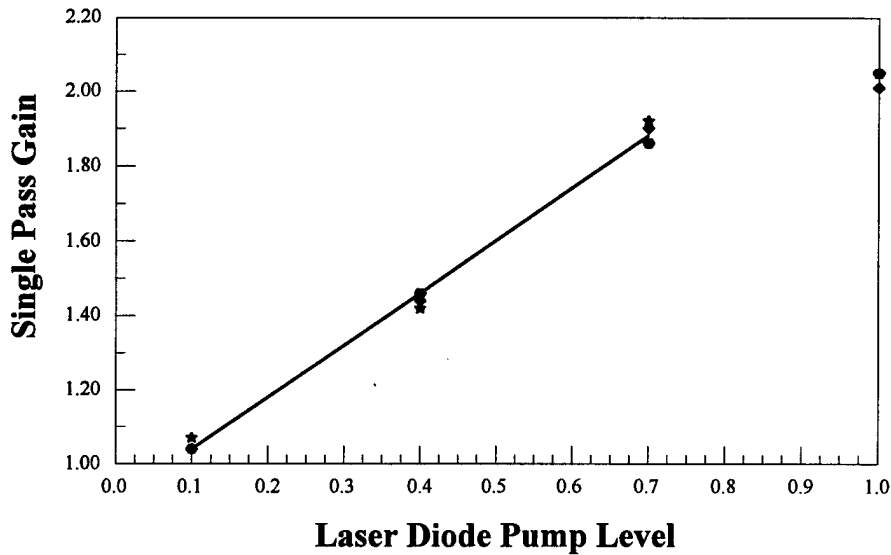


**Figure 16. Single Pass Gain vs. Laser Diode Pump Level**

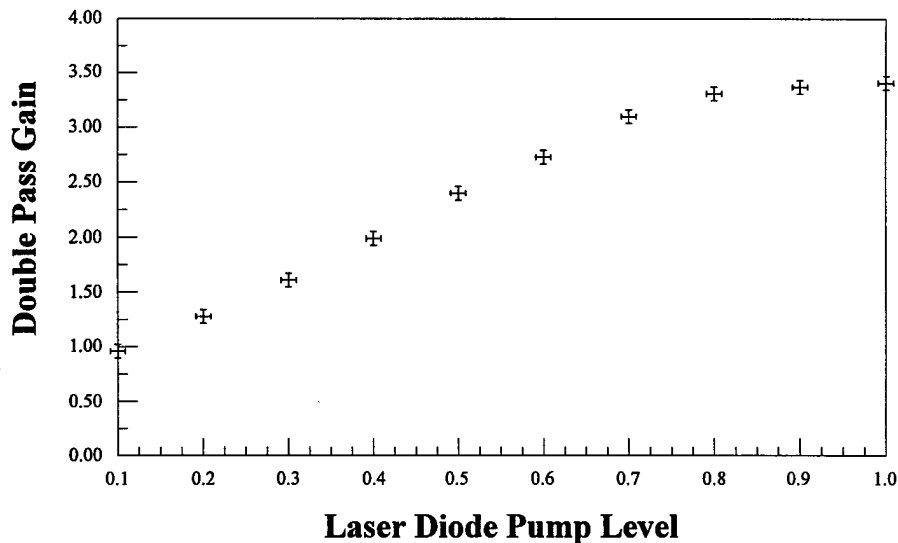


**Figure 17. Double Pass Gain vs. Laser Diode Pump Level**

Note the threshold values for gain at approximately 10% of maximum pump power. There after the amount above threshold scales linearly with the pump percentage. Loss through the slab on one pass was approximately 4% and between 11 and 16% on the double pass experiments, depending on the setup of mirrors and lenses. The amplifier was rarely run over 70% pump due to thermal loading and degradation of the fiber couplings into the laser head.  $r$  values (pump rate or number of times above threshold) scaled with % so that 30% was an  $r=3$ . These gain values indicate that the dynamic range of the experiment would not be very large.

This four level system is also easily and nearly completely inverted at low pump percentages. The inversion quality was verified by measuring the amplifier ASE in the same solid angle through an apertured detector at the same distance from amplifier. Complete inversion occurred at 10% pump power and remained linear to 70% pump power. Figure 18 shows the single pass and double pass ASE versus gain. The complete inversion was required as explained in the introduction to this chapter.

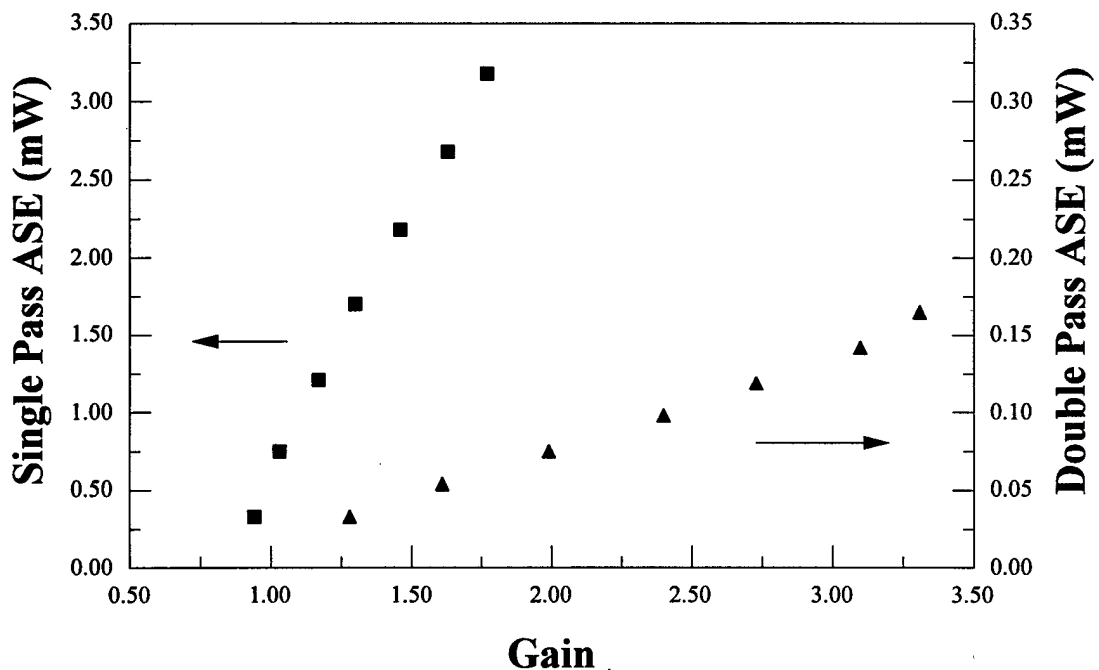


**Figure 18. Amplified Spontaneous Emission (ASE) versus Gain for Single and Double Pass Amplifier systems**

## 4.2 Detection Systems

Three different detection systems were considered for this study. They included direct homodyne detection, resonant homodyne detection and balanced detection. They are briefly discussed in this section and the detection system of choice is further characterized in the following section.

Direct detection of the homodyned “signal/ASE” and signal components was initially used to characterize the noise of the NPROs. The idea was simply to attenuate the NPRO and sample the photon stream with a fast detector at fairly high photocurrents. A large area silicon PIN detector ( $13 \text{ mm}^2$ ) was used that could handle high photon fluences, commensurate with tens of milliamps of photoelectrons that would be expected in LIGO dark fringe interferometer detectors. However, the photodiode had only moderate responsivity at  $1.06 \text{ }\mu\text{m}$ . Other problems, discussed below, also occurred with the Si direct detector. This led to a search for other direct detector candidates.

The next detection type considered, resonant homodyne detection, uses a resonant or tank circuit to enhance the signal (shot noise) measurement at a specific frequency. This would have been an acceptable solution for this particular experiment because the data set for this experiment was limited to  $15 \text{ MHz}$ , the LIGO phase modulation frequency. Though the basic idea of resonant homodyne detection is simple it requires the impedance matching of the detector to the amplifier to effect maxim power transfer. The device can also drift under normal operating conditions. Due to time constraints, the effort to construct, calibrate and maintain this more complex resonant detector design was stopped.

Balanced detection could also be used in noise experiments. This is the preferred approach for the Australian and German teams mentioned earlier. Its advantage is that it can reject common biases and leave only the noise components. It can be used over a very wide range of frequencies, but it does require two perfectly matched photo detectors. Again due to time constraints, this method was not used. However, commercial balanced detectors are becoming far more common and it may now be worthwhile to revisit this approach.

The direct homodyne approach was used in this experiment but it was done at much lower photoelectron currents than originally desired. A transimpedance amplifier design, coupled with an InGaAs detector material was operated at  $1 \text{ mA}$ . The following section details the steps leading up to this choice of design.

## Detectors

The first step in any experimental approach is to create a trusted measurement agent. In this case, the problem was to create a detector/receiver combination which could faithfully convert optical to electrical noise. The initial desire was to verify the possibility of operating a detector at very high photoelectron generation rates, and still have excellent linearity and absence of saturation effects.

Even before noise measurements were attempted it was most important to establish the linearity of the detector. There are two time constants which must be considered when determining whether or not a photodiode detector is linear at a particular frequency. The first consideration is the RC time constant limited capacitance of the diode structure and other parasitics. These capacitances can couple with device resistances to create unanticipated and undesired filters, usually the low pass type. This would be an obvious reason for DC behavior to be linear while the behavior at 15 MHz would be non-linear.

Also, though it is often tempting to use a larger active area to obtain high photocurrents and hence higher dynamic range, the larger area leads to transit time limited performance. It physically takes more time for the photoelectrons to be collected when they have to cross large distances. This would be more serious for the PIN structure due to the large intrinsic region in the center. It is also possible that extremely large photocurrents cause bunching which alters the very distributions of the photoelectrons.

The second most important characteristic of a detector is its responsivity. Responsivity is directly related to the quantum efficiency of the device, a parameter which allows more precise analysis of the experimental results. A detector without a uniform responsivity across its face would produce unusual behavior, especially if the beam position changes between measurements. The larger the detector area the more likely the responsivity would vary with position.

Steps were taken in this experiment to ensure the detector was linear, even at 15 MHz. Saturation effects were controlled by maintaining a low 1 mA DC current and ensuring no hot spots in the beam profile. A much smaller area detector was used to lower the chance of positional responsivity differences. The responsivity to varying photon fluences was measured at the 15 MHz frequency of interest. The actual measurements and detector characteristics are discussed in the experimental characterization section 4.3.1 below.

The detector/receiver was constructed around an Epitaxx ETX 300T high speed InGaAs detector. Linear operation of the detector was verified up to 4 mA of photocurrent while data was taken at 1 mA of photocurrent. It had a cutoff frequency well beyond the 15 MHz measurement point, in this particular case a bandwidth of 0.4 GHz. In general, direct bandgap materials such as InGaAs can be made much faster for a given quantum efficiency than indirect gap materials such as Si since the absorption coefficient of the direct gap material increases more rapidly with decreasing wavelength<sup>3</sup>. The schematic of the detector circuit is found in Figure 19. InGaAs detectors can also be used at much lower photocurrents because they have higher quantum efficiencies, 0.71 at 1.06  $\mu\text{m}$  vs. 0.3 to 0.4 for Si. The only disadvantage to the detector was its small diameter (300  $\mu\text{m}$ ).

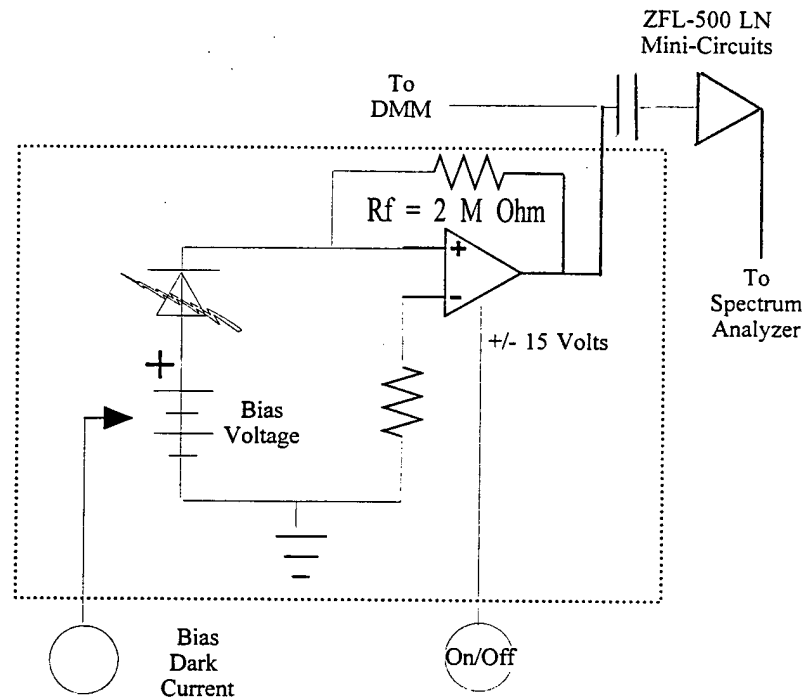


**Figure 19. Schematic of InGaAs Detector/Receiver**

A transimpedance amplifier converted the photogenerated current into the noise voltage registered in the spectrum analyzer. As can be seen in Figure 19, there is almost no voltage drop across the input terminals of the high gain operational amplifier, so the entire battery voltage appears across the photodiode no matter what the current flow from the photodiode. This is an example of a vertical load line. This improves the speed of the photodetector response at higher photoelectron fluences because the photoelectrons still see a high field situation. In addition, there is almost no current flowing into the input terminals of the op

amp. Hence, the entire diode current flows through the feedback resistor  $R_f$ . Since the negative op amp terminal is nearly at ground, the output voltage is just  $R_f$  times the photodiode current.

This set up is completely linear and if  $R_f$  is chosen to be  $2\text{ M}\Omega$ , the transimpedance conversion factor  $\gamma$ , which is the ratio of voltage to current, can be very large. Hence, a  $1\text{ mA}$  current registers  $2\text{ Volts}$  on the DMM. This detector/receiver combination had an additional biasing circuit to zero out the dark current background. A DC port, and an AC port with BNC for RG-58 cables was provided. A  $15\text{ Volt}$  power supply was provided to power the op amp and the photodiode biasing.

A commercial Mini-Circuits ZFL-500LN low noise amplifier followed the InGaAs detector/receiver. It had a Noise Figure of  $1.9\text{ dB}$  and a small signal gain of approximately  $28\text{ dB}$ . After the preamplifier the HP 71000 series RF spectrum analyzer system completed the sampling electronics. This system was impedance matched at  $50\ \Omega$  and provided linear operation at  $15\text{ MHz}$  with approximately a  $13\text{-}15\text{ dB}$  margin over the electronics noise floor, as shown in Figure 28. Linear operation was verified as shown in Figure 20. The system was capable of operation from  $100\text{ Hz}$  to  $2.96\text{ GHz}$ .

## 4.3 Experimental process

### 4.3.1 Characterization and Calibration

This section is devoted to understanding the idiosyncrasies or operational characteristics of the major components of the experiment. In particular, this section describes the characteristics of the InGaAs detector, the HP 71000 Spectrum Analyzer, the amplifier head and the NPRO 122-300 lasers.

The InGaAs detector efficiency and linearity were verified. This was accomplished by varying the DC photocurrent in multiples of 2 and watching for a commensurate  $3\text{ dB}$  difference between the noise levels. The results are shown in Figure 20.

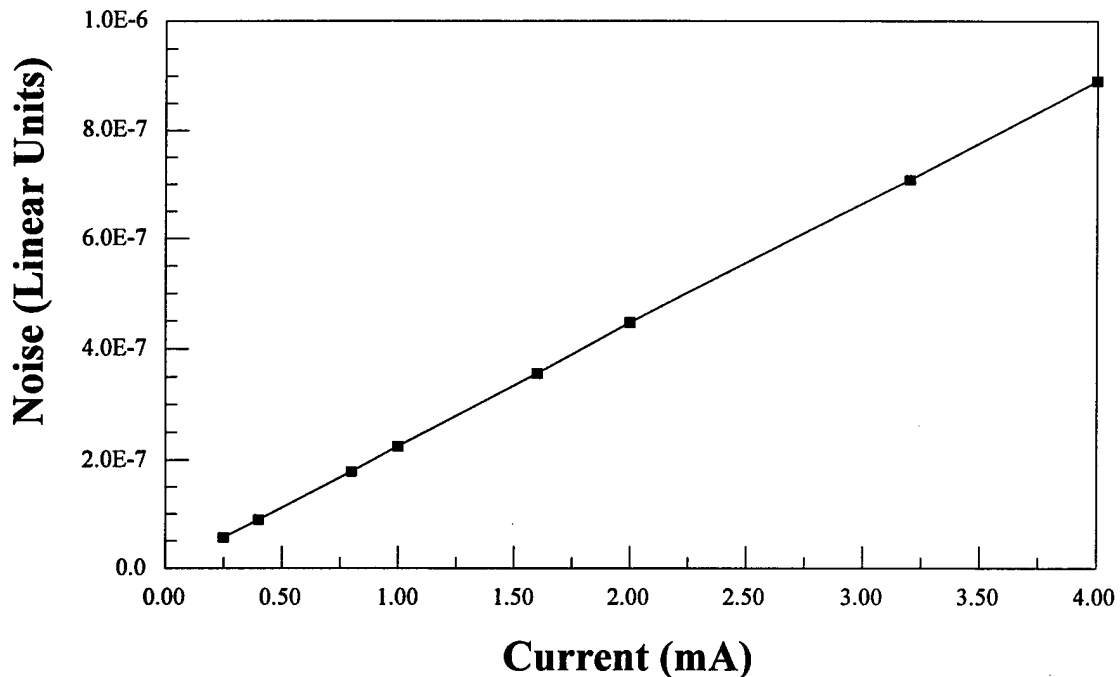


**Figure 20: InGaAs Detector Linearity at 15 MHz**

Though it was a minor activity, the reflection coefficients of the preamplifier towards the detector and towards the SA were checked. It was necessary to determine if there would be a substantial amount of noise power reflected back towards the detector. To verify the reflection coefficient,  $\rho$ , the voltage standing wave ratio, VSWR, from the amplifier specification sheet was used where  $\rho = \frac{VSWR - 1}{VSWR + 1}$ . Between the detector (50  $\Omega$  load) and the Mini-Circuits ZFL 500LN Amplifier at 5.4 and 53 MHz,  $\rho$  was measured to be 1.5 % and 4.3 % respectively. At 15 MHz the values were approximately 2% so this was within the error of the noise measurements. The VSWR between the preamplifier and the SA was 4.8 % at 5.4 MHz and 3.8% at 53 MHz, also acceptable values.

The characterization of the equipment proceeded with consideration of the noise floors and spectrum analyzer drift. There was more than a 10 dB margin above the SA noise floor which was deemed adequate. However, the averaging function of the spectrum analyzer led to an upward drift in the electronics noise floor which increased with increasing number of averages as depicted in Figure 21.

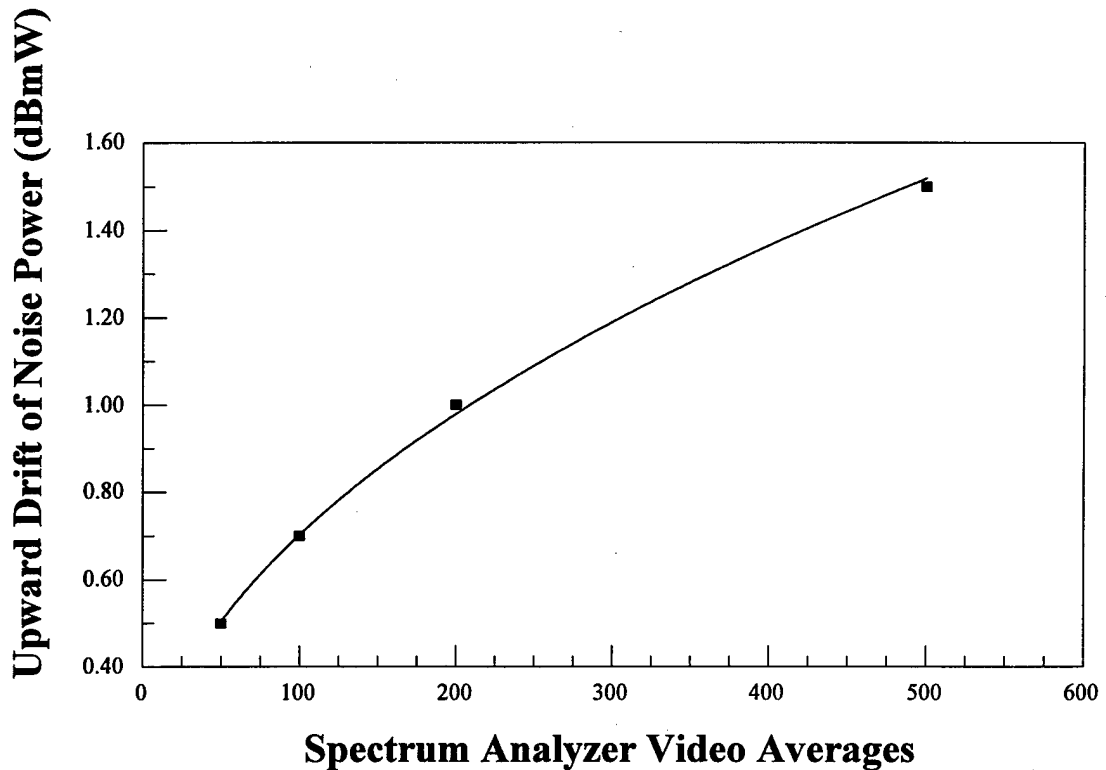


**Figure 21. Upward Drift in Spectrum Analyzer noise Trace vs. Video Averaging Function**

The video averaging function of the spectrum analyzer rounds and stores data. Eventually this continual rounding up and storing bumps up the readings. Based on this information, a tradeoff was made. At low video averages the variances in the noise signal are so great that it is difficult to find the mean. An average of 200 seemed an optimum choice between drift of the signal upwards and the large variances in the noise signal which make it unreadable.

The characterization of the amplifier included intensity profiles versus pump power to verify the thermal steering. At various pump power values the intensity profile would shift and broaden. The steering and subsequent clipping of the beam at the slab apertures and detector made it difficult to obtain power readings and noise measurements, especially with the double pass configuration. It was necessary to re-center the beam on the 0.3 mm diameter detector each time the pump percentage was changed. The following four figures depict the change in the vertical and horizontal intensity profiles for the single and double pass amplifier experiments. The beam steers mostly in the horizontal plane so, for the most part, it was only necessary to adjust one positioner. Though thermal lensing was reduced with the zig-zag slab design, it was not eliminated.

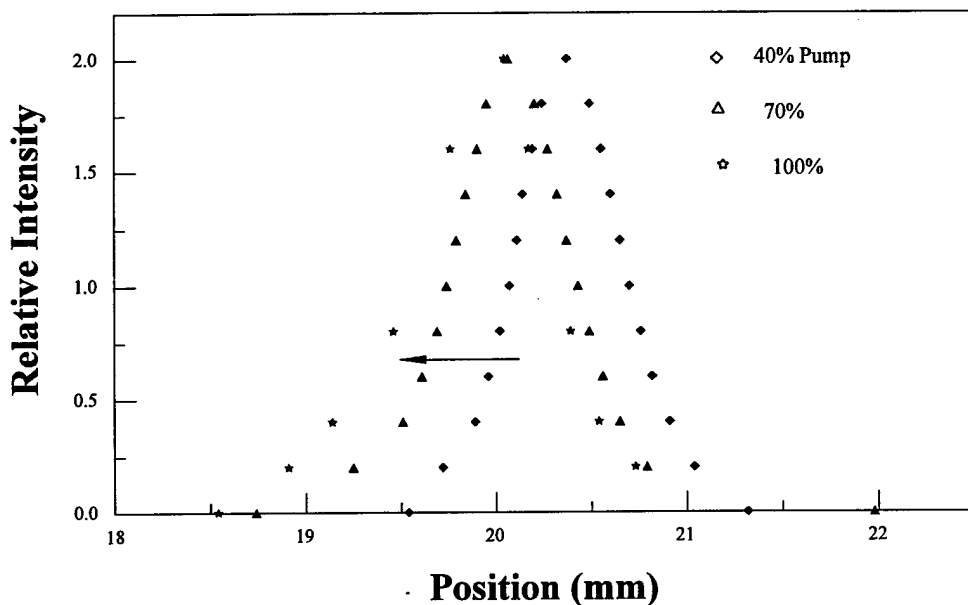


**Figure 22. Horizontal Intensity Profiles for the Single Pass Amplifier at three different pump levels. Notice the shift to the left of 0.5 mm.**

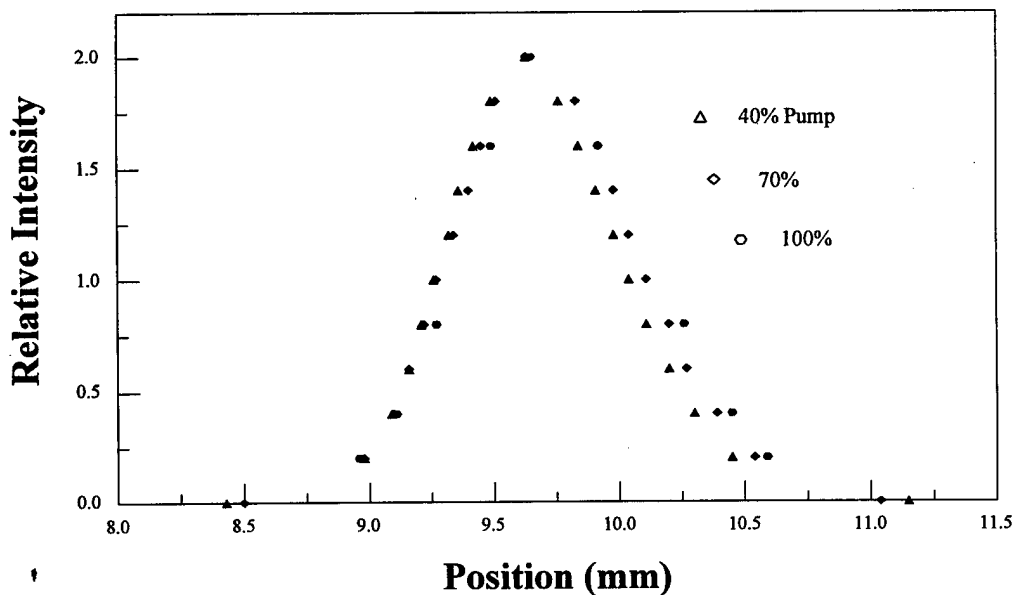


**Figure 23. Vertical Intensity Profiles for the Single Pass Amplifier at Different Pump levels. There was very little translation in this plane.**

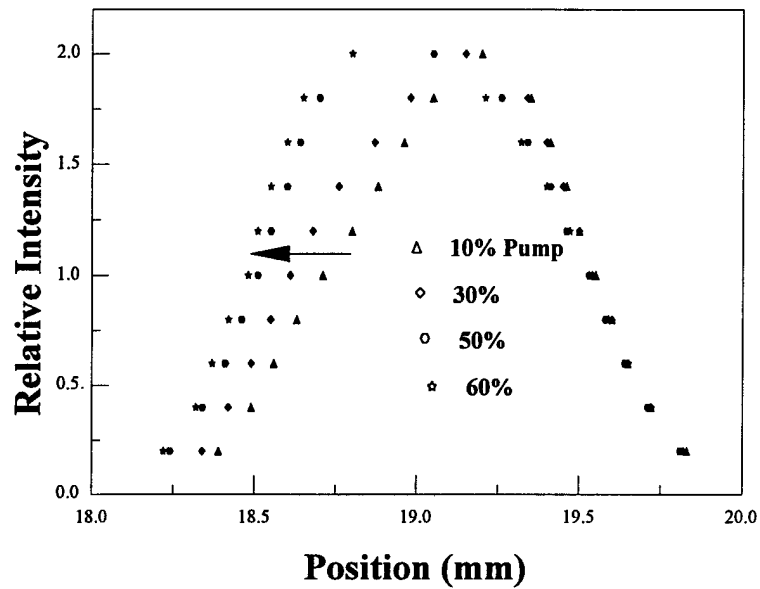


**Figure 24. Horizontal Intensity Profiles for the double Pass Amplifier. The beam profile has widened approximately 0.25 mm and shifted 0.5 mm left.**

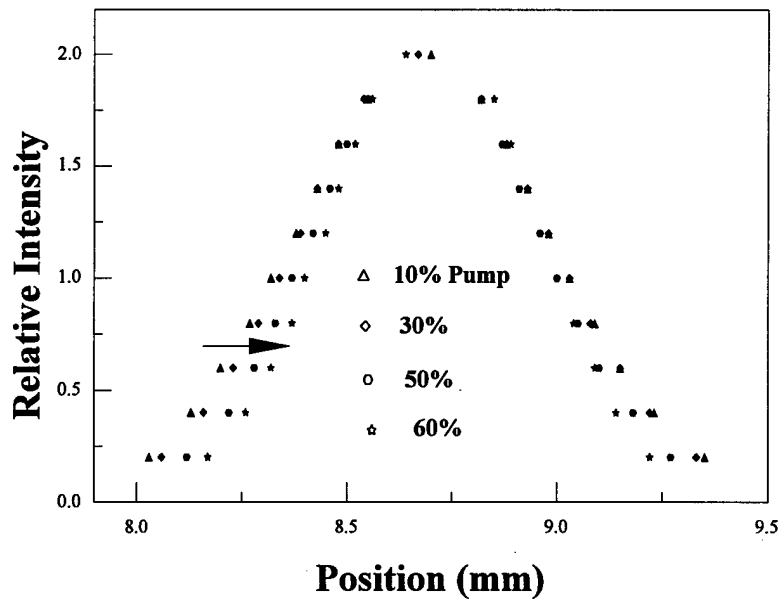


**Figure 25. Vertical Intensity Profiles for the double Pass Amplifier. The profile has narrowed slightly but remained centered.**

Saturated noise measurements on the slab amplifier verified that the gain did decrease as expected when the slab was flooded with additional 1.06  $\mu\text{m}$  radiation. A second Nd:YAG slab oscillator/amplifier head and a 7W Lightwave Laser were employed to make enough light to lower the gain in the main amplifier head. The main amplifier slab was pumped to various gain levels (30, 50%) and then laser light from the high power oscillator (1-18 Watts) was guided through a path which was angle multiplexed with the NPRO probe beam. The approach was to get enough overlap with the NPRO beam path through the head to saturate some of the gain region through which the probe beam passed. Figure 26 shows the saturation of the gain versus input power to the slab from the high power laser oscillator. It is apparent that 10's of Watts of power were needed to cause saturation. Total saturation was never attained. An additional 10 to 20 Watts of power would probably have been needed.

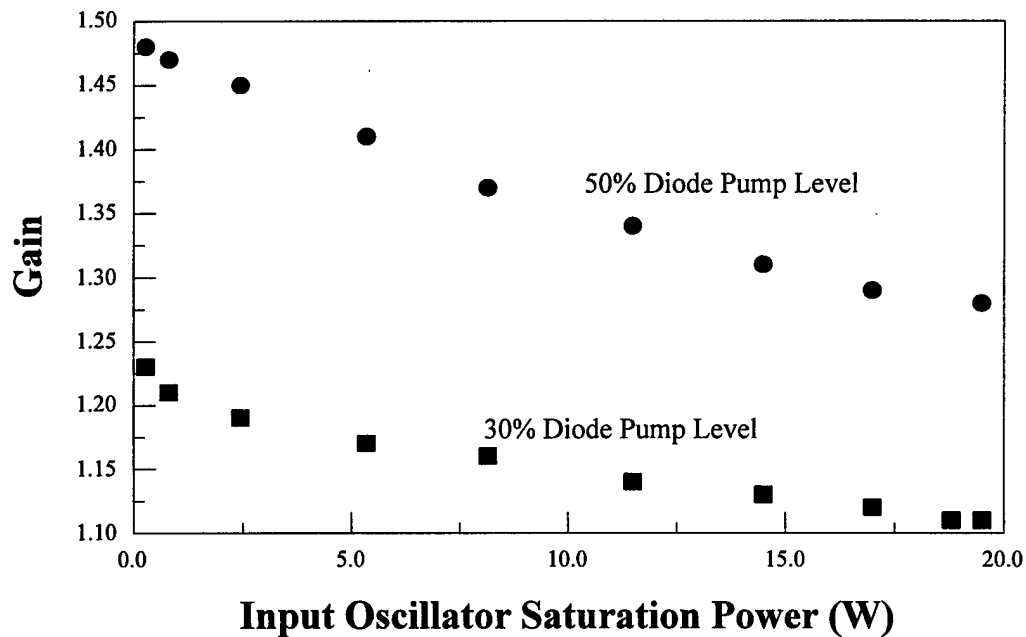


**Figure 26. Saturation Characteristics of the Nd:YAG Amplifier Slab. Two different amplifier pump levels were used to demonstrate saturation of the gain in the slab while oscillator input power varied from 1 to 18 Watts.**

The amplitude noise qualities for two NPRO 122-300 were characterized. (serial #118 and #282) These NPROs were different ages and run at different

currents. The plots below are in two different frequency regions. However, the RIN was expected to be within approximately 2 dB of the shot noise limit according to the manufacturer. They appeared to be shot noise limited at 15 MHz.

The NPRO #282 had a linewidth specified as 3 kHz. NPRO #118 had a linewidth specified as  $< 5$  kHz/msec. When the noise suppression circuit (noise eater) is active there is a slight increase of noise at 2 MHz. The NPRO favored the "s" polarization, showing an elliptical polarization of 89% i.e. normal to the plane of incidence, However, intensity plots indicated that the thermally induced birefringence of the slab may have lowered this from 89 to about 85%. This was deduced from a polarization extinction measurement performed on the head with the NPRO beam. The second NPRO was used as the probe laser throughout the experiment. There are several interesting things to note about the noise traces of NPRO #282 in Figure 28. The top two traces are the NPRO, which is shot noise limited at two different photocurrents (4 mA and 1 mA) at 15 MHz. The other thing to notice is the 14 dB of margin above the electronics floor, the lower trace.

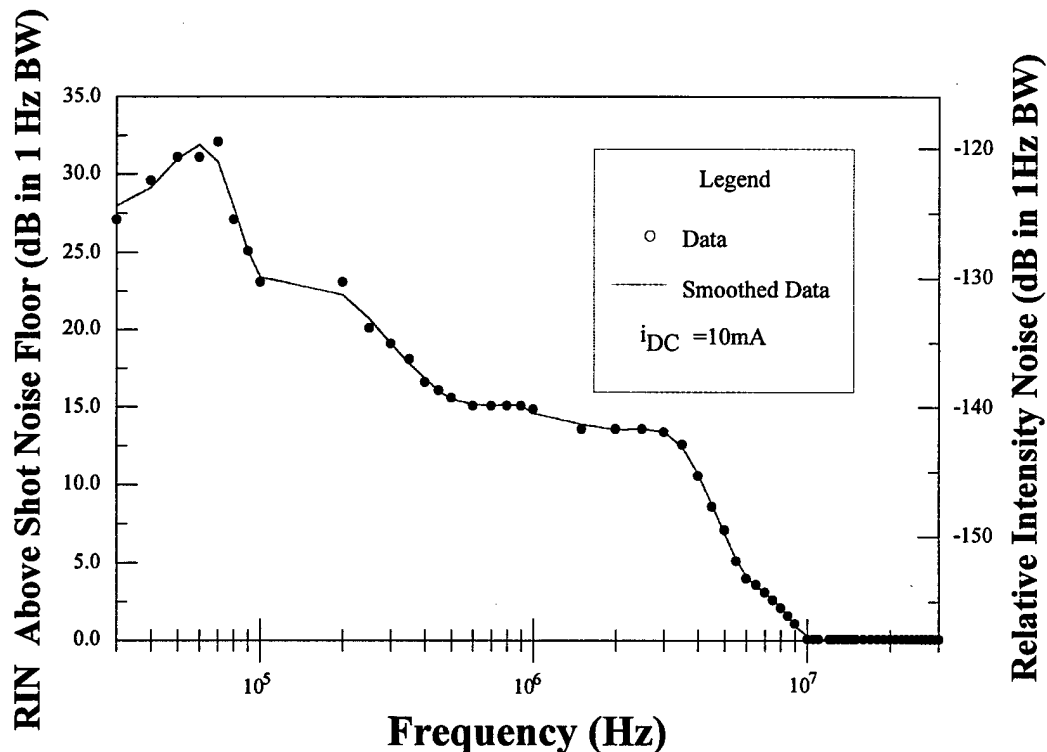


**Figure 27 NPRO Serial # 118 Noise Power Spectral Density Plot. This NPRO is shot noise limited at approximately 10 MHz.**

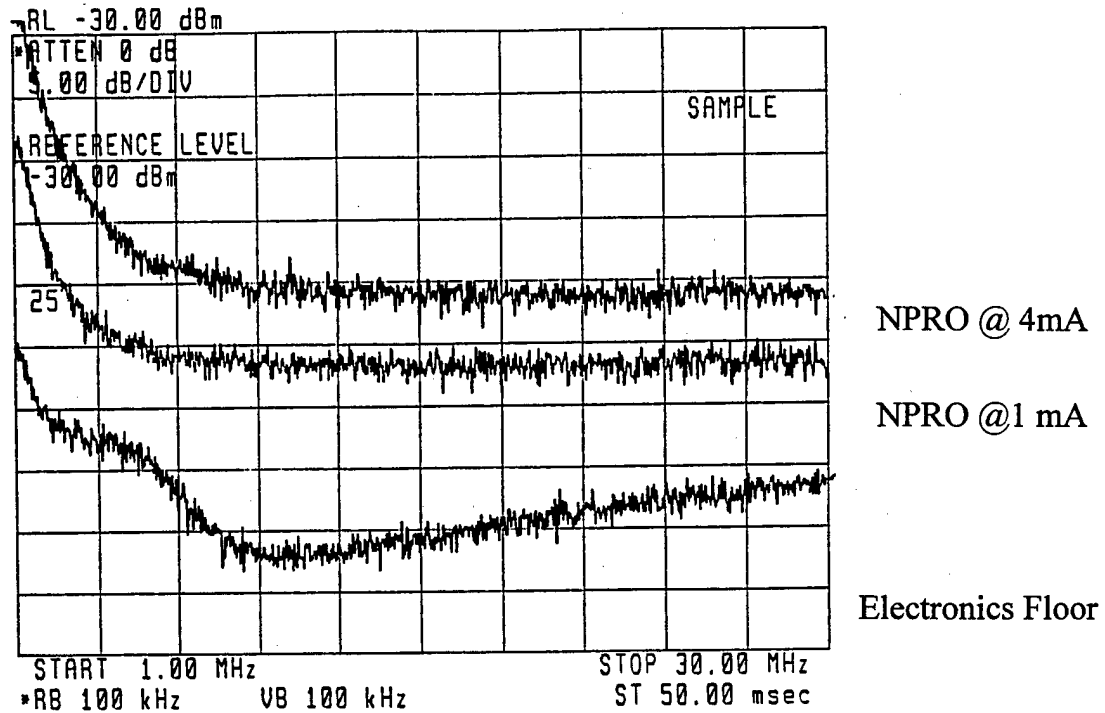


**Figure 28. NPRO Serial #282 Noise Power Spectral Density Plot.**

### 4.3.2 Experimental layout

Most of the components in the following diagrams have been described in detail elsewhere in this thesis. One note, however, concerns the optical isolator. It was an Electro-Optics Technology Model 1845 Faraday Isolator with greater than 30 dB isolation. It is known that even small feedback into a laser system can cause multi-mode instabilities. This was to be avoided in this experiment.

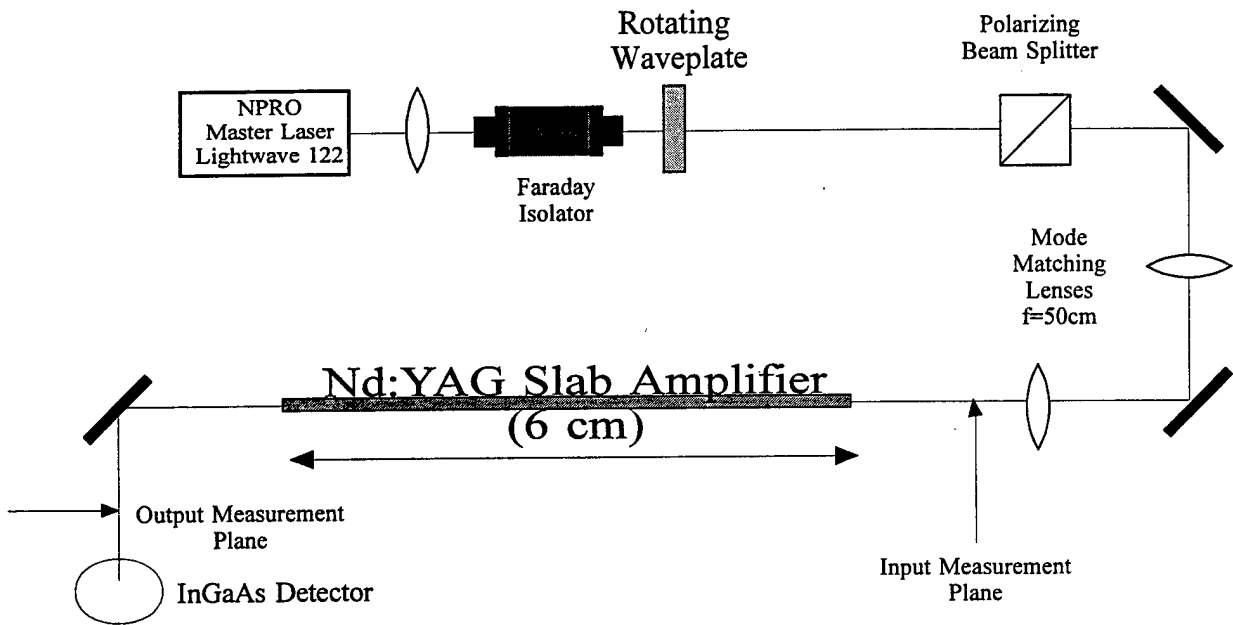


Figure 29. Layout of Linear Amplifier Single Pass Set up

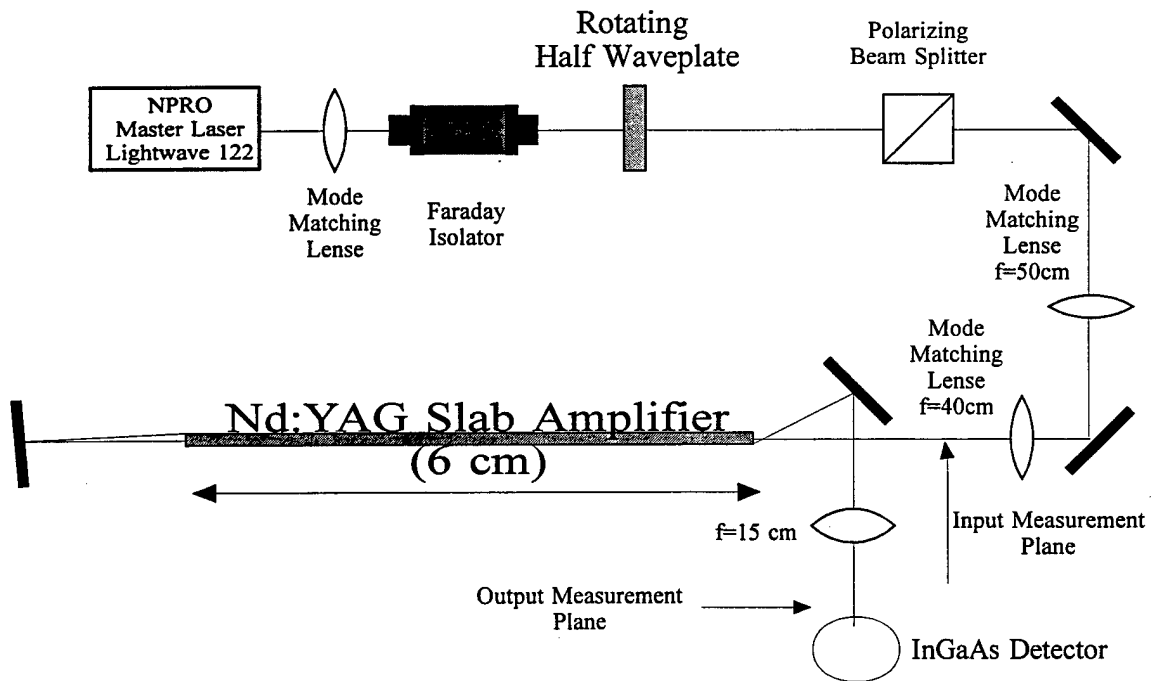
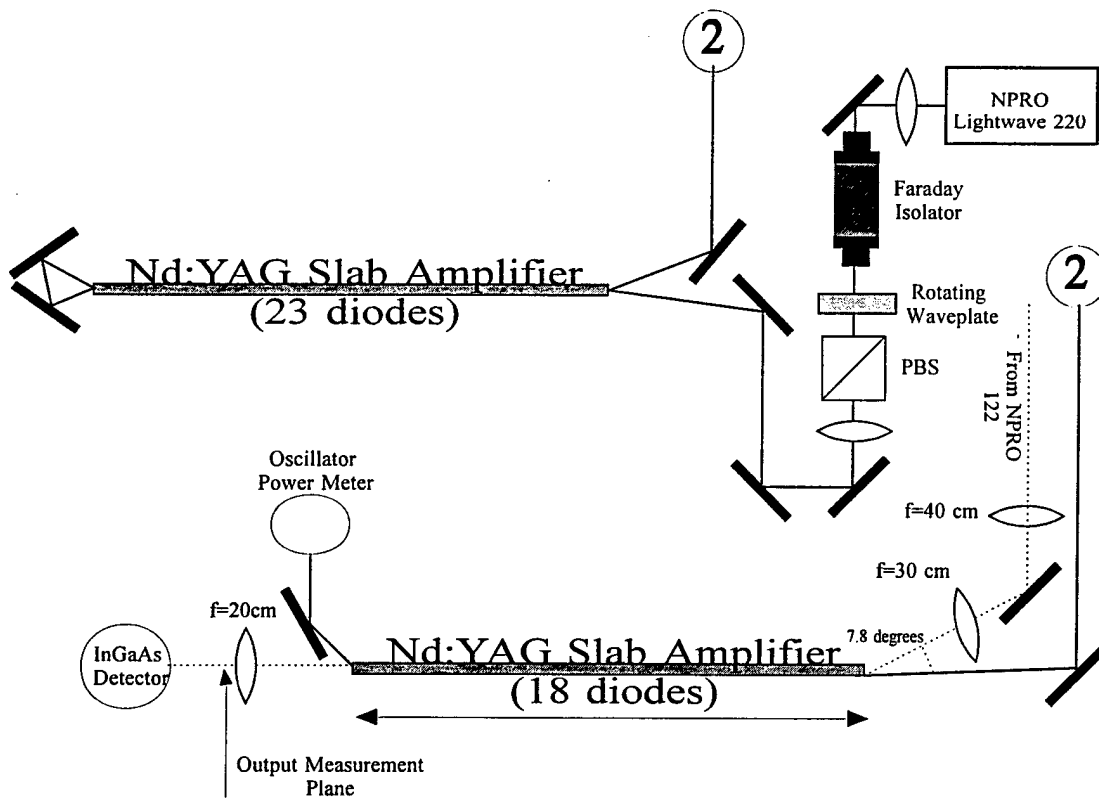


Figure 30. Layout of Double Pass Setup



**Figure 31. Layout of Saturated Amplifier**

### 4.3.3 Technique for Gain and Noise Measurements

#### Technique for Gain Measurements

Once the experimental equipment had been characterized and the layouts settled, two measurements were needed: the gain values experienced by the NPRQ probe beam and the noise plots from the spectrum analyzer. Of the two, the gain measurements required multiple steps and were more prone to experimenter error. Data was taken in most cases with 30% increments to conserve the diodes, fiber couplings and seals on the amplifier head. The thermo electric coolers (TEC's) would also get extremely hot, causing the diodes to drift and the gain to roll off. In some cases, the room was too warm to operate the system for long periods of time.

In theory the gain measurement was straightforward. Two different power meters, the Moletron 500D thermal power meter with the PM-10 head and a Newport 385 silicon large array detector power meter with the 883SL head were used to obtain the in and output powers of the Poisson stream and the ASE at the measurement planes indicated in the experiment layouts. Both meters were

eventually fitted with identical apertures. It was necessary to block the backs of the thermal meters to prevent pick up of stray ASE and drift.

As a first step in each measurement, the 1 mA photocurrent was established at the detector by modifying the NPRO probe input power into the amplifier. Then the power meters were shifted and inserted in the measurement planes before and after the amplifier. Each time the detector was shifted to the other measurement plane it was nulled to the ambient light conditions. ASE was measured at the output plane with the NPRO blocked. Then the NPRO beam after the amplifier was sampled. The power meters were then removed and the spectrum analyzer recorded the noise spectrum.

The spectrum analyzer video and resolution bandwidths were set to 100 kHz with a video average of 200. The center frequency of 15 MHz was bracketed by a 1 MHz wide spectrum trace. The shot noise floor was recorded with only NPRO light prior to amplifier turn on. The shot noise floor trace was stored in the spectrum analyzer, then noise power spectrums for various pump levels were recorded and displayed together to measure the relative noise power level above the shot noise floor.

Power gain,  $G$ , from the amplifier was calculated by taking the output power, subtracting the ASE and background and then dividing by the input power. At higher powers only the Coherent 100 Watt power meter was used. The use of two different thermal meters (PowerMax and Coherent) caused some discontinuity in the data taking because it was unusual to get them to agree precisely. The same Newport 385 detector was used to sample the NPRO beams before and after the amplifier. Prior to each power measurement the Newport 835 was nulled to the ambient light conditions. Thermal steering in the amplifier head, described earlier, required the detector to be re-centered and optimized to the highest voltage reading for each measurement.

Saturated gain measurements were more challenging. Ensuring high power (10-20 Watts) laser alignment and adequate overlap with the probe beam passed required numerous adjustments. Beam radius measurements were taken before and after the slab under various conditions to ensure no clipping. Also, due to the high power of the laser used to saturate the amplifier head it seemed safer to set the NPRO input probe beam power and not change it for the duration of the experiment. That ensured that there would be no need to reach across the area where the high power beam was traveling. The amplifier had to be pumped as high as possible and then saturated as hard as possible to get some dynamic range

to the measurements. The amplifier was run at 70% and the oscillator could be run almost to 20 Watts.

### Technique for noise measurements

As explained in the theory section the NPRO was used as a local oscillator and the ASE acted as the signal for homodyne detection. The NPRO was routed through both single pass and double pass (angle multiplexed) configurations. This was in an attempt to increase the amplifier gain  $G$ , and hence the dynamic range of the experiment. The intensity profiles of the beams after the single and double passes through the amplifier quantified the beam steering and provided a basis for estimating the optical efficiency values.

The second requirement was to always take noise power data in terms of the shot noise level for a specific DC photocurrent so that data would be comparable. A 1 mA current was established on the InGaAs detector and verified by a Fluke 83 DMM. This set the value of  $\langle n \rangle G \eta_{L1} \eta_{L2} \eta_d$  for the shot noise from Equation 3.10. Since  $G$  would be known by taking the gain measurements,  $\langle n \rangle \eta_{L1}$  would be known from the “power-in” measurements, that left the combination of  $\eta_{L2} \eta_d$  as the only unknown. Since this was also the only unknown factor appearing within the noise term, even if the  $\eta_{L2} \eta_d$  term was not known a priori, it could be calculated from the shot noise. Then this value would be inserted into the noise term to verify the theoretical fit to the data. With this approach, even if either efficiency,  $\eta_{L2}$ ,  $\eta_d$ , changed it would be transparent to the theory.

It is valid to criticize this fitting approach. However, the alternatives of determining all the constants in the shot noise power equation,  $\langle n \rangle$ ,  $G$ ,  $\eta_{L1}$ ,  $\eta_{L2}$ , and  $\eta_d$  would introduce even more error, due to the fact 4 or 5 measurements ( $\eta_d$  might be considered a true constant, in which case only 4 values would need to be measured) would be multiplied together. Also, if after the measurements the total multiplication did not result in the same photocurrent for each measurement, then each measurement would have to be normalized to one photocurrent shot noise value in order to be plotted on the same graph.

Another option would have been to alter the gain  $G$ , and  $\eta_{L2}$  and leave the rest of the terms, i.e.,  $\langle n \rangle \eta_{L1} \eta_d$  alone. This method would then assume that the detector quantum efficiency does not change, which is possible, and that the  $\eta_{L2}$  term could be measured with the same precision as the laser noise power. Based

on these considerations the choice of experimental method with the minimum number of measurements and minimum number of assumptions was used.

The saturated amplifier noise measurements were taken in a different way. In this case, for safety, the incoming beam was fixed in power. Then the gain was found assuming the input power and efficiency on the first leg did not change throughout the experiment.

Finally, the spectrum analyzer was calibrated at the factory just prior to the experimentation and carried a noise floor of (-150 dBm). The amplifier thermal noise was at -144 dBm, the detector and amplifier combination (electronics floor) produced a noise floor at -120 dBm and the shot noise floor for 1 mA was at approximately -105.5 dBm. This left a margin of approximately 15 dB for the measurements.

#### 4.4 Results and Analysis:

By far the measurements of gain were the most difficult and most prone to error. The steering and subsequent clipping of the beam at the Nd:YAG slab amplifier apertures made it difficult to obtain power readings with the double pass configuration. Hence, for the double pass configuration, the small signal gain was calculated separately from the noise data by using a 1 mW NPRO input beam and the output beam power as the pump percentage was increased. Data above 70% pump power was not used. This procedure improved the consistency of the gain measurements versus pump percentage.

The linear amplifier noise power stated as multiples above the shot noise is plotted versus the amplifier gain in Figure 32, with the dashed lines indicating the best linear fit. Error bars are given for both gain and noise power multiplier. The abscissa indicates the power gain,  $(PowerOut - ASE)/PowerIn$ , while the ordinate plots the  $(1 + 2(G - 1)\eta)$  noise multiplier above the shot noise floor, Equation 3.10. It is very important to subtract the ASE from the "Power Out" to obtain the correct gain value. The slope of the best fit line gives the overall "efficiency factor" for each configuration but it is not necessary to know this factor to verify the linear behavior. The power measurement errors represent half of the least significant digit value. The noise power error was derived from a slight drift (1 dBm) of the indicated noise power upward when the spectrum analyzer averaged 200 traces, and a 0.1 dBm error for reading the data from the spectrum analyzer plot. Error bars for the gain and noise measurements were calculated using Bevington<sup>5</sup>. The

results agree very well with the theory as is evidenced by the linearity of the data and the near unity intercept as power gain,  $G$ , decreases to 1.

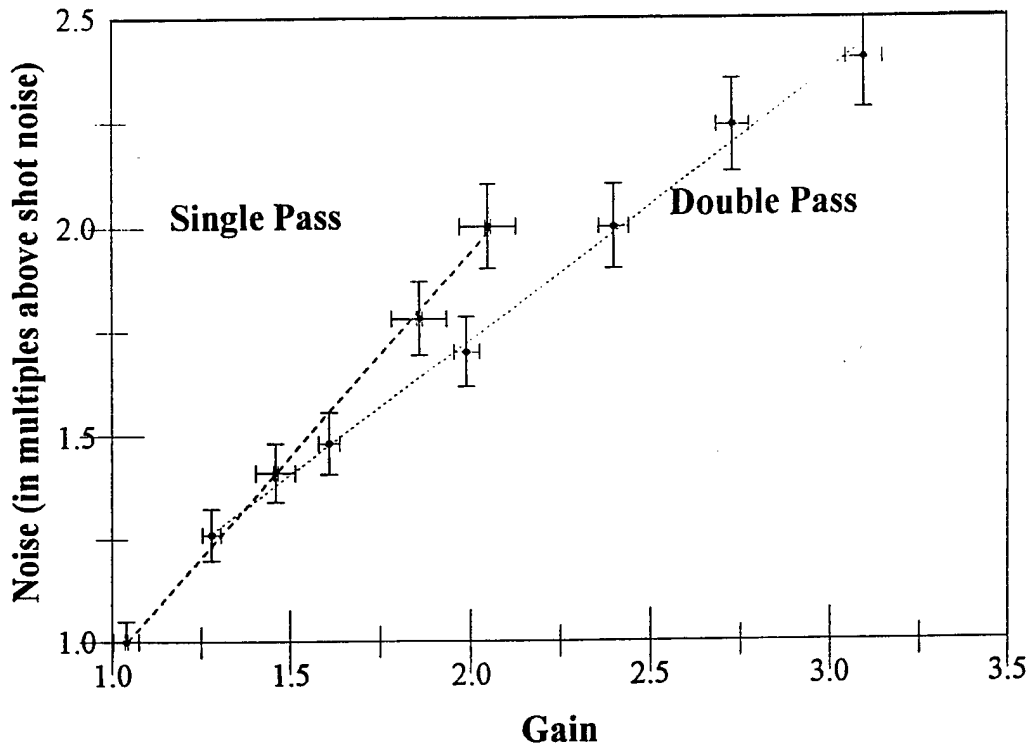


Figure 32. Nd:YAG Linear Amplifier Noise

The analysis becomes more complex when reviewing the overall efficiency factors. Recall that the requirement for taking the noise data was to always reset the DC photocurrent to 1 mA to ensure comparability of noise data points. While doing this procedure it became apparent that something unexpected was happening to the product of  $\eta_{L1}\langle n \rangle G$ . As the gain  $G$ , was turned up, the number of input photons  $\eta_{L1}\langle n \rangle$  was going down, i.e., the measured NPRO input power was decreasing, but the product  $\langle n \rangle G \eta_{L1}$  was not a constant. This implied that one of the other efficiencies out of  $\langle n \rangle G \eta_{L1} \eta_{L2} \eta_d$  was also changing. It was assumed that it was the  $\eta_{L2}$  value and hence the need to “fit” the points with a calculated  $\eta_{L2}$  value. Even after this fitting effort, the calculated efficiencies did not agree with the rough estimates of what  $\eta_{L2}$  should be. This residual error cannot be accounted for in the linear theory, Equation 3.10, unless it would be acceptable for the detector efficiency to vary greatly. This seemed an unlikely possibility due to the excellent linearity of the detector itself. Another possible explanation follows.

One of the assumptions used in deriving Equation 3.10 was that there would be a single mode and the overlap of these modes would be perfect. This is the

point at which that assumption probably broke down. An additional efficiency term needed to be added to take into account two different "geometric" problems occurring in the overlap of two photon fields. First, the NPRO beam is a Gaussian beam and the ASE is a much more uniform distribution of photon flux. This automatically creates a difference in homodyning efficiency. Also, the angle offset  $\Theta$ , of the phase fronts of the two modes would cause the homodyning efficiency of the two modes to decrease substantially. Based on a paper by Cohen<sup>6</sup>, the homodyne efficiency of a Gaussian beam overlapping a uniform intensity field was explored. The factors affecting the efficiency were the angle of the phase front misalignment,  $\Theta$ , the beam radius of the Gaussian distribution,  $w$  and the diameter of the detector active area,  $r_0$ .

Qualitatively, as the gain in the amplifier increased and the NPRO beam was being thermally steered, the angular alignment with the ASE was changing. At low gain, the NPRO and ASE overlapped with very little angle offset but this angle changed at higher gains. Also, at higher gains, the shape of the Gaussian got broader and the overlap with the ASE profile got better, especially in the double pass case. These two effects, depending on the ASE profile, could actually cancel each other somewhat, giving a situation where initially the angular offset dropped the homodyne efficiency quite a bit, but then the improved overlap with a larger area beam somewhat compensated. In Figure 33, the ASE profiles of the slab amplifier are plotted for the vertical and the horizontal. In the vertical case, the ASE was centered and uniform. In the case of the horizontal ASE, it was off centered and clipped on the positive displacement side. This asymmetry in ASE intensity profile was particularly disturbing because the horizontal beam steering was the greater of the two. Essentially, the NPRO beam, which is only about a millimeter across, is centered at zero in the horizontal and vertical dimensions. In the case of the vertical dimension, since there was almost no beam steer and very little beam spreading, the vertical geometry changes did not contribute to a change in the homodyning efficiency. However, for the horizontal case, the NPRO beam overlapped the horizontal ASE on the left slope of the curve. The NPRO beam shifted left and its cross section expanded with increasing gain from the amplifier. So, even though the intensity overlap was decreasing, the area of overlap was increasing.

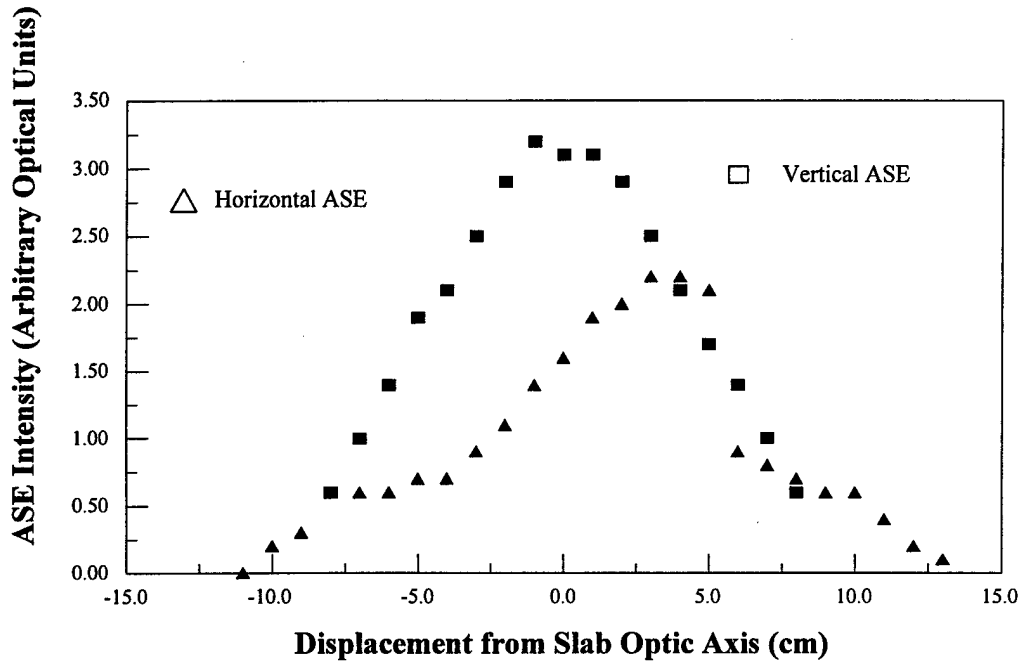


**Figure 33. ASE Intensity Profiles for Slab Amplifier. The asymmetric horizontal ASE profile contributed to a lower homodyning efficiency**

The corrections to the total efficiency using the homodyne efficiency are made to Equation 3.10 in the following way. The homodyning efficiency of the NPRO beam with itself is defined as one. The homodyne efficiency of the NPRO Gaussian beam with the more uniform distribution of ASE will be called  $\eta_{\text{hom}}$  and Equation 3.10 will be rewritten as

$$\sigma_d^2 = G\langle n \rangle \eta_{L1} \eta_{L2} \eta_d (1 + 2(G-1) \eta_{L2} \eta_d \eta_{\text{hom}}).$$

The interaction of the change in  $\eta_{L2}$  and  $\eta_{\text{hom}}$  can be described as follows. In the single pass case, the optical path efficiency decreased from 0.96 to 0.71, ( as the amplifier was increasingly pumped from 10 to 100% ) mostly due to aperturing inherent in overfilling the detector. ( 0.5 mm spot on a 0.3 mm detector ) At the same time, the homodyne efficiency went from about 70 percent to almost 100 percent. In the double pass case, optical path efficiency went from 0.87 down to 0.61 while the homodyne efficiency oscillated between 0.73 and 0.85. These trends are plotted in Figures 33 and 34. When these corrections are made, the homodyne efficiencies account for the discrepancies noted in the overall system efficiency.

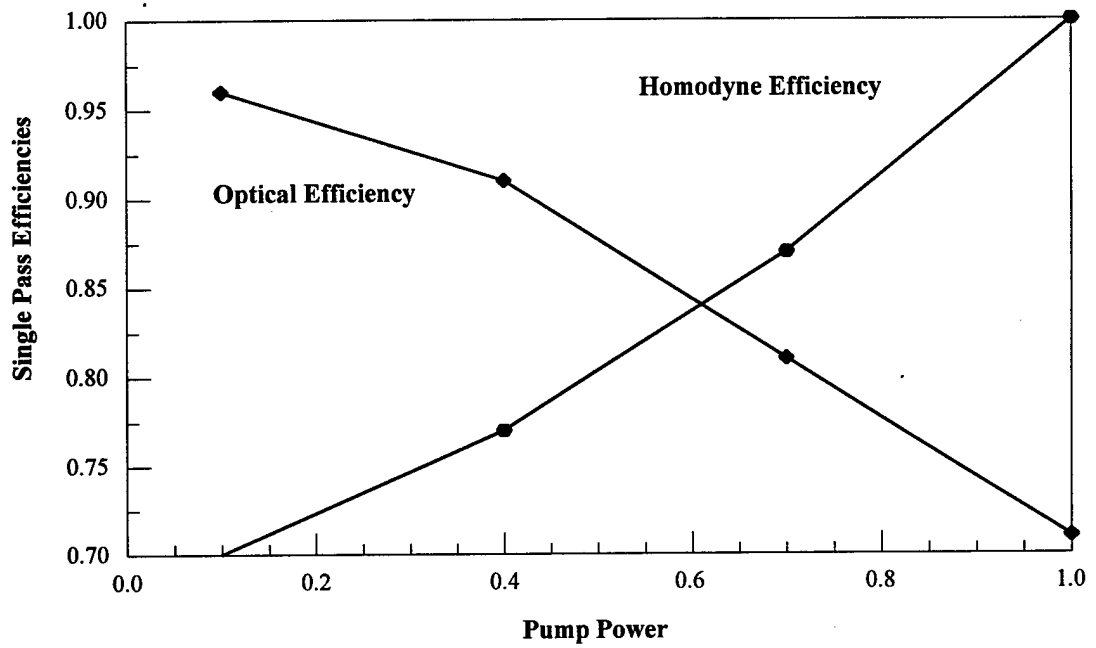


**Figure 34. Efficiencies for Single Pass Case. Overall optical efficiency appeared to decline, while homodyning efficiency improved with pump power level.**

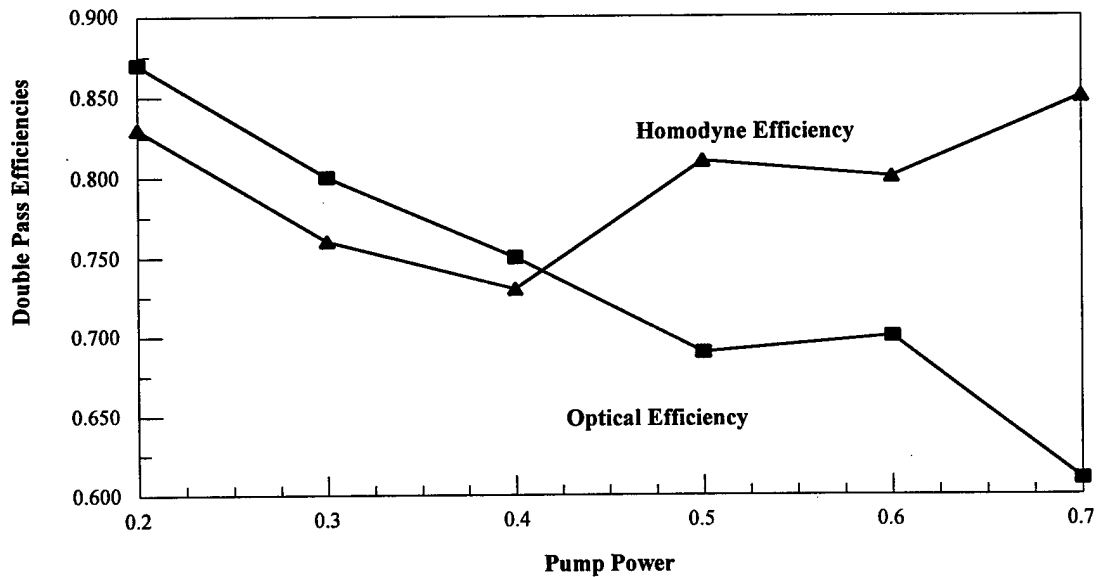


**Figure 35. Efficiencies for Double Pass Case**

The techniques for actually calculating the homodyne efficiency are fairly straightforward. First a few simple definitions. The homodyne detection parameter will be defined as

$$\gamma = \frac{\eta_{\text{hom}}}{\eta_o},$$

where  $\eta_{\text{hom}}$  has already been defined and  $\eta_o$  is the standard detector efficiency. This means that when  $\gamma$  is one, the homodyne efficiency is essentially one and only the detector quantum efficiency remains. The uniform ASE is essentially a constant over the area of the detector and zero elsewhere. This means that there is an aperturing function at work. The overlap integral essentially goes to zero outside the detector area. The Gaussian local oscillator parameter, in this case the one associated with the NPRO, is defined as

$$Z_o = \frac{r_o}{w}.$$

The governing equation for the small angle approximation for this particular homodyning situation is<sup>7</sup>

$$\gamma(Z_o, r_o, k, \Theta) = \gamma_o \left\{ 1 - \frac{1}{2} \left( \frac{kr_o \Theta}{2Z_o} \right)^2 \left[ 1 - \frac{2Z_o^2}{\exp(Z_o^2) - 1} \right] \right\}^2,$$

where

$$\gamma_o = \frac{2}{Z_o^2} \frac{[1 - \exp(-Z_o^2)]^2}{[1 - \exp(-2Z_o^2)]}.$$

Values for the homodyne detection parameters for the Gaussian-vs.-uniform and the uniform-vs.-uniform case for an optimum choice of  $Z_o$  are found in Figure 36.

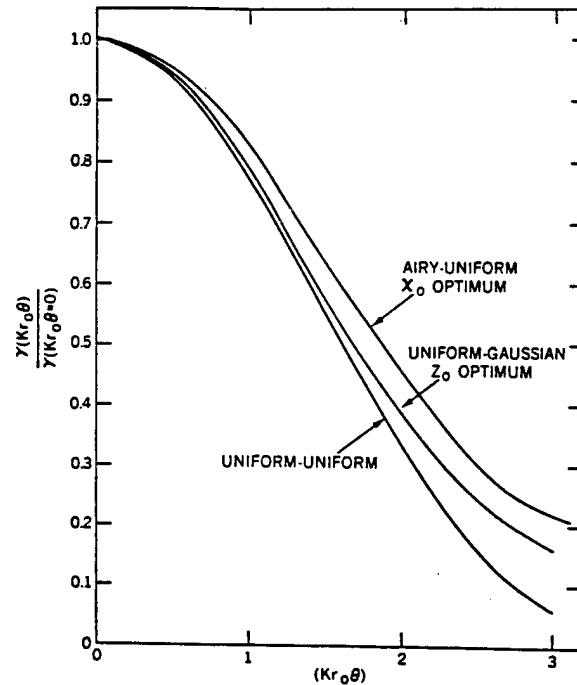


**Figure 36. Homodyne Detection Parameter Degradation with Increasing Phase Front Misalignment. [From Cohen<sup>8</sup>].** The vertical axis depicts the homodyne parameter value normalized to the optimum Gaussian beam size for a given detector radius. As the phase front misaligns, efficiency declines.

For non-vanishing phase misalignments,  $\Theta$ , there is a decreasing homodyne efficiency when normalized to the maximum detection parameter. For those situations where the phase front mismatch angles,  $\Theta$ , are zero, the homodyning efficiency approaches 1. As the angle of mismatch increases, the efficiency drops. In this particular case,  $kr_0 = 890$ . This makes the system very sensitive to the angle of misalignment.

The experimental data for the saturated amplification experiment was inconclusive. The dynamic range over which saturation occurred was not sufficient to obtain meaningful noise power readings.

In summary, the amplitude noise power of a linear traveling wave solid-state amplifier has been demonstrated to follow a simple quantum mechanical formulation as shown in Figure 32. A homodyning efficiency term was added to bring the experimental and the theoretical data into better agreement. The experimental techniques were focused on the relative noise power measurement above the shot noise floor in units of shot noise power for different power gains of the amplifier. The system was operated CW and data taken at 15 MHz in order to verify the noise properties of a laser system which could be used in the current LIGO design.

## Chapter 4 References

1. M. Harris, R. Loudon, T.J. Shepard, and J.M. Vaughan, "Optical Amplification and Spontaneous Emission in an Ar<sup>+</sup> Discharge", *Journal of Modern Optics*, Vol. 39, No. 6, p. 1195 (1992).
2. R.J. Shine, A.J. Alfrey and R.L. Byer, "A 40 W cw TEM<sub>00</sub> mode, diode-laser-pumped, Nd:YAG zig-zag miniature-slab laser", *SPIE Vol. 2379*, p. 112 (1995).
3. R.A. Marsland, "Selection and Application of High-Speed Photodetectors", *The Photonics Design and Applications Handbook*, (1993), p. 106.
4. T. Kane, "Intensity Noise in Diode-Pumped Single-Frequency Nd:YAG Lasers and its Control by Electronic Feedback", *IEEE Photonics Technology Letters*, Vol. 2, No. 4, p. 244 (1990).
5. P.R. Bevington, *Data Reduction and Error Analysis for the Physical Sciences*, (Mc Graw Hill, San Francisco, 1969).
6. S.C. Cohen, "Heterodyne detection: phase front alignment, beam spot size and detector uniformity", *Applied Optics*, Vol. 14, No. 8, p 1953 (1975).
7. S.C. Cohen, "Heterodyne detection: phase front alignment, beam spot size and detector uniformity", *Applied Optics*, Vol. 14, No. 8, p 1956 (1975).
8. S.C. Cohen, "Heterodyne detection: phase front alignment, beam spot size and detector uniformity", *Applied Optics*, Vol. 14, No. 8, p 1958 (1975).

## Chapter 5

### Conclusion

#### 5.1 Summary

The primary goal of this study was to characterize the amplitude noise properties of solid state laser amplifiers and oscillators. This amplitude noise knowledge, when coupled with the phase noise knowledge, will allow a more complete understanding of the engineering trade-offs in the design and construction of the LIGO system. In particular, this study effort was driven by the desire to make an early design decision between high power Nd:YAG amplifiers and injection locked oscillators for the ultra-quiet laser source embedded in the LIGO interferometer.

The theory portion of this study was devoted to the analysis of the linear and non-linear traveling wave amplifier and injection locked oscillator amplitude noise properties. After examining the classical (STT), semi-classical (Yamamoto) and quantum mechanical (Loudon, etc.) based approaches, the amplitude noise power of the traveling wave amplifier was shown to follow a simple quantum mechanical formulation given by Equation 3.10. Though there are demonstrated parallels with the semi-classical theory, the quantum mechanical approach demonstrates the amplitude noise is an artifact of the statistics of the photonic stream itself, not the photodetection process. The quantum mechanical theory ensures the proper interpretation of the effect spontaneous emission has on amplitude noise levels found on a photonic stream experiencing amplification. However, due to the assumptions of very high photon number and very low optical mode number, the quantum mechanically derived noise expression should only be used in high power solid state amplifiers. In addition, a simplified expression for the amplitude noise in an amplifier chain was included in anticipation of the need to use this approach in the LIGO design.

The analysis of the injection locked oscillators was based on a comparison of three recent and popular approaches to the amplitude noise problem, the

Transfer Function Approach (TFA), the electrical circuit model approach (RLC) and the Quantum Langevin Approach (QLA). Each approach has its advantages and disadvantages. The most important outcome of this portion of the study was the realization that sub quantum level noise performance was possible under particular circumstances. More precisely, it may be possible to attain sub shot noise limited performance from an injection locked system in the low frequency regime of interest (100 Hz to 10 kHz in LIGO). Since the injection locked laser is so sensitive to its pump source at these low frequencies, using sub quantum level amplitude noise pump sources would translate directly into similar noise performance for the injection locked laser system as a whole. This assumes there is no electronic feedback loop in effect in this region. If this system could be built, it would have the best possible amplitude noise performance. It may be possible to obtain quantum noise limited performance by filtering the laser output with a mode cleaner prior to entering the interferometer. Realistic engineering considerations are discussed below.

After completing a broad review of the theory area, the experimental efforts took a narrower scope. Since the amplifier studies appeared simpler to implement in the lab than the injection locked systems and with the knowledge that other groups were addressing the injection locked oscillator noise, this study only examined amplifier noise experimentally.

The experimental work had mixed outcomes. The linear single and double pass efforts supported the quantum mechanical theory to a point. The data supported the form of the amplitude noise power equation but indicated an inconsistency in the experimental efficiencies. The saturated amplifier work was inconclusive, most likely due to inadequate dynamic range. Basically, the linear amplifier experimental efforts uncovered the need to include a homodyning efficiency term. This was beneficial for several reasons. It exposed a shortfall in the theoretical assumptions, but it also opened up numerous areas for further characterization and application of this effect. Including this new efficiency term in the noise power equation provides excellent agreement between theory and experiment.

The original goal of this study was to determine whether the amplifier or the oscillator had the better amplitude noise performance for LIGO applications at 10 to 100 Watts. The answer is the injection locked oscillator is quieter in theory. It can be quantum noise limited at the phase modulation frequency of 15 MHz if its master laser is quantum limited at that frequency. Since there are already

quantum limited master oscillators available at this frequency this becomes an engineering problem to couple the two together. At the low frequency end of the spectrum, where the gravitational wave interaction occurs, the injection locked oscillator can always perform better than the amplifier if no electronic feedback systems are used. This assumes no additional filtering after the amplifier. In addition, as mentioned earlier, if injection locked oscillator pump sources, with sub quantum level performance are available, then this makes the comparison "no contest". In the amplification regime near the resonant relaxation oscillation, the amplitude noise properties of the injection locked system will be far worse than the amplifier system, but this should be inconsequential to the LIGO design. In summary, the amplifiers will always have greater than shot noise level amplitude noise due to the creation of amplified spontaneous emission, while the injection locked oscillators will not.

## 5.2 Further Work

### Theory

There are numerous areas for expanding and improving this research effort. In particular, further work could be aimed at refining this approach as it applies to the LIGO laser source. If so, there are several important engineering considerations to keep in mind.

Since the LIGO is built around very large and very carefully environmentally controlled optics, it is very important to consider the effect of the optical source on them. For example, it would be far better for the optical source to degrade gracefully rather than suddenly fail. This "soft failure mode" would maintain power on the interferometer mirrors, which is essential for maintaining thermal loading and hence maintaining the correct radius of curvature of these devices. Assuming the problem with the optical source was repairable while in operation, though the interferometer would not be usable for taking data during repairs, it would take less time to bring the interferometer back up to thermal balance. This would be an important feature to help ensure the LIGO can meet its operational availability requirement of  $> 99\%$ .

The second engineering consideration is the need to scale the system to ever higher optical power. Amplifiers by their nature allow power scaling. By adding amplifier modules, the laser can be geometrically scaled to hundreds to thousands

of Watts of low noise optical power. Would it be possible to do the same with injection locked oscillators without severely limiting the locking range?

The third requirement is that the system must be more efficient. This will probably mean the use of semi-conductor lasers in the design regardless of the solid state material chosen for the active medium. So, additional work in the noise properties of diode lasers is critical.

The LIGO system must be designed with all noise processes taken into consideration. As was mentioned in the introduction, the amplitude noise is only part of the problem. The frequency noise must also be characterized. Trying to optimize the amplitude noise solution all the way down to the quantum mechanical level will make the conjugate frequency noise problem more difficult. Technical noise from feedback systems and cooling systems will affect the optical control and hence the optics themselves. Designing the most sophisticated control system for the laser would be senseless if it destroyed the sensitivity of the interferometer.

To meet these engineering challenges, the first step would be to modify the assumptions of the linear theory for a more in-depth noise study. It is necessary to include the effect of multiple mode structures such as the super Gaussians in the noise calculations. The next step would be to work on improvements to the amplifier chain noise calculations and follow that with a double amplifier experiment. It would probably be worthwhile to revisit the parametric amplifier. It is possible to use the parametric amplifier to generate squeezed states. If there were a way to use more of the idler wave and increase the system efficiency, this could be a very good candidate amplifier.

The work on noiseless pump sources for the injection locked systems should be given a very high priority. Though the injection locked system may not be the current design choice for LIGO, due to the complexity involved in keeping it locked to the master laser, it is very important to verify whether the oscillator, with the low noise pumps, has enough noise advantage over the amplifier to employ in LIGO. The problem with these sub shot noise photon streams is that their noiseless properties are easily lost at beam splitters and ports, due to the coupling of the radiation partition noise. After examining the optical noise characteristics of the injection locked system, an in-depth study of the trade off between electronically controlled injection locked lasers versus amplifiers is needed. It is necessary to know if an electronic feedback system, with nested control loops for the master and the slave laser, can be used. Does the excess noise, 3 dB, added by the electronics and the more complex design necessarily

eliminate the oscillator from competition? For that matter, any system that relies on a sample beam as a comparison standard can be best attain the same SNR as that beam. So if the amplifiers have control systems which use beam sampling, they would not necessarily perform better than the injection locked systems. As a rule, weak sample beams have poorer SNR ratios, but even sampling up to 50% of the total beam power will still leave a system with the excess noise added by the electronics.

### **Experimental Apparatus**

There is always room for improvement in the experimental apparatus. One area of improvement that would pay big dividends would be to start work now on a low noise detector which could handle the much higher photocurrents expected on the LIGO interferometer dark fringe. While developing this detector it would be imperative to better characterize the photodetector frequency response by covering a much broader frequency range than was covered in this study. The detector studies could also include careful comparisons of the low noise balanced and resonant detectors at various frequency ranges.

In closing, probably the most important effort to improve these laser amplitude noise studies would be to improve the laser amplifier and oscillator. A laser head with low thermal induced steering, birefringence and beam jitter would have made this study much quicker, easier and more precise. Though it will not change the physics or the noise calculations per se, it would bring the ultimate LIGO laser closer to reality.

The techniques for characterization and control of optical amplitude noise can obviously be applied to even greater challenges than LIGO. A very careful definition of terms and most of all an understanding of the measurement planes used in taking and comparing experimental data would encourage even more rapid progress in overcoming these challenges. The demarcation between optical and electrical amplitude noise properties and units was maintained through out this study in order to achieve this additional goal.

**Appendix 1: Summary of Useful Equations**

Noise Power or Variance:  $\sigma^2 = \langle n^2 \rangle - \langle n \rangle^2$  (1.3)

Shot Noise Power in bandwidth  $\Delta f$ :  $\sigma_{SNL,i}^2 = 2qI_{DC}\Delta f$  (1.7)

Signal to Noise Ratio;  $SNR = \frac{\langle n \rangle^2}{\sigma_n^2}$

Fano Factor of Amplifier ASE:  $f = \frac{\sigma^2}{\langle n \rangle} = [1 + 2(G - 1)\eta]$  (1.8)

Photonic Linear Noise Equation:  $\sigma^2 = G\langle n \rangle[1 + 2(G - 1)]$  (2.3)

Photoelectron Linear Noise Equation:  $\sigma_d^2 = \sigma_{SNL}^2[1 + 2(G - 1)\eta]$  (3.10)

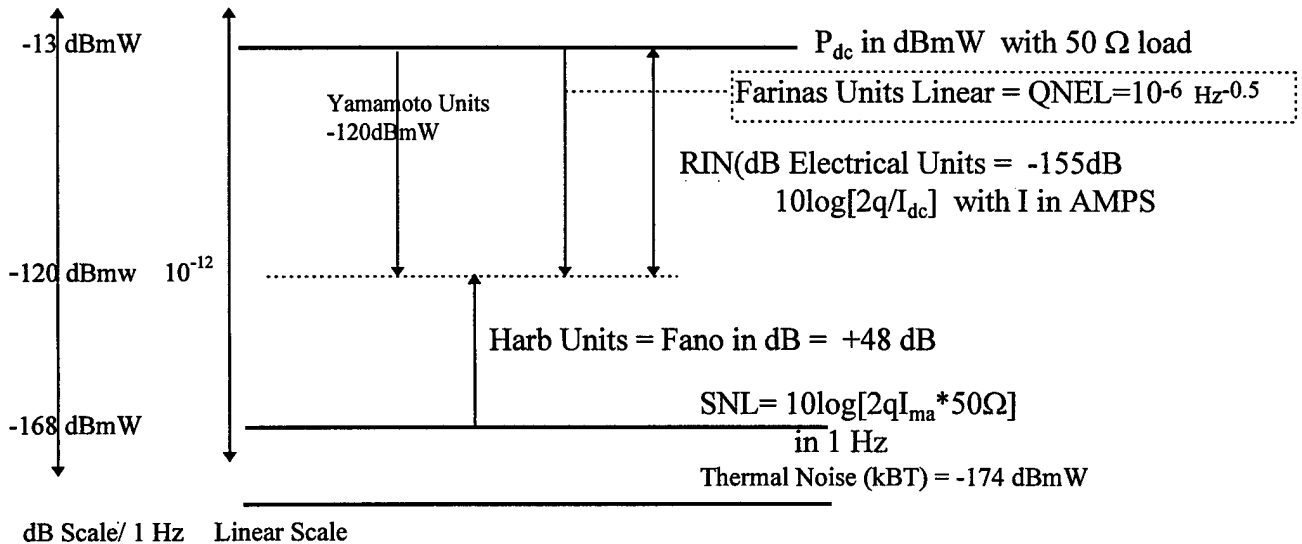
Linear Amplifier Chain (Type A) Noise Equation:  $\sigma_k^2 = \sigma_{SNL}^2[1 + 2(G - 1)\eta X_k]$  (3.14)

Non Linear Photonic Noise Equation:  $\sigma_s^{2^2} = G_s \langle n_o \rangle \left[ 1 + \left( 2 + \frac{1}{2} \right) (G_s - 1) \right]$  (3.16)

where  $X_k = \frac{1 - (\eta G)^k}{1 - \eta G}$ , k is the number of stages and  $\eta$  depends on type of amplifier.

$$RIN_{electrical\ units}(f) = \frac{Power_{RF}(f)}{P_{DC} \times Gain \times Resolution\ Bandwidth_{SA}} \text{ dB}$$

What 1 mA of photocurrent means in different systems:



## **Appendix 2: Optical vs Electrical RIN**

It was mentioned in section 2.1 that there are two types of RIN, optical and electrical. It was also stated that these two are not equivalent. This appendix explains this important difference.

As with any measurement theory, it is important to know the reference plane in which the measurement is taken. In the case of experiments designed to characterize optical noise power, there are two very important and distinctly different reference planes, the measurement reference plane just prior to the detector, described in optical units and the measurement plane just after the detector, described in electrical units. Whenever discussions of RIN occur it is very important to clarify which reference plane is being used for the comparison.

Though it is easy to talk about optical RIN, there is no way to actually measure it. This is not as difficult a situation as it appears. The photodetection process, due to its nature as a Bernoulli random deletion process, maintains the statistics of the particular photonic distribution it samples, and generates a faithful reproduction of the impinging optical signals. [D,159] There are known conversion factors for converting optical power to electrical current in the detector itself (the quantum efficiency and its derived unit the responsivity) as well as for the equipment used after the detector, the receiver. In this particular experiment the receiver is largely composed of an RF spectrum analyzer and it will receive the most attention. Note: though there are now what are called “optical” spectrum analyzers, these devices just perform the conversions internally. The basic concepts of what follows is still the same.

The conversion process in the spectrum analyzer is not one that can be represented by a linear multiplication factor, as it is for the detector. Rather there is quite a bit of uncertainty in the “absolute” measurements a spectrum analyzer does make, even when it is properly calibrated. Due to the use of heterodyning techniques and the need to integrate over fixed periods of time with imperfect filters, numerous conversion and adjustment factors need to be included to come up with a noise power measurement. For now, the two most important conversions are the square law conversion and the RMS conversion.

When an electrical spectrum analyzer measures “modulated” optical power, in this case, noise, that has been directly detected by a square law detector, the squared optical quantity (field amplitude), when converted to dB electrical units, causes a multiplier of 2 to move from the linear exponent to its position out in front of the logarithm. This is solely because of the choice to use units of dB. There is not twice as much electrical as

optical power. Secondly, an electrical spectrum analyzer is traditionally set up to provide an RMS value, which is a sinusoid centered on zero, squared, a mean taken and then the square root. Unfortunately, the mean of the optical signal is not centered on zero prior to the RMS process, rather it is centered at the average power of the optical signal, or for a sinusoid, half way up on the optical modulation curve. This creates a downward shift of half of the total amplitude or -3 dB when converted to the electrical units. (Note: this also means that as the noise measurements approach the noise floor of the analyzer (within a few dB optical), the lower excursion of the sinusoid (modulated noise) will actually dip below the noise floor of the spectrum analyzer. The signal above the noise floor will still be sampled, but there is an additional conversion factor which changes non-linearly in these last few dB. This additional factor was not taken into account in this experiment. The best thing is to get as much margin (at least 10 dB) as possible above the noise floor. See Appendix 3 for noise floor considerations.)

In summary the difference between optical and electrical RIN is:

$$\text{RIN}(\text{electrical dB}) = 2 * \text{RIN}(\text{optical dB}) - 3 \text{ dB.}$$

So, -70 dB of optical noise becomes, -143 dB in the electrical units. Though this may seem artificial, the use of relative units is very beneficial and avoids the problems encountered when attempting absolute measurements.

### Appendix 3: Conversion Calculations and Noise Floor Considerations

This appendix describes the noise floors and the spectrum analyzer conversion factors for those times when absolute noise measurements are to be derived from the displayed values. The conversion factors will be covered first.

The filters and amplifiers inside the spectrum analyzer modify the noise envelope and its mean. Reference Figure A1 for the following two effects.

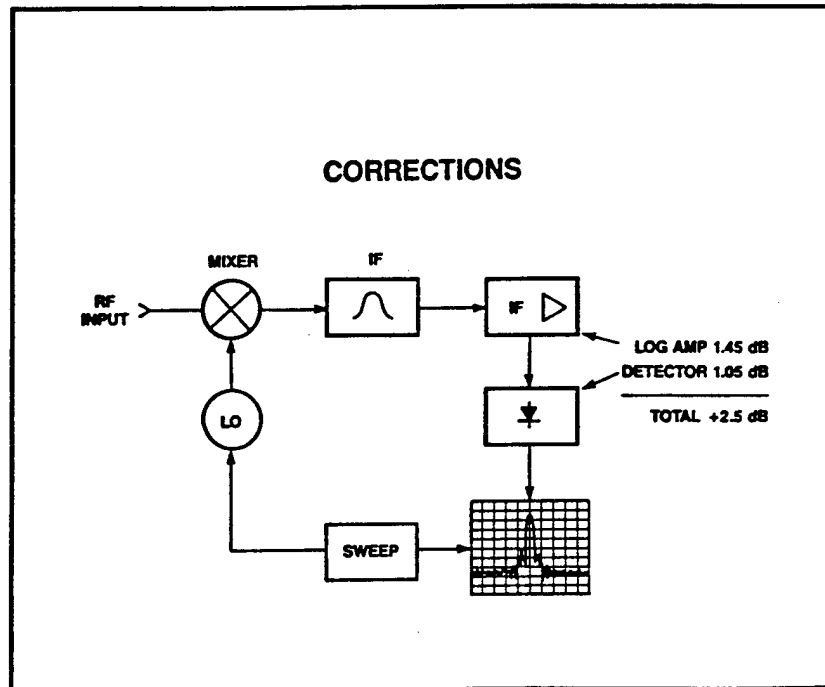


**Figure A1. Log Amplifier and Envelope Filter Noise Corrections**

The first effect is due to the logarithmic amplifiers. The gain of the logarithmic amplifiers (amplifiers used to increase the intermediate frequency (IF) amplitude after the front end mixing with the local RF oscillator) is inverse to the signal level. Lower level signals are expanded and higher level signals are compressed in amplitude. Just measuring the thermal noise on a spectrum analyzer which is not hooked up to anything gives an amplitude for the noise which is 1.45 dB too low.

Second, the envelope detectors read the RMS value of a sine wave, i.e. 0.707 of the peak value. In addition, the analyzer thermal noise sampled through its own filters (the Gaussian shape of these filters has an additional effect mentioned shortly) has the statistics of the Gaussian distribution, while the noise statistics that are actually being measured are Rayleigh distributed. The mean of Rayleigh statistics is 1.2533 times

higher than the mean of the Gaussian statistics. So the actual displayed mean of the noise is  $1.2533 \times 0.707 = 0.8862$ . In logarithmic terms this equates to  $20 \log(0.8862) = -1.05 \text{ dB}$ .

Taking these two effects together gives a displayed value which is 2.5 dB too low. Some spectrum analyzers will add the 2.5 dB back on automatically but this has to be verified on the operational noise menu and on the output CRT. For HP spectrum analyzers this is indicated by the Noise Marker tattletale.

The third effect is that the Gaussian shaped IF filters do not faithfully reproduce the ideal rectangular filter for a specified resolution bandwidth. See Figure A2.

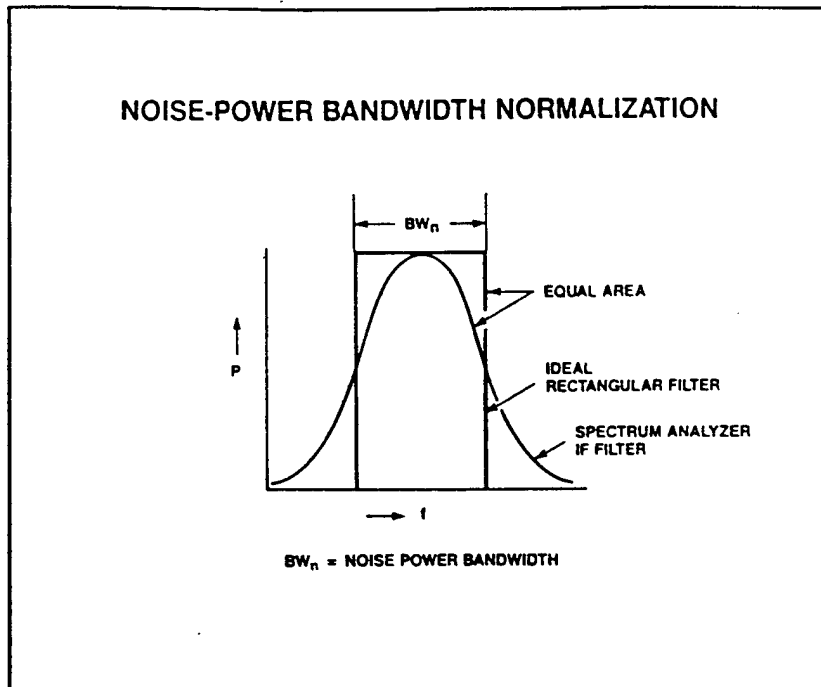


**Figure A2. Noise Power Bandwidth Resolution**

This means that every resolution bandwidth must be multiplied by 1.2 prior to its normalization back to 1 Hz.

As mentioned in Appendix 2, knowledge of the measurement reference planes is critical when comparing noise data from two different experiments. The concept is simple. The noise will always be given in terms of an equivalent 1 Hz bandwidth referenced to its measurement plane. Reference Figure A3. The most desirable plane of reference, especially for LIGO calculations is Plane A, the optical plane just before the detector. The next most desirable is Plane B immediately following the photodetector, where the conversion process from the detector material is straight forward. Plane C is probably the least desirable due to the need to take into account any additional amplifiers in front of the spectrum analyzer (this is experiment specific).

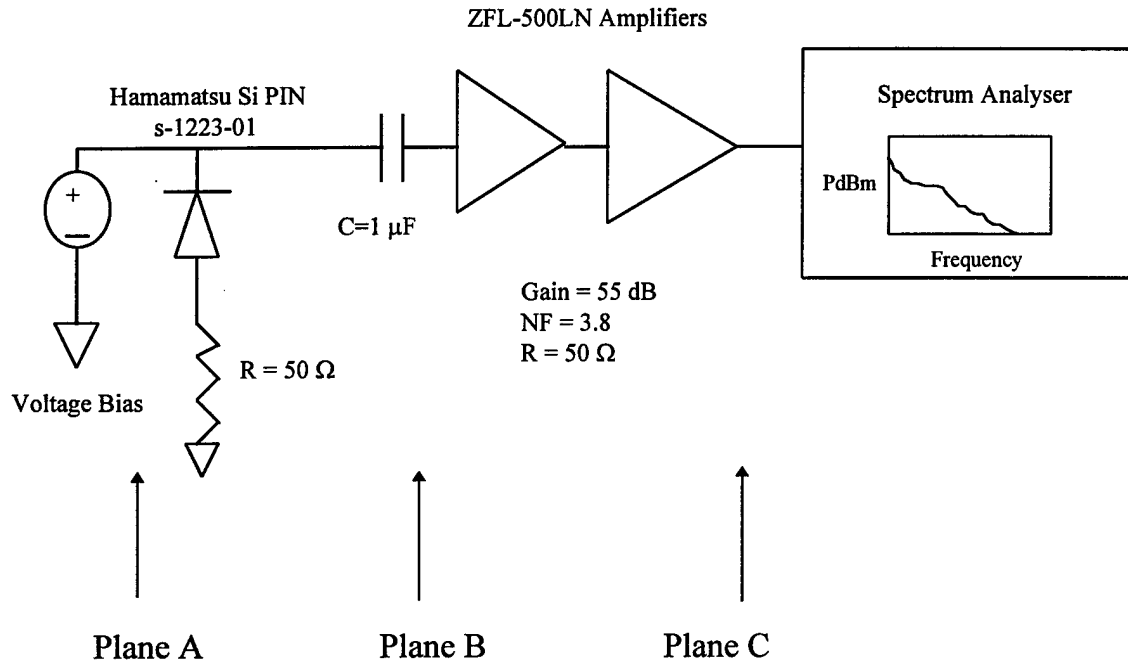


**Figure A3. Measurement Reference Planes for the Noise Experiments**

For this experiment the data was all taken and analyzed in electrical units at plane C. Since the shot noise level (SNL) was used as the unit of measure, all measurements were made relative to this SNL. Since shot noise level performance is indicative of photon quantum noise level performance, these results can be directly converted to optical units.

The key piece of equipment, the spectrum analyzer, was calibrated and certified by HP just prior to these noise measurements. This ensured linearity and a high probability that absolute noise measurements would have the lowest error. The HP 71000 series spectrum analyzer was specified to have a noise figure of 29 dB and a noise floor normalized to 1 Hz of -145 dBmW/Hz. These numbers will only be used as an example in this appendix. (They illustrate that the noise power gathered across a resolution bandwidth greater than 1 Hz must be normalized to 1 Hz and don't forget the corrections mentioned above.)

However, no matter how good the spectrum analyzer, it cannot distinguish whether a signal it has received is directly from the photodetector or has been processed in some way. All it can do is make corrections from its input connector at reference plane C and display noise powers referenced to this plane on its screen.

In the low noise experiments done in this study, it was necessary to have preamplifiers before reference plane C. Low noise preamplifiers can improve the sensitivity

of the noise measurement if the gain is greater than the loss due to the NF of the amplifier and if the NF is low enough relative to the NF of the spectrum analyzer. Recall from Appendix 2 that it is a good idea to be more than 10 dB above the SA noise floor. At plane C the noise is higher after the preamplifiers are inserted, but at plane B, the overall sensitivity is improved. This is explained in greater depth.

In general, from the amplifier chaining theory, it is well known that the lowest overall noise performance is attained when the amp with the lowest NF is the first in the sequence. This is because each gain stage multiplies the previous stages noise.

$$F_{total} = F_1 + \frac{F_2 - 1}{G_1} \dots \text{etc.}$$

If  $G_1 \gg F_2 - 1$  then  $F_{total}$  is approximately equal to  $F_1$ .

Though the NF s are given in dB, in order to do the calculations, the NF s must be converted back to noise factor or linear units to do the calculations.

$$NF_{SA} = 29 \text{ dB or } F_{SA} = 794.3 = F_2$$

$$NF_{amp} = 6 \text{ or } F_{amp} = 3.98 = F_1$$

$$G_1 = 50 \text{ dB or } G_1 = 100,000$$

Using the above equation,

$$F_{total} = 3.98 + \frac{794.3 - 1}{100,000} = 3.99.$$

This is approximately 6 dB, which is much closer to the preamplifier NF than the spectrum analyzer's NF. (Rule of thumb: when the sum of the preamplifier gain and noise figure are at least 10 dB greater than the SA NF, the NF is essentially the preamplifier's NF.)

Now it is possible to make the comparison of sensitivities at Plane B. With the total NF of 5.5 dB, the noise input at plane B is

$$NF_B = 6 \text{ dB} + \text{Resolution Bandwidth (in dB)} - \text{the thermal noise (50 Ohm load),}$$

where thermal noise (in 1 Hz) is (-174 dBmW) and assuming bandwidth units are converted to 1 Hz as well, gives

$$NF_B = 6 + 0 - 174 = -168 \text{ dBmW.}$$

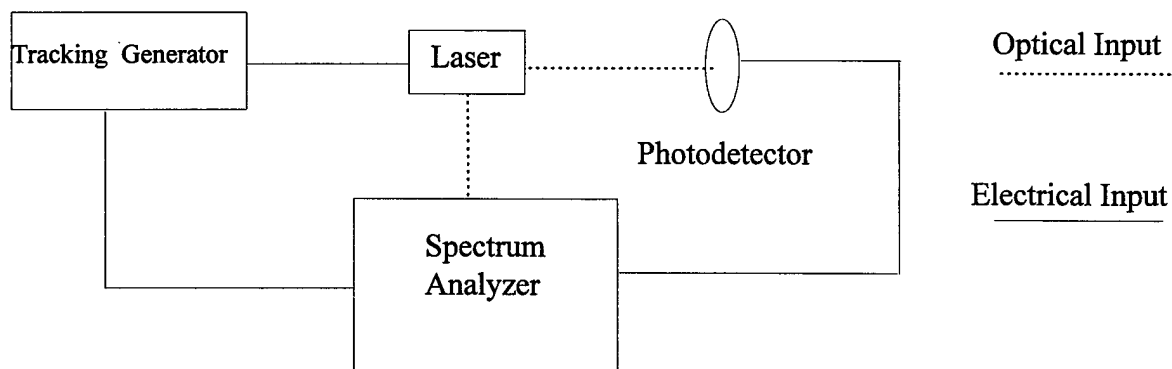
Since the original noise floor of just the spectrum analyzer was -145 dBmW, there is a 23 dB improvement with the addition of the amplifier. (Note that the improvement when adding the 55 dB of gain did not give 55 dB worth of noise improvement.) If the average optical input power and the responsivity of the detector is known, the change in sensitivity at reference plane A due to the addition of the preamplifier can be calculated in optical units.

## Appendix 4 - Set Up for Photodetector Frequency Analysis

Due to the advances in fiber optic communications, new diagnostic equipment has been developed which can be directly applied to the characterization of detectors. One characteristic which is of particular interest to the LIGO community is the frequency response of detectors to changing optical intensity. It is critical to ensure that a detector is not displaying saturation behavior at any frequency at which it may be used.

In this study, much time was spent determining the characteristics of detectors for the noise experiments. The detector under test (and in some cases a pre-amplifier) was connected to an RF spectrum analyzer. When illuminated from a known laser source, the detector generated a photoelectron current whose characteristic shot noise extended essentially over all frequencies. Only a small sample was taken over a narrow frequency range. (The optical source had to be calibrated prior to the test using another trusted detector). The optical intensity from the known source was then increased in known, calibrated steps, usually by using a beam splitter and wave plate combination. A commensurate increase in shot noise power levels indicated the detector was linear. It was a tedious and somewhat error prone process.

A much more efficient and consistent measurement technique is to use a sweep or tracking generator to drive a diode laser source and actually modulate the light at the source. The tracking generator would send a signal to the diode laser and to the spectrum analyzer. (If an optical spectrum analyzer is available then rather than sample the tracking generator signal, sample the light directly from the laser to get a ground truth for what the optical detector was receiving). The light from the optical source will not have a linear response to this sweep of current. By storing the first sweep trace in the spectrum analyzer and later subtracting it from the sampled noise, the non-linearity will be removed. Using diodes of different powers, a range of photocurrents can mimic the photocurrent expected during the operation of the photodetector device as shown in the figure below.



## Appendix 5: Calculations of the differences in quantum Efficiency for a Monochrome and Broadband Optical Source

Broadband thermal sources (flashlights) are often used in the lab to give a shot noise level input photon field to a detector to conduct linearity and responsivity experiments. However, it is known that thermal sources such as flashlights are not truly shot noise limited because they follow Bose-Einstein statistics. Two questions arise. How much noisier are the thermal sources than their coherent counterparts and how does the broadband nature of the light affect detector responsivity and hence efficiency. First some useful constants from Dereniak and Crowe, Chapter 1.

$$c_1 := 3.741 \cdot 10^{-16} \quad [\text{Watts meter}^2 \text{ K}^{-5}]$$

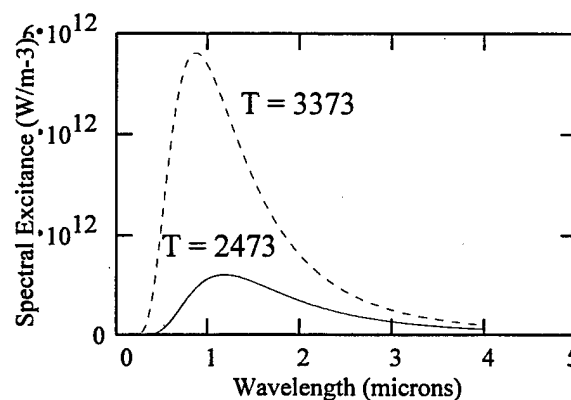
$$c_2 := 1.439 \cdot 10^{-2} \quad [\text{meter Kelvin}]$$

$$T := 2473, 2474.. 3373 \text{ Tungsten emission temperatures in Minimag Flashlight bulbs} \\ [\text{Kelvin}]$$

$$\lambda := 100 \cdot 10^{-9}, 101 \cdot 10^{-9}.. 4 \cdot 10^{-6} \quad [\text{Wavelength of optical radiation (m)}]$$

These constants are used in the equations describing any thermal source. The first descriptive equation is the spectral distribution of thermal radiation called spectral radiant exitance and it is in units of  $\text{W m}^{-3}$ .

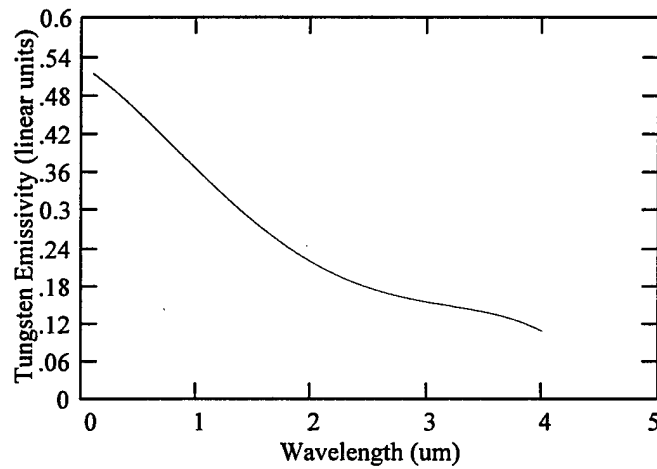
$$M(\lambda, T) := \frac{c_1}{\lambda^5 \cdot \left( \exp\left(\frac{c_2}{\lambda \cdot T}\right) - 1 \right)}$$



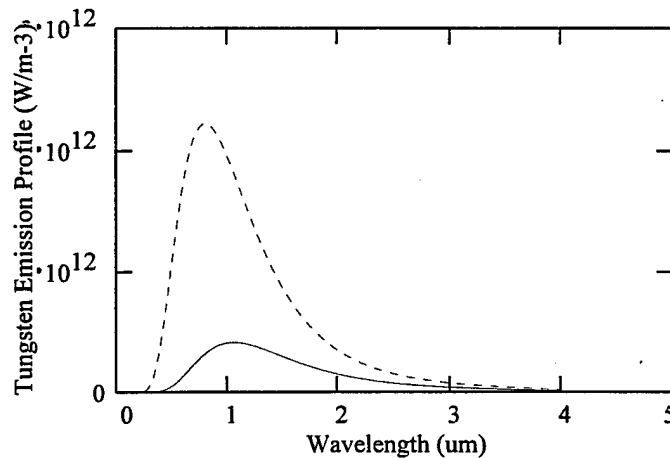
In this figure the spectral radiant exitance at two different temperatures for Tungsten bulbs are plotted. Notice that they both peak near the 1.06  $\mu\text{m}$  line of Nd:YAG.

Once the spectral radiant exitance of a thermal source is established it is necessary to impose the particular emission signature of the element on that source and establish the spectral radiant emission profile. Since most emission signatures are composed of discrete points, it is necessary to curve fit the data. This is a fourth order polynomial fit to the tungsten emissivity curve. Wavelength is in microns.

$$e(\lambda) := .52523472 + -.11452186 \cdot \lambda \cdot 10^6 + -.085972315 \cdot (10^6 \cdot \lambda)^2 + .044087598 \cdot (10^6 \cdot \lambda)^3 + -.0054929325 \cdot (10^6 \cdot \lambda)^4$$



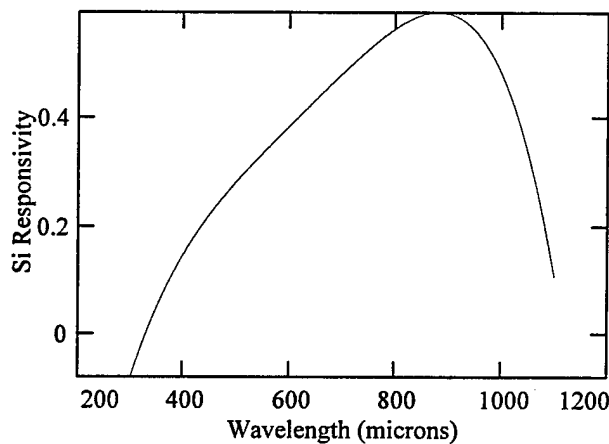
Now multiply the emissivity and spectral radiant exitance together to get the spectral radiation profile for Tungsten at two temperatures.



What is the total power emitted that can be intercepted by the detector? It depends on the overlap of the detector spectral responsivity with the source spectral radiation emission. This is the fourth order polynomial fit for the spectral responsivity of a Si pin photodiode. Using the wavelength range

$$\lambda := 300 \cdot 10^{-9}, 301 \cdot 10^{-9} .. 1.1 \cdot 10^{-6}$$

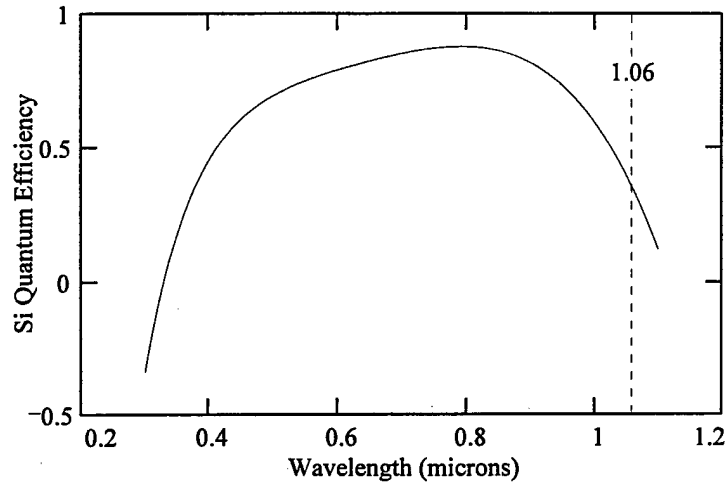
$$R(\lambda) := -2.5197336045919 + 0.0157702029358 \cdot \lambda \cdot 10^9 + -0.0000354732155619 \cdot (10^9 \cdot \lambda)^2 + 3.78299021106529 \cdot 10^{-8} \cdot (10^9 \cdot \lambda)^3 + -1.51308941009916 \cdot 10^{-11} \cdot (10^9 \cdot \lambda)^4$$



The responsivity can now be converted into the quantum efficiency using

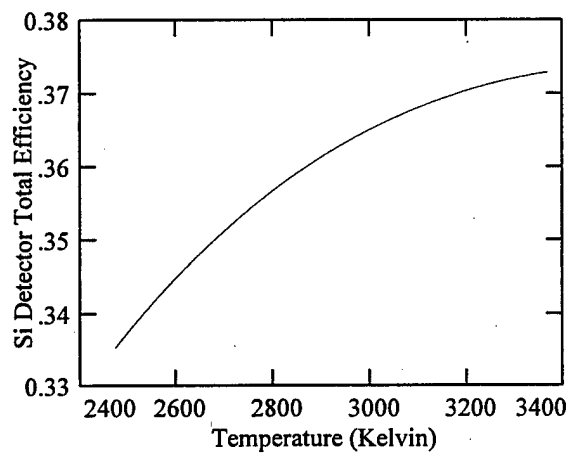
$$\eta(\lambda) := \frac{R(\lambda) \cdot 1.24}{\lambda \cdot 10^6}$$

This produces the familiar Si quantum efficiency plot.



The final step is to overlap the source emission and the detector efficiency curve and divide by the total emissivity to obtain the total efficiency.

$$F(T) = \frac{\int_{.25 \cdot \lambda}^{4 \cdot \lambda} R(\lambda) \cdot M(\lambda, T) \cdot e(\lambda) d\lambda}{\int_{.25 \cdot \lambda}^{4 \cdot \lambda} M(\lambda, T) \cdot e(\lambda) d\lambda}$$



This is the total efficiency on the Si detector for the Tungsten Vacuum Bulb. These values are very close to the values expected for Nd:YAG

So it appears the efficiencies for the laser and the mini-mag flashlight are the same. Now what about the noise? Take the equations for the first two statistical moments and insert the Bose Einstein Correction for the thermal source. Then find the noise power correction. The Bose-Einstein moments and variance are

$$\langle n \rangle = \frac{\exp(-h\nu/kT)}{1 - \exp(-h\nu/kT)},$$

$$\langle n^2 \rangle = \frac{\exp(-h\nu/kT) + \exp(-2h\nu/kT)}{1 - \exp(-h\nu/kT)^2},$$

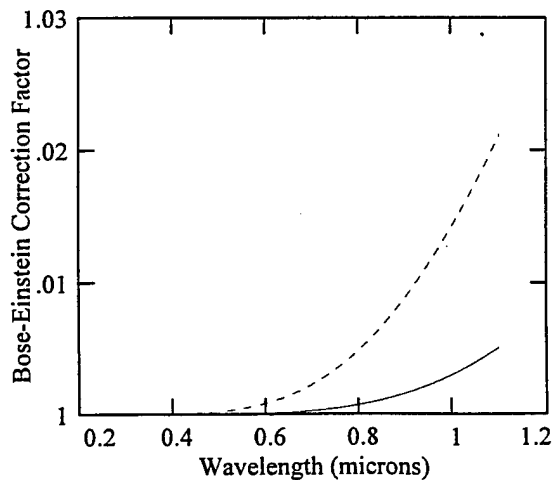
$$\sigma^2 = \frac{\exp(-h\nu/kT)}{(1 - \exp(-h\nu/kT))^2} = \langle n \rangle \frac{\exp(-h\nu/kT)}{1 - \exp(-h\nu/kT)}.$$

So the increase in noise over the Poisson source is contained in the last factor. The correction factor is calculated using the following constants.

$c := 299792458$  Speed of light  $h := 6.6260755 \cdot 10^{-34}$  Planck's const

$k := 1.380658 \cdot 10^{-23}$

$$E(\lambda, T) := \frac{\exp\left(\frac{h \cdot c}{\lambda \cdot k \cdot T}\right)}{\exp\left(\frac{h \cdot c}{\lambda \cdot k \cdot T}\right) - 1}$$



Notice the correction for the broadband source will be very small. It is certainly too small to give a 3 dB noise difference observed on the spectrum analyzer. Hence a flashlight is a good SNL source in the lab.

This appendix supports section 2.3, amplitude noise calculations for a simple oscillator. The goal is to determine whether a FP cavity imposed around gain material can give better SNR than a single pass system with the same gain material for single pass gains greater than 1. The following parameters and variable assignments are used throughout the derivation.

$G := 1, 1.01..10$  This single pass gain variable,  $G$ , represents what an actual Nd:YAG laser amplifier might be capable of supplying. This is in keeping with the experimental nature of this paper.

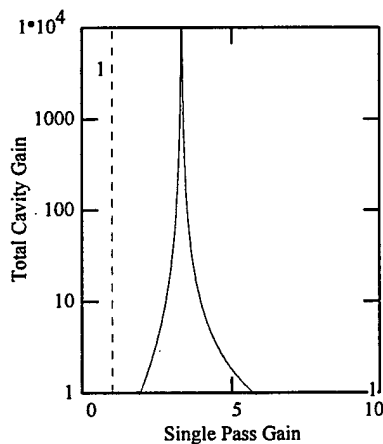
$R_1 := 0.01, 0.02..1$   
 $R_2 := 0.01, 0.02..1$  These are the mirror power reflectivities for the FP cavity.

The following equation provides the cavity gain based on the FP system where the numerator represents the transmissivity of the optical power through the two interfaces and the denominator represents the influence of gain. This is found in Saleh and Teich, *Photonics*, p. 316.

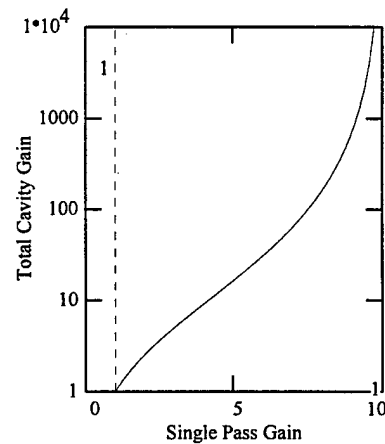
$$G_c(R_1, R_2, G) := \frac{(1 - R_1) \cdot (1 - R_2) \cdot G}{(1 - \sqrt{R_1 \cdot R_2} \cdot G)^2}$$

Notice there is no correction for gain saturation effects in this equation. There is also a symmetry here in that either way the reflectivities,  $R_1$  and  $R_2$  are ratioed, we will see the same effects.

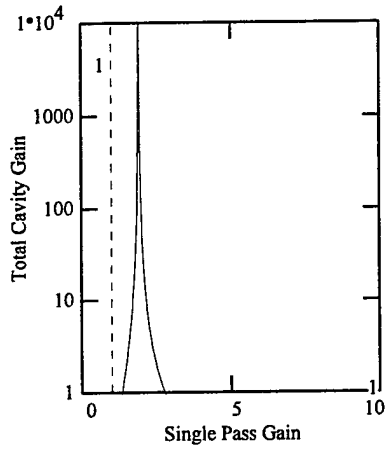
This first set of 9 plots provides the FP cavity gain,  $G_c$  for various combinations of mirror reflectivities. When the single pass gain is greater than one, indicated by the dotted vertical line, it is clear that the cavity gain can be a very large number.



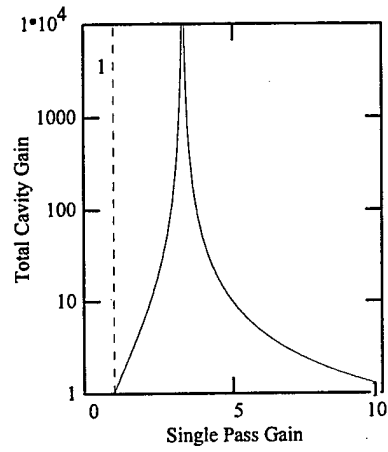
$R_1 = 0.1, R_2 = 0.9$



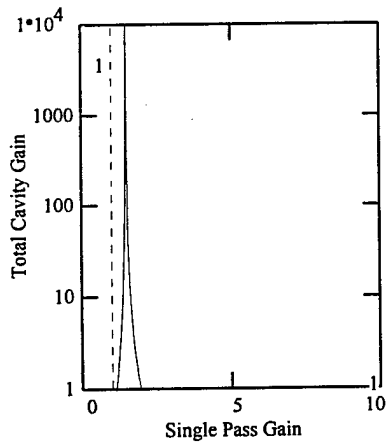
$R_1 = 0.1, R_2 = 0.1$



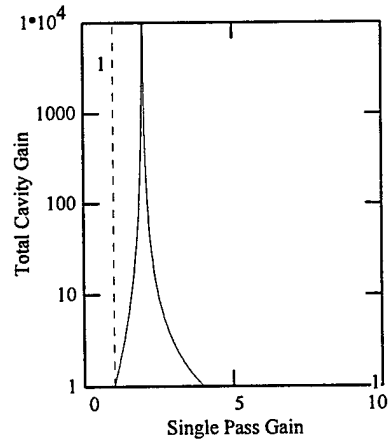
$$R_1 = 0.3, R_2 = 0.9$$



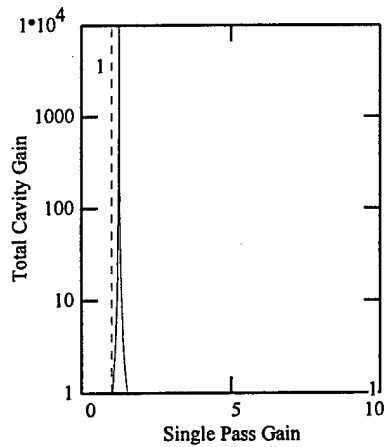
$$R_1 = 0.3, R_2 = 0.3$$



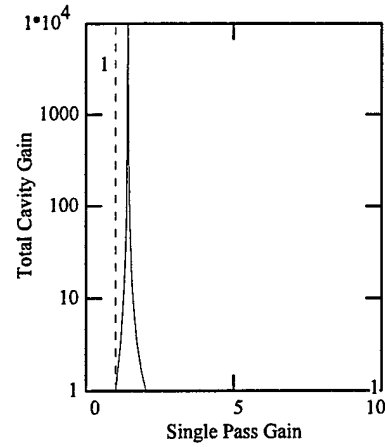
$$R_1 = 0.5, R_2 = 0.9$$



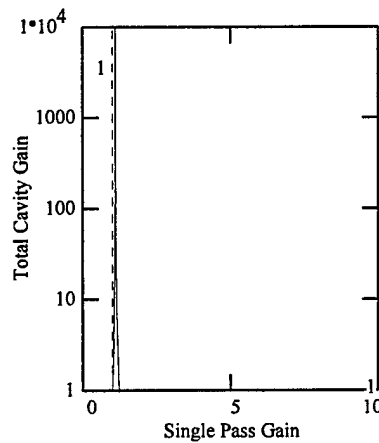
$$R_1 = 0.5, R_2 = 0.5$$



$$R_1 = 0.7, R_2 = 0.9$$



$$R_1 = 0.7, R_2 = 0.7$$



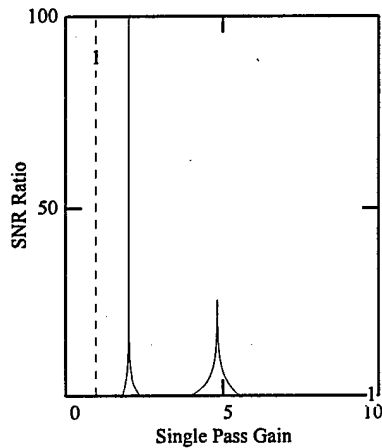
$$R_1 = 0.9, R_2 = 0.9$$

It appears from the first nine plots that very high gains are available from the FP cavities. However, does this mean they also have good noise performance? To answer that question use Yamamoto's equations from section 2.3 and compare the noise performance for the oscillators to the single pass amplifiers. The first equation is the gain parameter X.

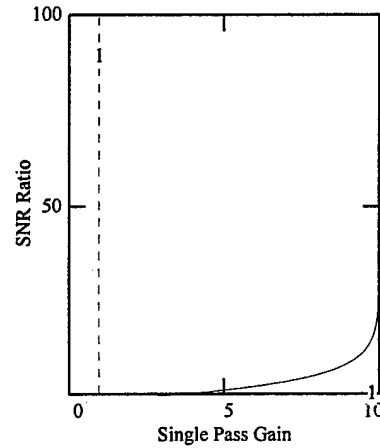
$$X(R_1, R_2, G) := \frac{R_1 \cdot \left( G - \sqrt{\frac{R_2}{R_1}} \right)^2}{\left( 1 - \sqrt{R_1 \cdot R_2 \cdot G} \right)^2}$$

If  $X$  can be made large enough to counter the added amplification noise, it may be possible to get shot noise performance out of a system at very low single pass gains but rather high cavity gains. To verify this hypothesis, we will compare the SNR for the cavity type system to the single pass system for cases where the cavity gains exceed 1. The ratio of SNRs for the single pass amplifier and the oscillator is given as follows

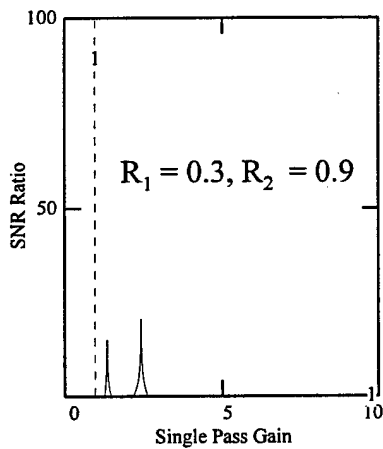
$$\text{SNR}(R_1, R_2, G) := 10 \cdot \log \left[ \frac{G_c(R_1, R_2, G) \cdot (1 + 2 \cdot (G - 1))}{G \cdot (1 + 2 \cdot (G_c(R_1, R_2, G) - 1 - X(R_1, R_2, G)))} \right]$$



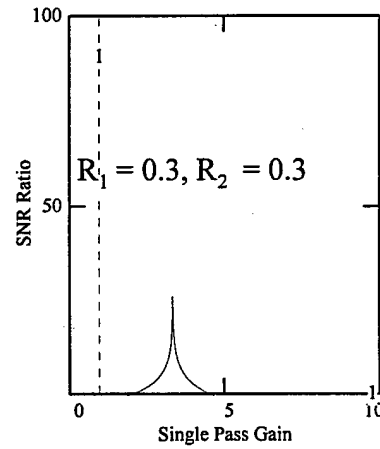
$R_1 = 0.1, R_2 = 0.9$



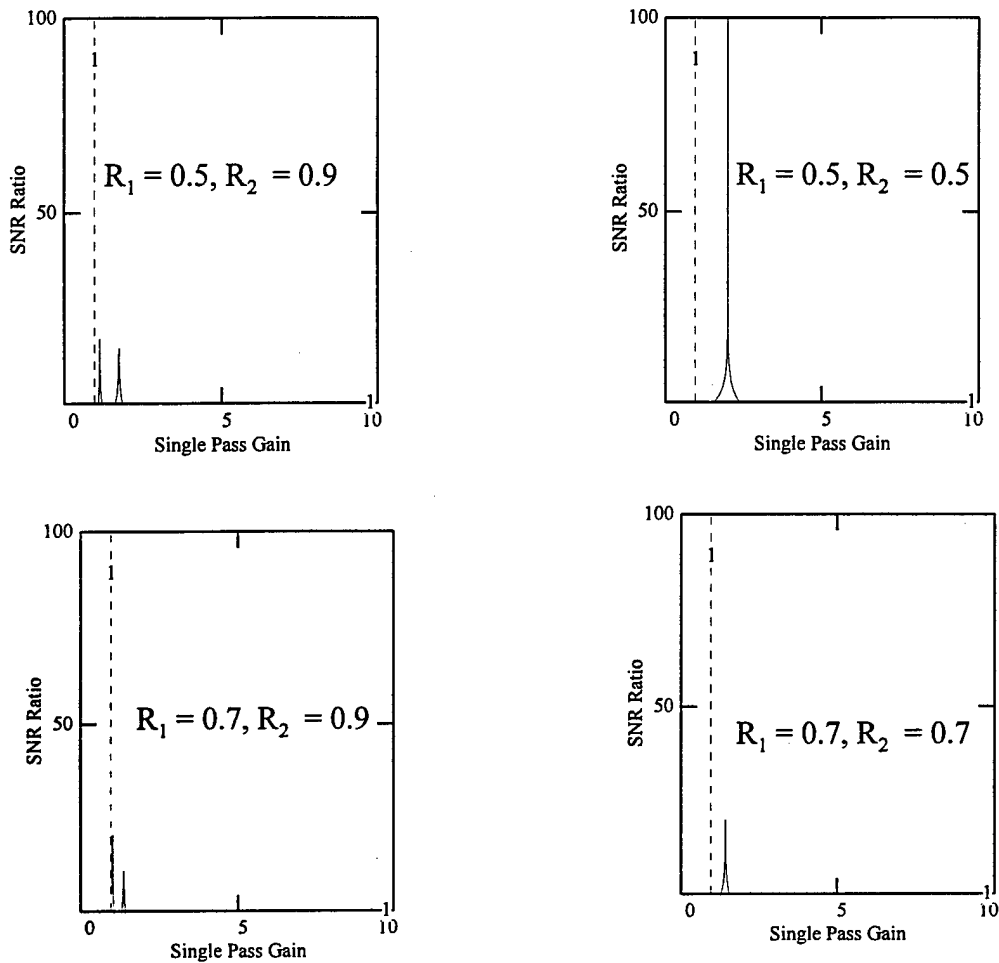
$R_1 = 0.1, R_2 = 0.1$



$R_1 = 0.3, R_2 = 0.9$



$R_1 = 0.3, R_2 = 0.3$



The simple oscillator with asymmetric mirror reflectivities has two "sweet spots" where it produces better noise performance than the single pass amplifier. The cavity with symmetric mirror reflectivities has a single spike where it has performance better than the single pass amplifier. As the mirror reflectivities increase, the sweet spot narrows and makes the control of the single pass gain value critical in order to maintain the excellent noise performance. The best noise performance for the FP cavity was for the cases where  $R_1 = 0.1, R_2 = 0.9$  and  $R_1 = 0.5, R_2 = 0.5$  and the gain was approximately 2. The remaining cases do not have as great an advantage over the single pass amplifier.

If the single pass gain can be controlled very precisely, this analysis shows that Fabry Perot oscillators can have superior gain and superior noise qualities compared to the single pass amplifier. This has direct bearing on the choice of design for the LIGO laser source.

This appendix calculates the amplitude noise for the 3 different injection locked oscillator theories and provides the material for Figure 15. The first calculation is Yamamoto's RLC approach to the Injection Locked Oscillator Noise. Throughout these calculations a 1 Hz unit of spectral width is assumed. The first statements assign values to constants used throughout the entire appendix.

$\gamma_e := 70$  This is the cavity resonance in MHz for the Shine injection locked laser.

$f := 0.0001, 0.001 \dots 20$  This is the value of the frequency in units of MHz. This covers the entire range of operation of the planned LIGO.

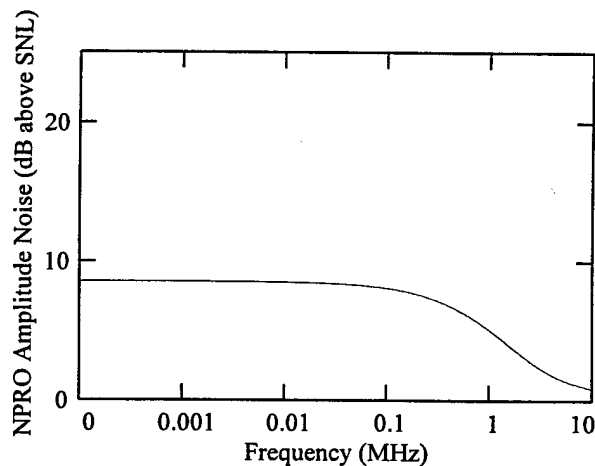
$h := 1.055 \cdot 10^{-34}$  This is the reduced Planck's constant

$\omega := 1.78 \cdot 10^{15}$  This is the frequency of light at 1.06  $\mu\text{m}$

$K := 0.01$  This is the power ratio of the master to the slave laser, 200 mW to 20 W.

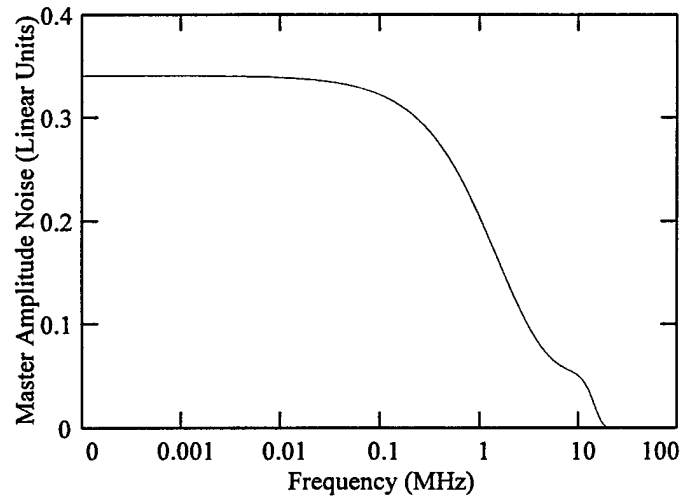
As described in section 3.4 the calculation begins with the Harb polynomial fit, Equation 3.17, to the NPRO noise spectrum in units of dB.

$$\text{ETC}(f) := -0.024 \cdot f^3 + 0.58 \cdot f^2 - 5.71 \cdot f + 21.42$$



Now taking the first term of Equation 3.18 and substituting in the known values gives the noise power due to the master laser input noise power.

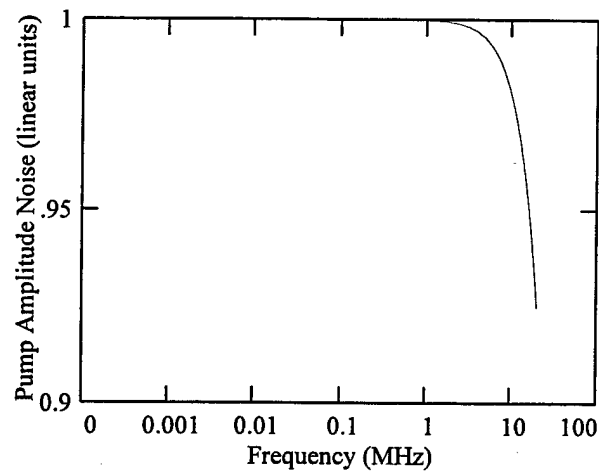
$$\text{PWRM}_{\text{mw}}(f) := \frac{\left[ \left( \frac{f}{\gamma_e} \right)^2 + 4 \cdot K \right]}{1 + \left( \frac{f}{\gamma_e} \right)^2} \cdot \exp\left(\frac{\text{ETC}(f)}{10}\right)$$



This is the noise due to only the master laser. The shot noise floor is at zero and the noise is given in linear units.

Taking the other term in Equation 3.18 will give the noise due to the pump source. (The pump is shot noise limited.)

$$\text{PWRS}_{\text{mw}}(f) := \frac{1}{1 + \left( \frac{f}{\gamma_e} \right)^2}$$

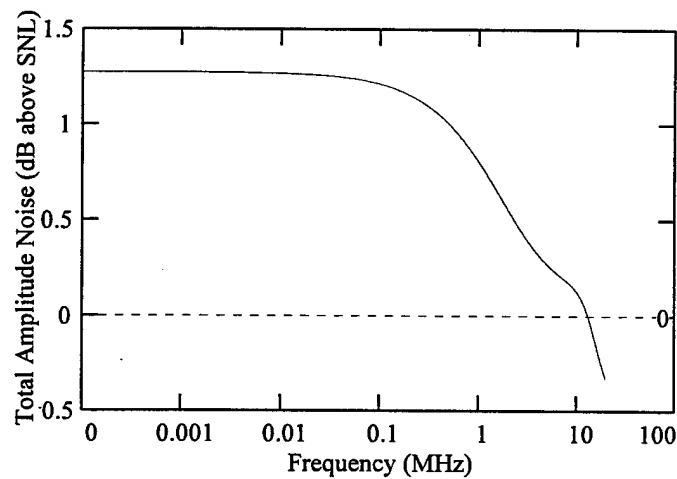


This is the amplitude noise due to the pump noise in the slave laser only.

Taking the noise due to the master and the noise due to the slave will give the total amplitude noise. Notice the pump is the predominant input of noise to the slave laser. The next two equations give the total noise in linear and dB units and the plot gives the total noise in dB units above the shot noise floor.

$$\text{PWR}_{\text{mw}}(f) := \text{PWRS}_{\text{mw}}(f) + \text{PWRM}_{\text{mw}}(f)$$

$$\text{dBPWR}_{\text{mw}}(f) := 10 \cdot \log(\text{PWR}_{\text{mw}}(f))$$



The system is shot noise limited at approximately 10 MHz. Otherwise it is very low noise at approximately 1.3 dB above the SNL.

The next section will calculate the Farinas Transfer Function Approach (TFA) to the Injection Locked Oscillator Amplitude Noise using the same parameters as the Yamamoto approach. This calculation also starts by defining variables and constants

$f := 0.0001, 0.001 .. 20$  Frequency range of interest. (MHz)

$i := \sqrt{-1}$  Definition of the imaginary number.

$\gamma_c := 111.8 \cdot 10^6$  This is the cavity decay rate

$\gamma_2 := 4350$  This is the population decay rate from Siegman.

$\gamma_e := 70 \cdot 10^6$  This is the cavity resonance in MHz for the Shine injection locked laser.

$r := 5$  This is the number of times pumped above threshold

$\omega_{sp} := \sqrt{(r-1) \cdot \gamma_c \cdot \gamma_2}$  This is the spiking frequency

Note: the spiking frequency and the spiking decay rates are actually squared values. Mathcad has trouble with designating squared functions in assignment statements.

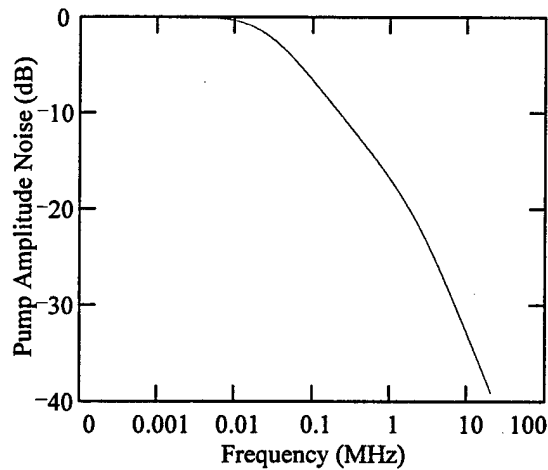
First is the equation for the spiking decay rate.

$$\gamma_{sp} := \frac{r \cdot \gamma_2}{2} + \gamma_e \cdot \left( r \cdot \frac{\gamma_2}{\gamma_c} + 1 \right) \cdot \sqrt{.01}$$

This is the transfer function for pump modulation to cavity photon number noise in linear and dB units.

$$G_p(f) := \frac{\omega_{sp}}{\left[ \omega_{sp} - (2 \cdot \pi \cdot f \cdot 10^6)^2 \right] + 2 \cdot i \cdot (2 \cdot \pi \cdot f \cdot 10^6) \cdot \gamma_{sp}}$$

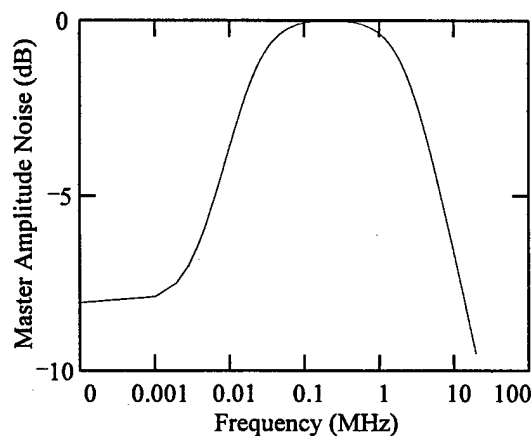
$$dBG_p(f) := 10 \cdot \log(G_p(f))$$



The pump modulation transfer function to internal photon noise spectral density is basically a low pass filter. Now look at the expression for the transfer function for the master laser amplitude power spectral density to internal photon noise spectral density. Note: the equation has been scaled by a factor of two to bring the transfer function response in the resonant relaxation oscillation (RRO) regime to the 0db level. This expression is provided in both linear and dB units.

$$G_m(f) := 2 \cdot r \cdot \gamma_2 \cdot \gamma \cdot e^{\sqrt{.01}} \cdot \frac{1 + \frac{i \cdot 2 \cdot \pi \cdot f \cdot 10^6}{r \cdot \gamma_2}}{\left[ \omega_{sp} - (2 \cdot \pi \cdot f \cdot 10^6)^2 \right] + 2 \cdot i \cdot (2 \cdot \pi \cdot f \cdot 10^6) \cdot \gamma_{sp}}$$

$$dBG_m(f) := 10 \cdot \log(G_m(f))$$



Lastly, the expression for the total noise using the TFA approach is a combination of the noise attributable to the master and the pump.

$$\text{dB PWRM}(f) := 10 \cdot \log \left[ (G_m(f)) \cdot \sqrt{\exp\left(\frac{\text{ETC}(f)}{10}\right) + G_p(f)} \right]$$

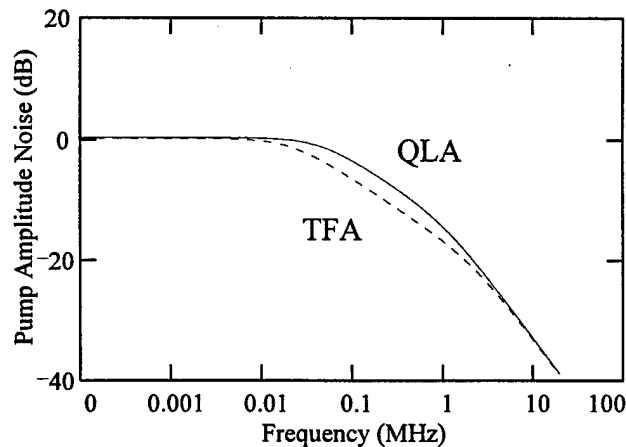
Third and last is the calculation for the QLA Approach to the Amplitude Noise of the Injection Locked Laser. Only two definitions are needed.

$\Delta l := \gamma_e \cdot \sqrt{K}$       The locking range will be set at  $\gamma_e \cdot 1$ , reflecting the square root of the ratio of powers between master and slave.

$\gamma_{\text{Lin}} := 0.01 \cdot \Delta l$       The damping rate for master laser will be set to be less than the locking range.

The QLA approach transfer functions are for squared units. To compare to the other approaches they must be rooted. They are also referenced to the SNL so the "1" used in the original equation has been subtracted. The first equation is the transfer function for the pump to slave noise.

$$V_{ps}(f) := \sqrt{\frac{3 \cdot 10^4 \cdot \gamma_e \cdot \omega_{sp}}{\left[ \omega_{sp} - (2 \cdot \pi \cdot f \cdot 10^6)^2 \right]^2 + (2 \cdot \pi \cdot f \cdot 10^6)^2 \cdot (\gamma_{sp})^2}}$$

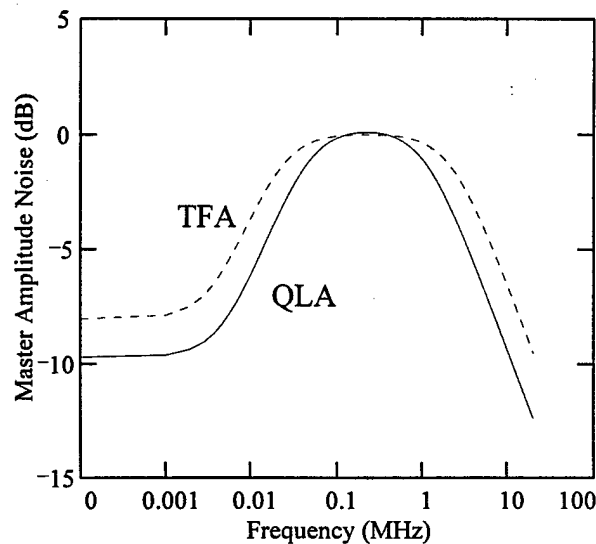


The plots of the QLA and TFA pump-to-slave amplitude noise agree very well. This implies that the semi-classical and QLA approach treat pump amplitude noise in a similar fashion. This was expected.

Now the QLA equation for the transfer of amplitude noise from the master laser to the injection locked system amplitude noise. It looks like the Farinas result--more like an asymmetric bandpass filter. A factor was inserted to bring the function to 0 dB at the RRO.

$$V_{ms}(f) := \sqrt{\frac{\gamma e^2 \cdot \left[ (2 \cdot \pi \cdot f \cdot 10^6)^2 + \gamma_{Lin}^2 \right] - \left[ 2 \cdot \gamma e \cdot \omega_{sp} \cdot \gamma_{Lin} - 2 \cdot \gamma e \cdot (2 \cdot \pi \cdot f \cdot 10^6)^2 \cdot \Delta l \right]}{\left[ \omega_{sp} - (2 \cdot \pi \cdot f \cdot 10^6)^2 \right]^2 + (2 \cdot \pi \cdot f \cdot 10^6)^2 \cdot (\gamma_{sp})^2}} \cdot 10.7^1$$

$$dBV(f) := 10 \cdot \log \left( V_{ms}(f) \cdot \sqrt{\exp\left(\frac{ETC(f)}{10}\right) + V_{ps}(f)} \right)$$



This plot shows the TFA internal photon noise number due to the master laser and the QLA rendition of the amplitude noise of the injection locked system from the master laser noise inputs. They show great similarities.

Finally the plot which compares all three theories for total amplitude noise. This is Figure 15.

